A Biochemical and Biophysical Study of Dystrophin

A DISSERTATION
SUBMITTED TO THE FACULTY OF THE GRADUATE SCHOOL
OF THE UNIVERSITY OF MINNESOTA
BY

Davin Michael Henderson

IN PARTIAL FULFILLMENT OF THE REQUIREMENTS
FOR THE DEGREE OF
DOCTOR OF PHILOSOPHY

Advisor, James M. Ervasti Ph.D.

July, 2011

Acknowledgements

I would like to thank my advisor Jim Ervasti for mentoring me to become a better scientist and writer. I also would like to thank Jim for establishing a laboratory environment that is enjoyable to work in and productive. I could not have asked for a more patient and enjoyable advisor to work with.

I would like to thank my parents Janis and Kallen Henderson for their support and patience they have given me throughout my oft-winding path to this point. I would like to thank my sister, Kirsten, for her support and humor. I can always count on her to call me out when I start to talk too much about science.

I would like to thank my wife, Julia, for her support, encouragement and willingness to listen to all of my science related rambling.

I would like to thank Laura Breshears, Jess Curtis, Zach and Shana Demorest, Medora Huseby, David Kast, Drew Kile, Andy Lane, Clint Matson, Colin and Laura Ramsey, Eric Rahrman, Brad Scutvick, Matt and Katie Smith, Mark Stenglein and everyone else I have had the pleasure to meet and spend time with in Minnesota for their friendship and comradery.

I would like to thank my graduate committee: Tim Griffin, Lincoln Potter, Kathleen Conklin and Natalia Tretyakova for the time they have taken to mentor me and the advice they have given me along the way.

I would like to thank all members of the Ervasti lab past and present for their willingness to help and for making daily lab life enjoyable.

I would like to thank the Thomas lab, specifically Dave Thomas for access to instrumentation and experimental advice, Ewa Prochniewicz for her sage like knowledge of actin biochemistry and Eva Yun Lin for her willingness and openness to collaborate.

I would like to thank David D. Thomas and the Minnesota Muscle Training grant (AR007612) for supporting my graduate career.

I would like to acknowledge the Minnesota Medical Foundation, the University of Minnesota College of Biological Sciences, and the Department of Biochemistry, Molecular Biology and Biophysics for awards I have received.

I would also like to thank every trout in Minnesota and Wisconsin because I have probably caught and released every one since I came to the Midwest.

Dedication

This dissertation is dedicated to my family and my wife Julia.

Abstract

The primary role of a muscle cell is to contract and produce force that moves an organism. A vast majority of a muscle is made of the proteins in contraction machinery and nearly all energy utilized by the cell is consumed in this process. However, an equally important but substantially smaller portion of the muscle cell is dedicated to the preservation of cell membrane integrity. The costamere is an elaborate matrix of cytoskeleton associated and transmembrane proteins that form a support lattice between the plasma membrane and contractile apparatus. The dystrophin glycoprotein complex (DGC) is a structurally important member of the costamere and has been shown to link microtubules, thin and intermediate filaments of the cytoskeleton with major components of the extracellular matrix. In the DGC, dystrophin is responsible for attachments with intracellular cytoskeletal components and the transmembrane protein dystroglycan.

One of the most common diseases afflicting muscle is Duchenne muscular dystrophy (DMD), which is caused by mutations in the gene encoding the protein dystrophin. The focus of my thesis is to better understand the biochemical and biophysical properties of dystrophin. Specifically, I investigated the actin binding properties of dystrophin in the context of its functional domains as well as the consequences of disease causing missense mutations localized to actin-binding domain 1 (ABD1). Additionally, I characterized the biophysical properties of internally truncated dystrophin proteins under development for treatment of DMD.

It has been twenty years since dystrophin was hypothesized to bind actin and even today we are learning more about this fascinating interaction. My thesis expands our understanding of the dystrophin-actin interaction in three ways. First, I showed that full-length dystrophin interacts with the actin isoforms expressed in muscle with equivalent affinities. Second, I showed that the thermally stable C-terminal domain of dystrophin is required for full actin binding activity. Third, in collaboration with the Thomas lab, we showed that dystrophin and utrophin uniquely alter the physical properties of actin filaments.

Disease causing missense mutations in the dystrophin gene are scattered in many functional domains but we chose to study a cluster localized to ABD1 with hope that we would find amino acids important for actin binding. We hypothesized that mutations in ABD1 would disrupt actin binding and therefore lead to disease though loss of an essential interacting partner. However, no mutation dramatically disrupted actin binding but instead lead to loss of thermal stability and protein aggregation. My thesis work was the first to show evidence that protein stability and aggregation may play a role in the pathogenesis of dystrophinopathies.

DMD currently has no effective treatment but many promising therapies are being pursued. Many laboratories are pursuing therapies for DMD and multiple techniques are being pursued including adeno-associated viral gene therapy, protein replacement therapy, exon skipping therapy and stop codon read though therapy. For gene therapy and protein therapy, the size of the dystrophin

or utrophin coding sequence has been reduced by deletion of internal domains, which retains important N- and C-terminal ligand binding sites. I set out to test the stability of internally deleted therapy proteins to ensure that no unwanted structural perturbations were caused by internal deletion. Additionally, I tested a set of N-and C-terminal truncations of dystrophin and a dystrophin related protein, utrophin for comparison to internally deleted versions of these proteins used in therapy. I found that the thermal stability of utrophin was uniform from N- to C-terminus and that internal deletion did not affect protein stability. I also found that the N-terminal half of dystrophin had a lower thermal stability compared to the C-terminal half and, to our surprise, internally deleted dystrophin proteins showed marked thermal instability and aggregation.

Table of Contents

List of Tables

List of Figures

Chapter One: Introduction

Muscle composes a larger percentage of our body weight than any other tissue and is the cellular machine that powers all movements. Multicellular animals have evolved a number of unique muscle adaptations to accomplish an impressive diversity of movements from a cheetah chasing prey to a worm inching across the ground. Muscle is captivating because of the ubiquitous role it plays in our lives. We cannot speak without muscle and the ever-present beat of our hearts reminds us of our utter reliance on the contractile properties of muscle. The three types of muscle- skeletal, cardiac and smooth- have evolved unique features to accomplish diverse tasks. Smooth muscle evolved separately from skeletal and cardiac muscle and is controlled involuntarily by the nervous system (1). Cardiac muscle of the heart pumps blood that carries oxygen throughout tissues. Skeletal muscle powers both voluntary and involuntary movements of our skeleton.

During contraction skeletal and cardiac muscle cells endure significant stresses and have developed a wide range of structural support systems to mitigate damage. Structural integrity of muscle cells is compromised in a number of diseases that range in severity from moderate muscle impairment to complete muscle degeneration and subsequent death. One of the most common muscle diseases is Duchenne muscular dystrophy (DMD) (2). DMD is a lethal disease

that affects both cardiac and skeletal muscles and is caused by loss of the protein dystrophin (3, 4). Understanding the molecular basis of dystrophin related disease is the focus of this thesis.

Duchenne Muscular Dystrophy

DMD affects one out of every 3700-4200 males born and is the second most common genetic disease (2, 3). DMD is typically caused by mutations within the dystrophin gene, which is found on the X-chromosome and is the largest gene known in nature (3-5). The X-chromosome location of the gene explains the male inheritance pattern and the remarkable size of the gene helps to explain the high rate of de novo mutation, which accounts for 30% of DMD cases (2, 5). To date, there is no effective cure and life expectancy ranges from the mid-twenties to the early thirties.

DMD can be caused by chromosomal rearrangement or deletion at the dystrophin locus or by nonsense, missense or point mutations (4, 5). Rearrangements or splice site mutations that produce an in-frame loss of coding sequence usually result in a rarer disease called Becker's muscular dystrophy (BMD) (5, 6). BMD symptoms range from nearly as severe as that of DMD to almost undetectable muscle weakness for reasons that are not well understood (6, 7).

Dystrophin and Disease

Dystrophin is a key protein in a large protein assembly called the dystrophin glycoprotein complex (DGC) that establishes a mechanically strong link between the intracellular cytoskeleton and the extracellular matrix (Figure 1-1) (8-10).

Dystrophin is a cytosolic protein that forms two key linkages required for membrane stability: one with the cortical actin cytoskeleton and the other with the membrane spanning dystroglycan complex (8, 11-14). The dystroglycan heterodimer is composed of alpha and beta-dystroglycan, which are transcribed as a single mRNA but are post-translationally cleaved to form two polypeptide chains (15). Beta-dystroglycan is a single-pass transmembrane protein with an extracellular domain responsible for alpha-dystroglycan dimerization and a small cytoplasmic domain that interacts with dystrophin (16, 17). Alpha dystroglycan is extracellular, highly glycosylated and supports interactions with multiple extracellular matrix proteins including laminins, agrin and perlecan (8). Mutations in the dystroglycan gene or genes that are required for proper glycosylation of dystroglycan result in many diseases with varying clinical manifestations which include presentations similar to DMD (18).

The DGC also contains a number of other proteins including the sarcoglycans, alpha-dystrobrevin, alpha1-syntrophin and sarcospan (Figure 1-1). Mutations in the sarcoglycans lead to limb girdle muscular dystrophies 2C-F,

which can be clinically similar to DMD but are often more variable and less severe (19-21). The alpha-dystrobrevin null mouse has apparent muscle degeneration but retains normal muscle function (22). Alpha1-syntrophin and sarcospan deficient mice have no apparent muscle phenotypes (23, 24). Importantly, while loss of DGC components can produce variable muscle phenotypes, loss of dystrophin protein expression alone leads to DGC destabilization indicating that dystrophin is an essential component of the DGC (11).

In muscle, the DGC is localized to a lattice-like structure called the costamere (25-27). Costameres link the sarcomeric Z-line in the contractile apparatus with the extracellular matrix though multiple membrane spanning complexes, one of which is the DGC (28). Functionally, costameres transmit force radially to neighboring muscle fibers and physically couple the force generating contractile apparatus with the sarcolemma (28). As a member of the costamere, the DGC links the cortical actin cytoskeleton with the membrane and the extracellular matrix (8, 10, 28). Although the costamere has many protein complexes that link the extracellular matrix to the intracellular cytoskeleton, loss of dystrophin or the DGC is sufficient to cause lethal muscle wasting disease (29, 30).

The Dystrophin Protein

Dystrophin is a member of the spectrin superfamily of cytoskeletal-associated proteins (31-33). By sequence comparison between dystrophin and other spectrin-like proteins, it was hypothesized that dystrophin may bind filamentous actin due to the presence of an N-terminal tandem CH domain (3, 32) (Figure 1-2 A and B). As predicted, the isolated tandem CH domain of dystrophin, or ABD1, bound to actin filaments with K_d of 40 μM (13). Later a peptide/nuclear magnetic resonance (NMR) based approach delineated specific regions of ABD1 that interacted with actin (34). NMR studies showed that peptides corresponding to amino acids 17-26 and 128-156 had a reduced mobility upon the addition of actin (34). The identified peptides were conserved in all other tandem CH-domain containing proteins and spectrin super-family members (34).

At its C-terminus, dystrophin has a globular cysteine-rich region that contains multiple domains including a WW domain, two EF hand domains, and a ZZ domain that facilitate an interaction with beta-dystroglycan (17, 35-37) (Figure 1-2 A and C). Each domain is required for full biochemical activity and, as a whole, interacts with the specific target sequence PPxY found in the cytoplasmic domain of beta-dystroglycan (36, 37).

Between the two globular regions of dystrophin lies a series of 24 triple helical spectrin-like repeats (SLRs) and four hinge regions that are thought to

give dystrophin an elongated, flexible, rod shape with an approximate contour length of 120 nanometers (32, 33, 38) (Figure 1-2 A and D). SLRs are typically found in elongated proteins that are localized to mechanically challenged cellular structures such as alpha-actinin at the Z-line and spectrin at the membrane of red blood cells (39). SLRs are composed of approximately 100 amino acids in a triple helical bundle and are organized in a conserved heptad pattern (40, 41) (Figure 1-2 D). The heptad pattern marks conserved amino acids along the primary sequence with a specific letter (A-G) (40). Conserved hydrophobic residues are found in the A and D positions, which places them along the same plane when found in an alpha-helical secondary structure and serves to establish a hydrophobic core within the SLR domain (40, 41). The helices that make up the bundle are not perfectly parallel but twist slightly to form a structurally stable coiled coil (41, 42). Moreover, SLRs in divergent family members have been shown to support multiple protein-protein interactions and dimerization, suggesting that SLR structure is adaptable to a wide variety of cellular functions outside of its traditional role as a structural/linker domain (43-49).

In addition to ABD1, dystrophin has a second site of interaction with actin (ABD2) localized within SLRs 11-17, which are a series of predominantly basic repeats that form an interaction with acidic actin filaments (47, 50) (Figure 1-2 A). The electrostatic nature of ABD2 binding to actin has been hypothesized to function as a molecular shock absorber between ABD1 and the C-terminal beta-dystroglycan binding domains (11). As isolated fragments, ABD1 and ABD2 bind

to actin filaments with low affinity but together in the full-length protein they confer sub-micromolar affinity for actin filaments (51, 52).

The thermal stability of the rod domain of dystrophin has been widely examined by multiple laboratories using small rod domain recombinant proteins (42, 53-57). Although spectrin-like repeats found in dystrophin have a similar predicted fold, the stability of individual repeats varies widely (57). Moreover, certain repeats are unstable without the presence of a neighboring repeat suggesting that neighboring repeat structure positively influences the structure of more unstable repeats (42, 54, 57). The thermal stability of two larger fragments of dystrophin containing SLRs 11-17 and 8-15 have been characterized and demonstrate that individual repeats with varying stabilities cooperatively unfold with a single transition when expressed in conjunction with neighboring repeats (47, 54). However, no study has examined the stability of the full-length dystrophin, or internally-deleted proteins containing its globular N- and C-terminal domains connected via non-native junctions.

Actin Isoforms in Muscle

Dystrophin is a critical actin binding protein and actin filaments play a multitude of key roles in all cells. Actin forms many important structures in the cell such as stress fibers and the cortical actin network, which are responsible for maintaining cell shape and membrane integrity. Actin is also required for cell locomotion and cell division where interactions with the molecular motor protein myosin can illicit dynamic changes in cell shape. Actin is a 43 kDa protein capable of reversibly polymerizing into filaments. Monomeric actin (G-actin) can polymerize into filamentous actin (F-actin) under ionic conditions and in the presence of a divalent cation such as those found within the cell (58). Actin polymerizes into a helical bundle that repeats approximately every 28 monomers (59) and is referred to as a thin filament in muscle and a microfilament in all other cell types. Polymerization of actin filaments occurs at different rates at each end due to the polarity of actin filaments (60). The polarity can be readily observed by decoration of actin filaments with a proteolytic fragment of myosin called S1 (61). S1 binds F-actin with a directionality that forms a barbed end and a pointed end when viewed in images from electron microscopy (61). Actin monomers preferentially add to the barbed end and dissociate from the pointed end (60).

Actins are a six member gene family, and each gene is referred to as a different actin isoform (62). β_{cyto} and γ_{cyto} are two cytoplasmic actins found in all

cell types while $\alpha_{skeletal}$-actin, $\alpha_{cardiac}$-actin, α_{smooth}-actin, and γ_{smooth}-actin are expressed in skeletal, cardiac or smooth muscle cells, respectively. All actin isoforms are remarkably conserved from birds to mammals (63). The cytoplasmic actins differ by only 4 biochemically conserved resides and all actin isoforms share at least 93% identity (64).

In skeletal muscle, $\alpha_{skeletal}$-actin is the predominant isoform and it comprises the thin filament in the contractile apparatus. In addition, β_{cyto} and γ_{cyto}-actin are expressed in muscle, albeit with a distinct localization from that of $\alpha_{skeletal}$-actin and at significantly lower levels (10, 65-67). γ_{cyto}-actin is specifically expressed at the cortical actin cytoskeleton and associates with dystrophin at the DGC (10). Genetic ablation of γ_{cyto}-actin in muscle results in a progressive myopathy (66). β_{cyto}-actin is also expressed in muscle with a similar localization pattern as γ_{cyto}-actin. Conditional knock out of β_{cyto}-actin in skeletal muscle results in a quadriceps myopathy and a decrease in dystrophin protein levels (65). Importantly, in each case where an actin isoform is ablated from muscle the total level of actin remains unchanged. Therefore, a specific attribute of the missing actin isofom is necessary to maintain normal muscle function. These genetic studies demonstrate that cytoplasmic actins play an important role in muscle biology but the mechanism by which their absence leads to disease remains unknown. We hypothesized that there is a biochemical interaction

between dystrophin and cytoplasmic actins that is not rescued by expression of other actin isoforms.

Early studies showed that recombinant fragments of dystrophin bound β_{cyto}-actin with increased affinity compared to $\alpha_{skeletal}$-actin. Moreover, recombinant fragments of dystrophin have showed differing results when compared to the full-length protein. Experiments determining the affinity of full-length dystrophin for actin isoforms expressed in muscle would shed more light on the previously reported difference using recombinant fragments and possibly account of the pathological conditions observed when cytoplasmic actins are ablated from skeletal muscle.

Disease Causing Missense Mutations in the Dystrophin Gene:

72% of dystrophinopathies are caused by large deletions of the dystrophin gene that result in loss of protein production (2, 68-70). Another 5 to 10% of cases are caused by insertions in the dystrophin gene that result in an aberrant reading frame ultimately causing the introduction of a premature stop codon (2, 68-70). Roughly 20-25% of cases are caused by point mutations that produce a premature stop codon, a non-functional splice site or an amino acid change (2). Small deletions or splice site mutations typically lead to the introduction of a premature stop codon and cause DMD. BMD is typically caused when the reading frame is retained after exonic exclusion from a splice site mutation or small in frame deletions. BMD patients typically display dystrophin products that are smaller than normal and at a reduced level (71). Missense mutations that result in a single amino acid substitution out of 3686 typically produce lower levels of full-length protein for reasons that are not clear (66-69).

The severity of disease caused by dystrophin missense mutations is heterogeneous with symptoms ranging from mild muscle weakness to DMD (72). Single amino acid changes such as the L54R mutation result in DMD (73), whereas other mutations such as K18N and F3228L result in X-linked cardiomyopathy (74). Overall, the majority of missense mutations result in a diagnosis of the milder BMD (72, 75).

Early genetic studies discovered and mapped the location of disease causing missense mutations in the dystrophin gene and found that many were localized to essential ligand binding domains (72, 76, 77). For example, two mutations, R82P and L172H, are localized to highly conserved regions of the N-terminal ABD, suggesting that these mutations would disrupt the dystrophin:actin interaction (71) (Figure 1-2 B). In addition, reduced dystrophin protein levels were observed for each of these mutations (71). The location of the mutations in the crystal structure of ABD1 suggested that known disease-causing mutations would lead to destabilization of ABD1 folding due to replacement of amino acids found in the hydrophobic core of ABD1 with large polar amino acids (78). However, it remained unclear what affect these changes would have on the full-length protein since ABD1 composes of only 256 amino acids of the full-length 3686 amino acid protein. In contrast, another mutation (D3335H) found in the beta-dystroglycan binding domain, caused severe disease but protein levels and membrane association of DGC proteins were normal (76). Thus, the mechanism underlying disease associated with missense mutations was unresolved and was hypothesized to involve disruption of ligand binding, reduced protein levels or a combination of both. Clearly, like other dystrophinopathies, missense mutations can lead to complex phenotypes with multiple mechanisms of action. Therefore, more diagnostic and biochemical studies are needed to better understand the pathogenesis of disease causing missense mutations in the dystrophin gene.

Therapies for DMD and Dystrophin Related Disease

Currently there is no effective cure for DMD or BMD. However, many therapies are currently under investigation in clinical trials or in animal models of disease (79, 80) including: gene therapy approaches, protein replacement therapy, stop codon read through compounds, and exon skipping molecules, (79, 80).

From the beginning it was thought that reintroduction of dystrophin through any of the above treatments would result in non-self antigen recognition, since DMD patients typically have never been exposed to dystrophin protein. In an attempt to mitigate an immune response, utrophin, an autosomal homolog of dystrophin, was used as a surrogate for dystrophin in gene therapy and protein replacement studies.

Utrophin is another member of the spectrin super family of proteins and is most closely related to dystrophin (33, 40, 81). Dystrophin and utrophin share a remarkably similar domain structure but the spatio-temporal expression of utrophin is distinct from that of dystrophin (33, 40, 81). Utrophin, like dystrophin, has a N-terminal tandem CH domain and a C-terminal globular domain that interacts with beta-dystroglycan (40, 82). However, utrophin lacks ABD2 found in dystrophin but instead has a series of spectrin-like repeats located adjacent to the tandem CH domain that increase the overall affinity for actin filaments (46, 50). Perinatally, utrophin is expressed throughout muscle fibers, and as development progresses to adulthood the expression of utrophin becomes

restricted to the myotendinous and neuromuscular junctions (81). At these sites, utrophin is associated with the same cast of proteins that associate with dystrophin in the DGC forming the UGC or utrophin glycoprotein complex (81-83). Importantly, utrophin is expressed in DMD patients but with a similarly restricted localization as healthy individuals. Both dystrophin and utrophin are thought to function interchangeably in muscle due to their shared ligand binding partners (83). Consistent with this hypothesis, overexpression of utrophin in dystrophin deficient or *mdx* mice fully rescues all known parameters of disease (84-86).

Gene therapy for DMD has been extremely successful in large animal models of disease but was unsuccessful in a clinical trial due to immune responses in DMD patients (79, 87). Current approaches use adeno-associated virus (AAV) carrying an internally deleted dystrophin or utrophin to deliver expression to muscle cells (80). The capacity of the AAV capsid requires the miniaturization of the dystrophin and utrophin cDNA. Therefore, a portion of the middle rod domain and the far C-terminal region that does not participate in β-dystroglycan binding of dystrophin or utrophin were deleted. It appears that, under higher than native dystrophin expression levels, miniaturized dystrophin and utrophin gene therapy constructs are effective at restoring muscle membrane integrity in *mdx* mice and larger animal models (79). Given the promise of this therapy coupled with the negative immune response seen in patients (87), additional studies were necessary to move this type of treatment forward.

Protein replacement therapy has also been employed to rescue the dystrophic phenotype of the mdx mouse (88). Due to expression limitations and possible immune responses to injected protein, utrophin and an internally deleted utrophin protein were used instead of dystrophin. In order gain entry to muscle cells, a protein transduction domain derived from the human immune deficiency virus TAT protein was added to the N-terminus. Injected micro-utrophin protein was observed in muscle cells associated with the DGC, and mdx mice showed significant histological and functional muscle improvement (88). Further studies in larger animals will be necessary to determine if the injected protein elicits an immune response.

Stop codon read through compounds target mutations that introduce nonsense mutations, which would result in DMD (89). About 10-15% of DMD patients could be treated with this approach, but recent clinical trial data suggest that the technology needs further development (80).

Exon skipping has shown a great deal of promise in large animal models and patient trials (80). In a clinical trial with DMD patients that would benefit from exon 51 skipping, nascent dystrophin expression was seen in 64-97% of muscle fibers (90). However, skipping exons with non-sense mutations would lead to an internally deleted dystrophin protein and may not completely cure DMD but, instead, result in clinical symptoms more similar to those of BMD.

Exon skipping, gene therapy and protein replacement rely on internally deleted dystrophin or utrophin and would result in or contain non-native junctions

between spectrin like repeats in dystrophin or utrophin. Although much work has been done to investigate the phenotypic improvement of treated animals no one understands the biochemical and biophysical consequences of creating non-native protein junctions at the protein level. In order to establish the most robust therapy, the stability and half-life of proteins containing internal deletions should be determined before clinical trials are initiated.

Questions Addressed in This Thesis

A remarkable amount of work has revealed a more detailed picture on the structure, biochemical properties and actin binding activity of dystrophin (10, 13, 47, 50-52, 82, 91, 92). However, key questions remain to be answered.

Does dystrophin have differing affinities for the actin isoforms expressed in muscle?

Early studies with ABD1 demonstrated that dystrophin and utrophin had increased affinities for β_{cyto}-actin compared to $\alpha_{skeletal}$-actin (13, 82). We know that dystrophin predominantly associates with γ_{cyto}-actin at costameres and that dystrophin has a similar affinity for γ_{cyto}-actin and $\alpha_{skeletal}$-actin (10, 93). The finding from our lab that muscle specific knockout of β_{cyto}-actin leads to reduced dystrophin protein levels (65) prompted us to examine the affinity of the full-length dystrophin protein for each of the actin isoforms expressed in muscle. To that end, we performed actin cosedimentation assays with full-length dystrophin and each actin isoform in parallel (Chapter 2).

Does the C-terminal half of the dystrophin protein influence actin binding?

A number of studies from our laboratory have delineated the specific regions of the dystrophin protein that interact with actin (47, 51). Interestingly, it was noted that a fragment of dystrophin that contained both ABDs but lacked the remaining C-terminal region had a lower affinity and stoichiometry compared to the full-length protein (51). To better understand the specific actin binding

contribution of the C-terminal third of the dystrophin protein I designed and performed a series of experiments to better understand the scope of the dystrophin actin interaction (Chapter 2). The assays I established to analyze dystrophin fragments later helped to examine disease-causing mutations in ABD1.

How do single amino acid changes in ABD1 cause disease?

We hypothesized that mutations in ABD1 would lead to a decrease in actin affinity and cause disease through loss of this interaction. However, evidence from structural analysis of ABD1 hinted that disease causing mutations may lead to domain destabilization. ABD1 composes a small fraction of the large dystrophin protein and it seemed unlikely that a structural disruption in this domain would have global effects on the full-length protein. In order to understand how these single amino acid changes in a very large protein lead to disease, I engineered 9 mutations into ABD1 and examined their biophysical and actin binding properties (Chapter 3).

What are the biochemical and biophysical consequences of creating non-native SLR junctions in dystrophin and utrophin?

Therapies to cure DMD are increasingly reliant on the functionality of non-native junctions between SLRs. Gene therapy, protein replacement therapy, and exon skipping all create non-native SLRs and no studies have examined the stability or protein half-life of the unnatural proteins produced for these therapies. To investigate the stability of internally deleted dystrophin and utrophin proteins

created for therapy we performed a detailed biophysical analysis of these proteins and compared them to the native proteins as well as a series of N- and C-terminal fragments (Chapter 4).

Figures

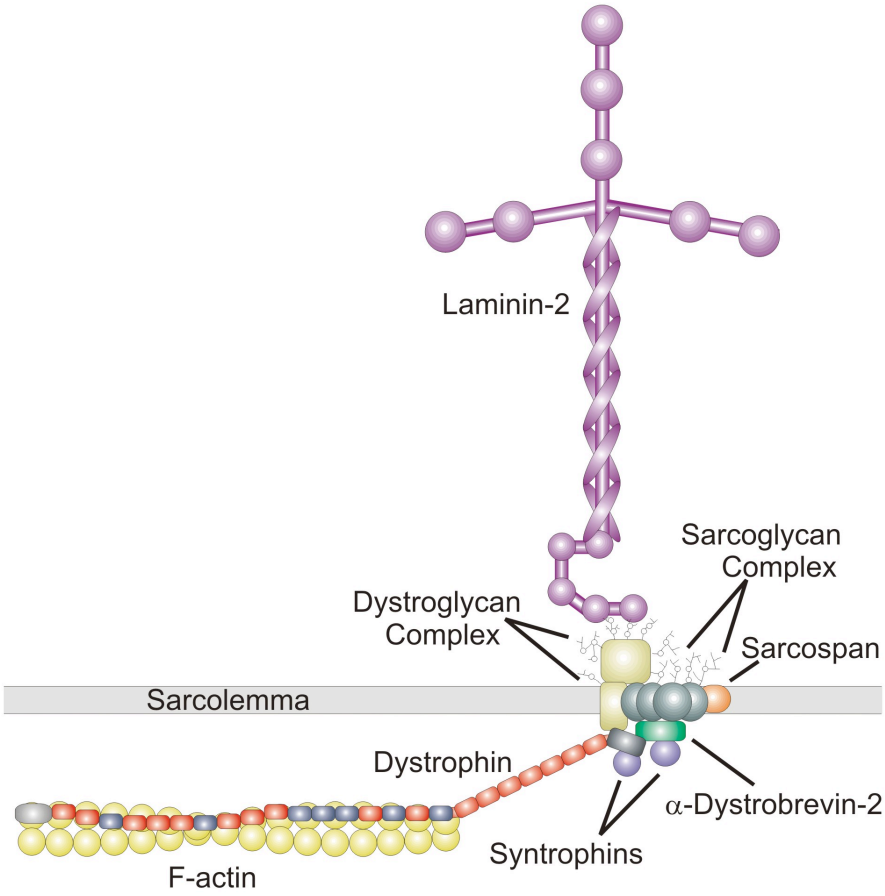

Figure 1-1: **The dystrophin glycoprotein complex.** Dystrophin interacts with the F-actin cytoskeleton and the transmembrane heterodimer dystroglycan. Dystroglycan forms a strong interaction with the extracellular matrix protein laminin-2.

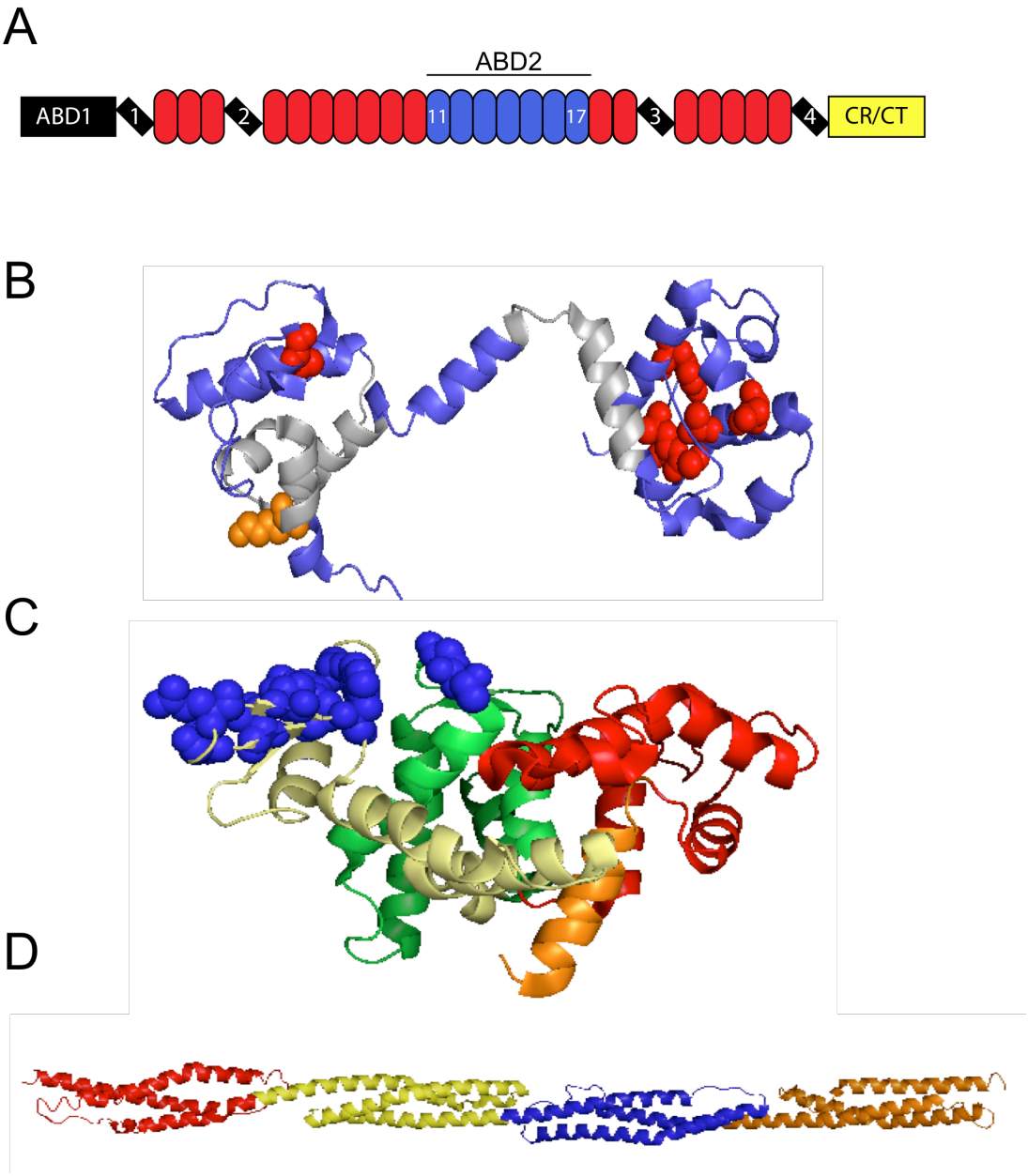

Figure 1-2: **Domain cartoon and structural representations of ABD1, the dystrophin dystroglycan binding domain and spectrin-like repeats (36, 78).** (A) Diagram of dystrophin domains including ABD1, ABD2, hinges (diagonal black rectangles) and SLRs (colored ovals, blue for SLRS in ABD2 and red for all others). (B) Ribbon diagram of ABD1 showing CH1 (left) and CH2 (right) in blue.

Actin binding sites are colored grey. Disease causing mutation locations are marked in red for buried amino acids and orange for surface amino acids. (C) Ribbon diagram of the C-terminal dystroglycan interacting portion of dystrophin containing part of the WW domain (yellow), EF hand domain 1 (green), and EF hand domain 2 (red). Residues that contact the cytoplasmic tail of dystroglycan are shown as spheres and are blue. Remaining region is colored orange. (D) Ribbon structure of 4 SLRs from alpha-actinin

Chapter 2: The Carboxy-Terminal Third of Dystrophin Enhances Actin Binding Activity

Davin Henderson expressed and purified all proteins and performed all experiments except for the following. Bin Li purified proteins used in Figure 6. Ava Yun Lin performed experiments in Figure 6. All constructs were generated in previously published work from our laboratory (94).

Chapter Summary

Dystrophin is an actin binding protein thought to stabilize cardiac and skeletal muscle cell membranes during contraction. Here, we investigated the specificity of dystrophin binding to different actin isoforms and delineated the contributions of each dystrophin domain to actin binding function. Contrary to previous studies of isolated actin binding domains (ABD) 1, actin cosedimentation assays with full-length dystrophin demonstrated no preferential binding to filaments comprised of three different actin isoforms. Cosedimentation assays and pyrene-actin fluorescence experiments confirmed that a fragment spanning two-thirds of the dystrophin molecule (from N-terminal ABD1 through ABD2) bound actin filaments with high affinity and protected filaments from forced depolymerization, but was less effective in both assays compared to full-length dystrophin. While a construct encoding the C-terminal third of dystrophin displayed no actin binding activity or competition with full-length dystrophin, our data show that it confers an unexpected regulation of actin binding by the N-terminal two-thirds of dystrophin when present in cis. Time-resolved anisotropy experiments demonstrated that the presence of the C-terminal third of dystrophin in cis also influences actin interaction in terms of restricting actin's rotational amplitude. We propose that the more thermally stable C-terminal region of dystrophin allosterically stabilizes an optimal actin binding conformation or orientation of dystrophin.

Introduction

Dystrophin is an essential component of the dystrophin-glycoprotein complex (DGC) that functions to protect the muscle cell membrane from contraction-induced injury (9). The DGC is localized to a lattice-like structure in muscle called the costamere that is thought to transmit force radially from the z-disc to neighboring muscle fibers (25-28). Dystrophin is a multidomain protein with two globular domains at its N- and C-termini that are connected by a large rod domain consisting of 24 spectrin-like repeats with 4 interspersed hinge regions (32, 38). The C-terminal domain of dystrophin encodes a WW domain, a ZZ domain and two EF hand domains that interact with the cytoplasmic tail of β-dystroglycan (35, 37, 95-97). Dystrophin interacts with actin filaments at two sites; ABD1 at its N-terminus composed of a tandem calponin homology domain (12, 98) and ABD2 within spectrin-like repeats 11-17, which interacts with actin filaments via electrostatic attraction (47). Through the concerted action of these two distinct binding interactions, dystrophin is thought to physically anchor the sarcolemma to the costameric actin cytoskeleton thereby stabilizing the membrane against mechanical damage during muscle use. Recent biophysical characterization of the dystrophin-actin interaction showed that binding of full length dystrophin restricts actin microsecond rotational amplitude but increases the rate (99). This paradoxical combination is novel to dystrophin and utrophin (99), and is hypothesized to effect a strong but resilient dystrophin-actin interaction to prevent contraction-induced damage.

Multiple actin isoforms are expressed in skeletal muscle cells including α_{sk}-actin, which forms the thin filaments of the contractile apparatus, and β_{cyto}- and γ_{cyto}-actin (10, 65, 100, 101). All three actin isoforms are required for normal muscle function (65, 66, 102), and γ_{cyto}-actin in particular is thought to be important for mediating interactions between dystrophin and the cortical actin cytoskeleton (10). However, efforts to biochemically characterize dystrophin's interaction with different actin isoforms have been limited and produced disparate results (13, 82, 103, 104). Early studies focused on the isolated ABD1 and reported K_d values ranging from 15 to 40 μM (13, 82). Our laboratory later identified ABD2 in the central rod region, which also bound actin with a low affinity similar to ABD1 (47, 50). In contrast, studies with purified DGC and recombinantly-expressed full-length dystrophin protein established its affinity for actin filaments in the sub-micromolar range (51), but did not address whether full-length dystrophin bound preferentially to different actin isoforms.

Here, we have performed cosedimentation assays to directly measure the affinity of full-length dystrophin for actin filaments comprised of α_{sk}-, β_{cyto}-, or γ_{cyto}-actin. We find that dystrophin displays no quantitative preference for any of three different actin isoforms. We also systematically measured the specific contributions of each dystrophin domain on its actin binding function through actin cosedimentation, depolymerization, and time-resolved phosphorescence anisotropy (TPA) assays. Large fragments containing a single ABD tested

showed similar affinities for actin as isolated ABDs. Most interestingly, while the C-terminal third of dystrophin displayed no measurable affinity for actin, or competition with full-length dystrophin binding to actin, our data suggest a regulatory function for the C-terminal domain in the stabilization of a dystrophin conformation that binds actin with maximal affinity.

Results

Actin isoform specificity: To more completely understand dystrophin's interaction with different actin-based structures of skeletal muscle, we first quantitatively assessed whether dystrophin exhibits different affinities for the three actin isoforms expressed in adult muscle. We performed a high-speed cosedimentation assay where a fixed concentration of actin (6 mM) was incubated with increasing concentrations of full-length dystrophin (52), which eliminates effects caused by differences in the critical concentration for different actin isoforms. Consistent with our previous studies (14, 51), we found that full-length dystrophin bound α_{sk}-actin filaments with a K_d of 0.30 +/- 0.099 μM and with a B_{max} of 0.065+/- 0.0024 (Figure 2-2A). Dystrophin bound β_{cyto}-actin filaments with a K_d of 0.41 μM +/- 0.17 and a B_{max} of 0.064 +/- 0.0013 (Figure 2-2B) and to γ_{cyto} -actin with a K_d of 0.33 μM +/- 0.22 and a B_{max} of 0.051 +/- 0.0011 (Figure 2-2C). From this direct comparison of dystrophin binding to α_{sk}-, β_{cyto}- and γ_{cyto} actin filaments, we conclude that dystrophin binds to all three actin isoforms with similar affinities.

Dystrophin domain contributions: Several previous studies from our laboratory reported the affinities of the dystrophin N-terminal ABD1 (93), middle rod ABD2 (50), ABD1 plus spectrin repeats 1-10 (51), or both ABD1 and ABD2 linked by spectrin repeats 1-10 (51). Here we directly compared the affinities of two previously studied constructs (DysN-R10, Dys N-R17) as well as ABD2 in context

of the DP260 isoform of dystrophin to determine whether the small, unique N-terminus of DP260, or the presumed actin non-binding C-terminal third of dystrophin influences actin binding affinity (Figure 2-1). We also measured the actin binding affinity of a therapeutically relevant miniaturized dystrophin protein (94) retaining ABD1 and the C-terminus but lacking ABD2 (DysΔH2-R19). For all constructs, we varied the concentration of actin in our cosedimentation assay and fixed the concentration of the dystrophin fragment at 0.5 μM. Varying the actin concentration is advantageous because any self-pelleting protein can be easily subtracted from the protein cosedimenting with actin filaments (105). Full-length dystrophin, DysN-R17, and DysN-R10 each bound actin filaments with affinities (Figure 2-3A-C) similar to those previously published (82, 103). DP260 bound actin filaments with a K_d of 6.85 μM +/- 4.62 (Figure 2-3D), which is in good agreement with the previously published value (7.3 μM) for isolated ABD2 (50). These results suggest that neither the unique N-terminus of DP260 nor the C-terminal region influences actin-binding affinity of ABD2. DysΔH2-R19 bound with a K_d of 3.53 μM +/- 1.73 (Figure 2-3E), which is consistent with other fragments containing only ABD1. These data confirm the two ABD model for dystrophin binding to actin (47, 51).

The DysN-R17 construct, which contains both ABDs, was previously shown to bind with a Kd of 0.76 μM when DysN-R17 concentration was varied around a fixed actin concentration (51). Here, we measured a K_d of 0.6 μM +/- 0.24 when varying the actin concentration with a fixed DysN-R17 concentration

(Figure 2-3B), while full-length dystrophin bound F-actin with a K_d of of 0.11 μM +/- .0082 (Figure 2-3A). Binding analyses of DysN-R17 and full-length dystrophin reported similar B_{max} values of 0.66 +/- 0.0087 mol/mol and 0.065 +/- 0.006 mol/mol respectively (Figure 2-3A and B). While the similar stoichiometries suggest that DysN-R17 encodes the full actin binding domain of dystrophin and spans similar lengths of actin filaments, the lower affinity of DysN-R17 in comparison with full-length dystrophin suggests that the C-terminal third of dystrophin may play a role in actin binding. However, an isolated C-terminal fragment encoding spectrin repeat 18 though the C-terminus of dystrophin (DysR18-CT), showed no measurable binding to actin filaments up to a concentration of 25 μM actin (Figure 2-3F).

To further address whether DysN-R17 binds actin filaments with lower affinity than full-length dystrophin, we measured the ability of each protein to protect actin filaments from forced depolymerization (51). Consistent with previous studies (14, 52), none of the large dystrophin fragments containing only ABD1 or ABD2 (DP260, DysN-R10, and DysΔH2-R19) was able to protect actin filaments from forced depolymerization, confirming that both ABD1 and ABD2 must be present in cis to afford protection (Figure 2-4A-C). DysN-R17 significantly protected actin filaments from depolymerization, albeit with reduced capacity compared to the full-length protein (Figure 2-4D).

Effect of the C-terminal region of dystrophin on actin binding: Although Dys-R18-CT exhibited no measureable actin-binding activity (Figure 2-3F) DysN-R17

exhibited a 5 fold lower affinity compared to full length dystrophin. Therefore, we hypothesized that the actin non-binding C-terminal third of dystrophin may facilitate a cooperative interaction between adjacent dystrophin molecules docked on an actin filament analogous to the cooperative model of actin binding in tropomyosin (106). To test if DysR18-CT may participate in actin binding through a head to tail association with a second dystrophin molecule, we assayed the ability of Dys-R18-CT to inhibit the binding of full-length dystrophin to actin filaments. However, increasing concentrations of DysR18-CT had no measureable effect on dystrophin's affinity for actin, as measured in both the high-speed cosedimentation (Figure 2-5A and B) and forced depolymerization assays (Figure 2-5C and D).

We recently demonstrated that dystrophin binding increases the torsional flexibility of actin filaments (99). To test possible effects of the dystrophin C-terminal region on actin torsional flexibility, we performed TPA to compare the effects of dystrophin constructs with and without the C-terminal region on actin dynamics. TPA was performed with erythrosine-iodoacetamide (ErIA) on Cys-374 of each actin protomer, and the degree of filament anisotropy (orientational order) was measured as a function of time after excitation with a pulsed laser. From the calculated anisotropy decays, the amplitudes and rates corresponding to filament bending and twisting motions of actin (Figure 2-6A) were calculated (107). Our previous TPA studies (99) showed a cooperative restriction of actin rotational amplitude and an increase in rotational rate when full length dystrophin was

bound (Figure 2-6B and C, red). In contrast, DysN-R17 lost functional cooperativity, as its titration caused a linear decrease in the angular amplitude of actin rotational motion (Figure 2-6B, blue). Loss of the C-terminal region from DysN-R17 also ablated the effect on rate observed with full-length dystrophin (Figure 2-6C, blue). These results suggest that the decreased protection of DysN-R17 on actin depolymerization was also the result of an altered mode of interaction between the ABDs and actin.

Despite its lower affinity and lack of protection in depolymerization assays, DP260 showed a dramatic rescue of the cooperative effect in restricting actin rotational amplitude in TPA (Figure 2-6B, green). However, DP260 failed to increase actin rotational rate (Figure 2-6C, green). These results suggest that the C-terminal region allosterically influences ABD2 to restrict actin's rotational amplitude, but both ABDs and the C-terminal region appear to be necessary to influence rotational rate. Despite the high sensitivity of the TPA assay to detect changes in actin dynamics, a large range of Dys-R18-CT (0.3uM to 13.5um) to ErIA-actin (1μM) concentrations had no significant effect on actin rotational motion (Figure 2-6D and E). The effect on actin rotational amplitude (Fig. 6D) or rate (Figure 2-6E) was minimal and mostly within range of ErIA-actin alone. The occasional outlier showed at most a 15% change in actin rotational amplitude and a 6% change in rate, which are quite minimal compared to the average 26% and 80% changes, respectively, observed when dystrophin was bound to actin (red dotted lines in Figure 2-6D and E). The TPA results are congruent with both

the co-sedimentation and actin-depolymerization data. We conclude that the C-terminal third of dystrophin neither directly participates in actin binding nor enhances binding through a head-to-tail interaction with neighboring dystrophin molecules (analogous to the tropomyosin model), but its presence in cis with ABD1 and ABD2 enhances the ability of dystrophin to bind and regulate actin filament dynamics.

Discussion

Early studies on the isolated ABD1 of dystrophin and the dystrophin-related protein, utrophin, reported that these fragments exhibit a four-fold greater affinity for filaments comprised of β_{cyto}-actin compared to α_{sk}-actin (82). However, these conclusions were based on experiments performed by different laboratories. Experiments from our laboratory showed that the isolated ABD1 of dystrophin exhibited no difference in affinity for γ_{cyto}-actin versus α_{sk}-actin, while our measured affinities were very similar to those reported by Winder et al (82) for ABD1 binding to β_{cyto}-actin. Here we directly compared the binding of full-length dystrophin for filaments comprised of α_{sk}-, β_{cyto}- or γ_{cyto}- actin. We conclude that full-length dystrophin exhibits no preference for binding to filaments comprised of different actin isoforms.

It is well established by multiple studies that dystrophin binds actin filaments with sub-micromolar affinity through the concerted action of ABD1 and ABD2 (47, 50, 51). While previous studies have measured the actin binding properties of ABD1 and ABD2 in isolation and reported ~10-fold lower affinities than measured for full-length dystrophin, ours is the first to directly compare the properties of ABD1, ABD2 and the C-terminal third of dystrophin with full-length protein. We found that large constructs containing only one ABD (DP260, DysN-R10 and DysΔH2-R19) exhibited actin binding affinities that matched well with those previously reported for isolated ABD1 and ABD2, and none of these single

ABD-containing fragments were able to protect actin filaments against forced depolymerization. Ablation of one ABD also weakened the effect of dystrophin on actin filament dynamics. Loss of either the N-terminal region in DP260 or the C-terminal region in DysN-R17 eliminated their effect on actin rotational rate, although their restriction of rotational amplitude was preserved at higher titrations.

While DysN-R17, containing both ABD1 and ABD2, bound actin filaments with similar stoichiometry as full-length dystrophin and significantly protected filaments from depolymerization, it bound with lower affinity than full-length dystrophin. This suggests a role for the C-terminal region of dystrophin in increasing actin affinity. On the other hand, the isolated C-terminal region (Dys-R18-CT) exhibited no measureable actin-binding activity in both cosedimentation (Figure 2-3F) and forced polymerization assays (Figure 2-5C).

We hypothesize that the dystrophin C-terminal region must be in cis with both ABDs to allosterically influence their binding to actin. The coiled-coil domains of tropomyosin demonstrate end-to-end interactions between adjacent molecules, which contributes to cooperative actin binding (106). However, we measured no actin-binding activity in Dys-R18-CT, and competition experiments showed it had no effect on full-length dystrophin binding to actin. Nevertheless, our TPA experiments demonstrated a cooperative effect on the ability of the dystrophin ABDs to restrict actin rotational amplitude only when the C-terminal region was present in the construct (Figure 2-6B). Thus cooperativity must arise

from an allosteric effect of the C-terminal region on ABDs 1 and 2, and not through a conformational change in actin. Recently, we demonstrated that the isolated C-terminal region (Dys-R18-CT) exhibits markedly greater thermal stability compared to N-terminal constructs (Dys-N-R17) or even full-length dystrophin (94). Since the N- and C-terminal regions of dystrophin have drastically different thermal stabilities (50˚C and 70 ˚C respectively), one would expect to observe two melting transitions but instead only a single transition exactly halfway in between each is observed (60˚C). We propose that when present in cis, the highly stable C-terminal third of dystrophin allosterically influences the N-terminal region of the protein to effect increased thermal stability and orient or stabilize a conformation required for optimal actin binding (Figure 2-7).

Experimental Procedures

Cloning, protein expression and purification: All constructs used to express protein in this manuscript were previously generated for other studies (94). Each cDNA was N-terminally Flag tagged using PCR and cloned into either pFastbac1 or pFastbac duel downstream of the polyhedrin promoter. Once in pFastbac, bacmids were generated using the Bac-to-bac system from Invitrogen. High titer virus was used to infect Sf21 insect cells at a density of between 1.0 and 1.5 $x10^6$ cells/ml with a volume of 250 milliliters. Proteins were purified by Flag affinity chromatography and dialyzed against two changes of phosphate buffered saline pH 7.5 to remove excess flag peptide. Proteins were concentrated in Millipore Amicon Ultra centrifuge-based concentrators with cutoffs of either 100 kDa or 10 kDa depending on protein molecular weight.

Actin isoform preparation: α_{sk}-actin (Cat# AKL99) and platelet non-muscle actin (Cat# APHL99) were purchased from Cytoskeleton. γ_{cyto}-actin was expressed in the Bac-to-Bac insect cell expression system from Invitrogen. Mouse γ_{cyto}-actin cDNA was amplified by PCR and cloned into the p10 promoter of pFastbac Dual by restriction digest. No affinity tags were added. γ_{cyto}-actin was purified by lysing 3 grams of insect cell paste in G-buffer (10 mM Tris pH 8.0, 0.2 mM $CaCl_2$ and 0.2 mM ATP) by sonication. Actin was purified using DNAseI and ion exchange chromatography similar to Renley et al 1998 (93). Briefly, the lysate was clarified by centrifugation for 20 minutes at 14,000 *x g* and passed over a DNase column.

The DNAse column was prepared from 400 g DNAseI (Roche Cat# 10104159001 100) and 25 ml affigel 10 active ester agarose (BioRad Cat# 153-6099) following the BioRad coupling instructions and equilibrated with G-buffer with protease inhibitors (PI) as in (93). The Column was washed with 50 ml of G-buffer with PI, 50 ml G-buffer with 1.0 M NaCl, then 50 ml G-buffer without PI. Actin was eluted from DNAseI with 50 ml 50% formamide in G-buffer onto a 1 ml DEAE sepharose (Sigma Cat# DFF100-50ML) column. The DEAE column was washed with 50 ml G-buffer then eluted with G-buffer containing 0.3 M KCl. Actin was dialyzed into 500 ml G-buffer overnight, concentrated to approximately 1 mg/ml and polymerized with 10x polymerization buffer (500 mM KCL, 20 mM $MgCl_2$ and 10 mM ATP). Polymerized actin was centrifuged at 100,000 *x g* for 1 hour. Pelleted actin was resuspended in 1x polymerization buffer and stored for experiments at 4 ˚C for up to a week.

Actin cosedimentation assays: Sedimentation assays where the concentration of dystrophin was varied were performed as previously described in Rybakova et al. (52). Briefly, actin concentration was fixed at 6 μM and dystrophin concentration was varied past saturation (approximately 2 μM for full length dystrophin). Each reaction was incubated at room temperature for thirty minutes and centrifuged at 100,000 x g for 30 minutes. Resulting supernatant and pellet fraction we subjected to SDS-PAGE and stained with Coomassie blue. Supernatant and pellet fractions were determined by densitometry with UVP analysis software. Sedimentation assays where the concentration of actin was varied instead of

dystrophin were performed identically to Henderson et al 2010 (105). The same experimental details as above were used except the concentration of actin was varied past saturation and the concentration of dystrophin or dystrophin fragment was fixed at 0.5 μM. Additionally, the fraction of dystrophin protein found to pellet without actin was quantitated by densitometry from Coomassie stained gels and the self-pelleting fraction was subtracted from subsequent reactions where actin was present.

Actin depolymerization assays: Depolymerization protection assays were performed with pyrene labeled actin from Cytoskeleton as previously described (105). In short, pyrene labeled actin at 2 μM was incubated with dystrophin or dystrophin fragments at ratios of 1:6, 1:12 or 1:24 (dystrophin:actin). Actin was forced to depolymerize by dilution below critical concentration with g-buffer (10 mM Tris pH 8.0 and 2 mM $CaCl_2$). Samples were immediately read on a Gemini (Molecular Devices) fluorescence plate reader and every minute for 30 minutes.

C-terminal competition experiments: Dystrophin actin-binding was performed as described above at a near Kd concentration of 0.75 μM actin and incubated with increasing concentrations of DysR18-CT (1:5, 1:10 and 1:15). Results were complied by analyzing the scanned Coomassie stained gel by densitometry and plotted as a bar graph. Student's t-test was used to determine significance. Actin depolymerization protection assays were performed as described above except that DysR18-CT was added at ratios of 1:10 and 1:20

(dystrophin:DysR18-CT) to a reaction containing full-length dystrophin at a ratio of 1 dystrophin per 12 actin monomers.

Time-resolved phosphorescence anisotropy: Actin preparation and labeling with phosphorescent erythrosine-iodoacetamide (ErIA) (Anaspec) was as described in (99). Phalloidin-stabilized ErIA-actin was diluted in U/D buffer (100 mM $NaCl_2$, 2 mM $MgCl_2$, 0.2 mM ATP, 1 mM DTT, 10 mM Tris pH 7.5) to 1uM. Increasing concentrations of dystrophin and fragments (Fig 1) were added to 1 μuM ErIA-actin. An oxygen removing system containing glucose oxidase (55ug/ml), catalase (36ug/ml), and glucose (45ug/ml) was added to the sample prior to each experiment to maximize the phosphorescence signal (108, 109). The phosphorescent dye was excited at 532nm with a vertically polarized 1.2 ns laser pulse from a FDSS 532-150 laser (CryLas) with a 100 Hz repetition rate. Emission was detected through a 670 nm glass cutoff filter (Corion) using a photomultiplier (R928; Hamamatus) and transient digitizer (CompuScope 14100; GaGe) with a resolution of 1 μs per channel. Time-resolved anisotropy is defined by

$$R(t) = \frac{I_v(t) - GI_h(t)}{I_v(t) + 2GI_h(t)} \qquad \textbf{Eq 1}$$

Where $I_v(t)$ and $I_h(t)$ is defined by the vertical and horizontal components of the detected phosphorescent emission, using a single detector at 90° and a rotating sheet polarizer alternating between the two orientations every 500 laser pulses. The instrument response function G was calibrated by detection of the signal with

horizontally polarized excitation pulse, and correcting so that the anisotropy is zero. All time-resolved anisotropy experiments were recorded with 30 cycles, with 500 pulses each in the horizontal and vertical planes.

The anisotropy decays were analyzed by fitting to the function:

$$r(t) = r_1 \exp(-t/\phi_1) + r_2 \exp(-t/\phi_2) + r_\infty \qquad \textbf{Eq 2}$$

Where rotational correlation times ϕ_1 (slow) and ϕ_2 (fast) and amplitudes r_1, r_2 and r_∞ were varied and using a least-squares minimization procedure (110). Results were validated by comparison of residuals and chi-squares of the fits at one, two and three exponential terms. Increase in final anisotropy r_∞ indicates a decrease in the amplitudes of microsecond rotational dynamics, which is attributed to a decrease in actin filament flexibility. A maximally flexible molecule (isotropic) would exhibit a final anisotropy value of 0. The slower motions (ϕ_1, r_1) represent mainly the actin filament bending, while the faster motions (ϕ_2, r_2) represent mainly the actin filament twisting. The combined rates of the filament twisting and bending motions were evaluated by ϕ_{Ave} which is calculated by a weighted average of ϕ_1 and ϕ_2. The overall angular amplitudes of the microsecond motions in actin were calculated using the wobble-in-a-cone model (107)

$$\theta_c(\mu s) = \cos^{-1}\left[-0.5 + 0.5(1 + 8\sqrt{r_\infty / r_0}\right] \qquad \textbf{Eq 3}$$

This reflects the combined amplitude of microsecond filament bending and twisting motions depicted in Fig 6A.

Rates of the corresponding angular amplitudes were calculated by:

$$rate(\mu s^{-1}) = {}^{1}\!/\!_{\phi_{Ave}} \qquad \textbf{Eq 4}$$

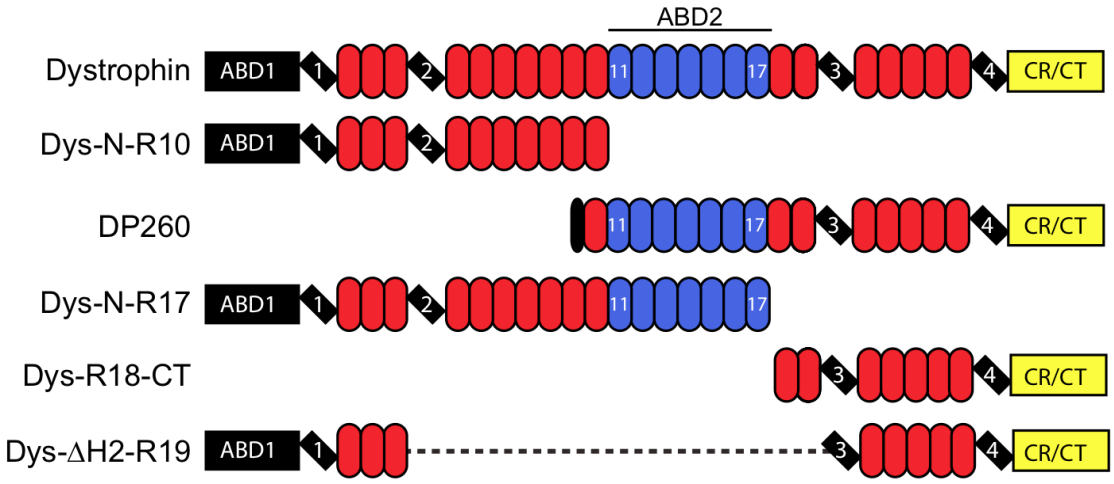

Figure 2-1: **Domain map of proteins assayed.** Globular N- and C-terminal domains are represented by rectangles. Hinge regions are marked by tilted rectangles. Spectrin-like repeats are represented by ovals and colored blue for actin binding repeats. Non-actin binding spectrin-like repeats are yellow.

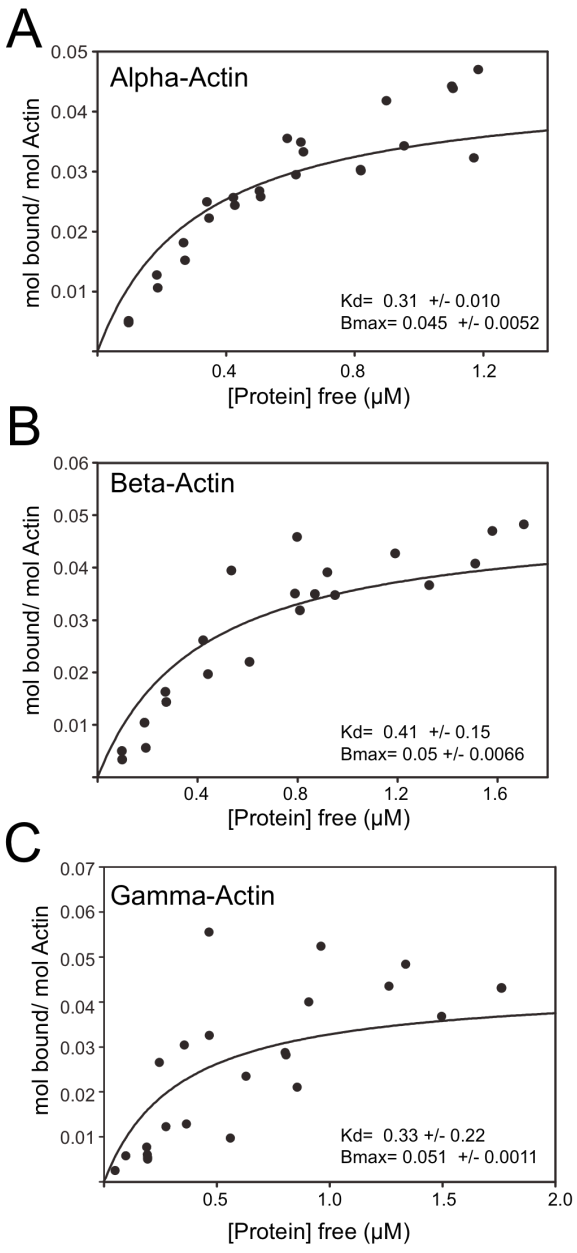

Figure 2-2: **Full-length dystrophin actin cosedimentation assays for actin isoforms.** Dystrophin protein is varied with a constant concentration of 6 μM α_{sk}-actin (A), β_{cyto}-actin (B) or γ_{cyto}-actin (C). The results from three independent

experiments are plotted on each graph. Binding isotherms were fit using regression analysis to determine K_d and B_{max} values (inset) from plotted data.

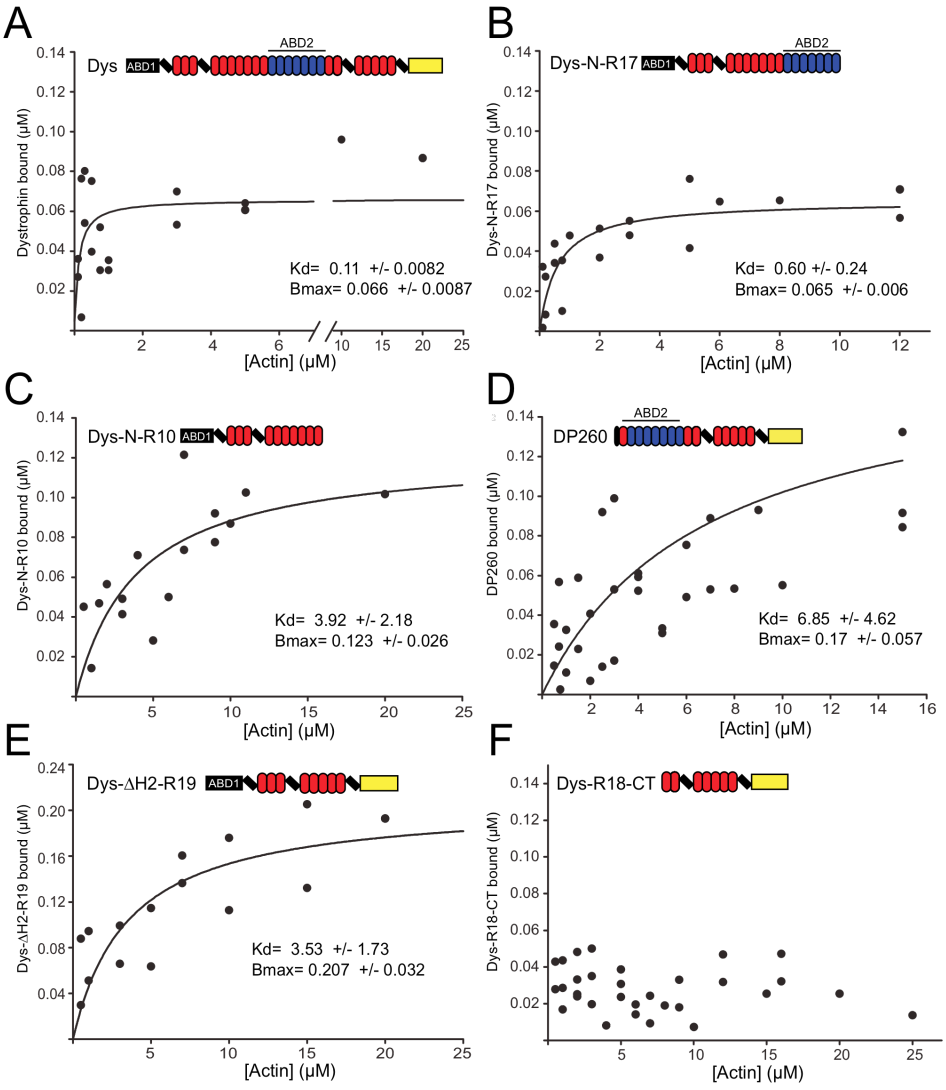

Figure 2-3: **Analysis of dystrophin actin binding domains.** Binding isotherms from actin cosedimentation assays with increasing actin concentration and a constant concentration of FL-Dystrophin (A), DysN-R17 (B), DysN-R10 (C), DP260 (D), DysΔH2-R19 (E) and DysR18-CT (F). Plots display the results from at least three independent experiments on each graph. Binding curves were fit

using regression analysis to determine K_d and B_{max} (inset). The color code for domain diagrams is the same as in figure 1.

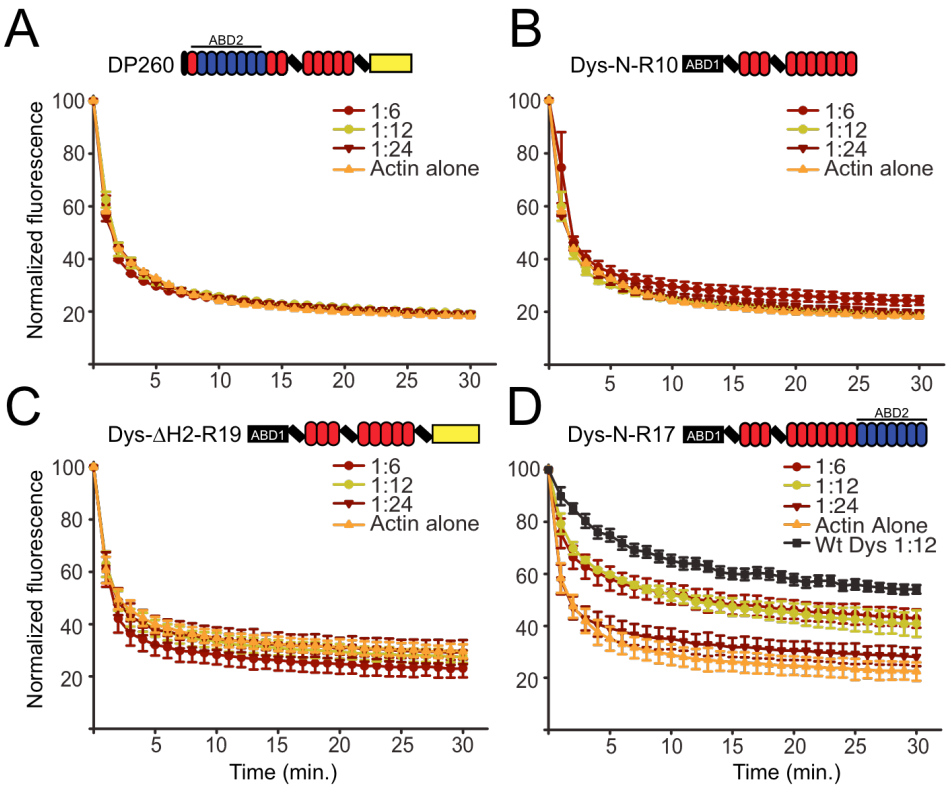

Figure 2-4: **Actin depolymerization protection analysis of dystrophin fragments.** Actin depolymerization was monitored by measuring the decay of pyrene actin fluorescence after dilution into low salt buffer below critical concentration. Actin was measured alone or in the presence of molar ratios of 1:6, 1:12, 1:24 (Dys:actin) DysN-R10 (A), DP260 (B), Dys-ΔH2-R19 (C) and DysN-R17 (D). (A-D) Error bars represent standard error of the mean (SEM). Black curve in (D) represents values from full-length dystrophin measured previously (105).

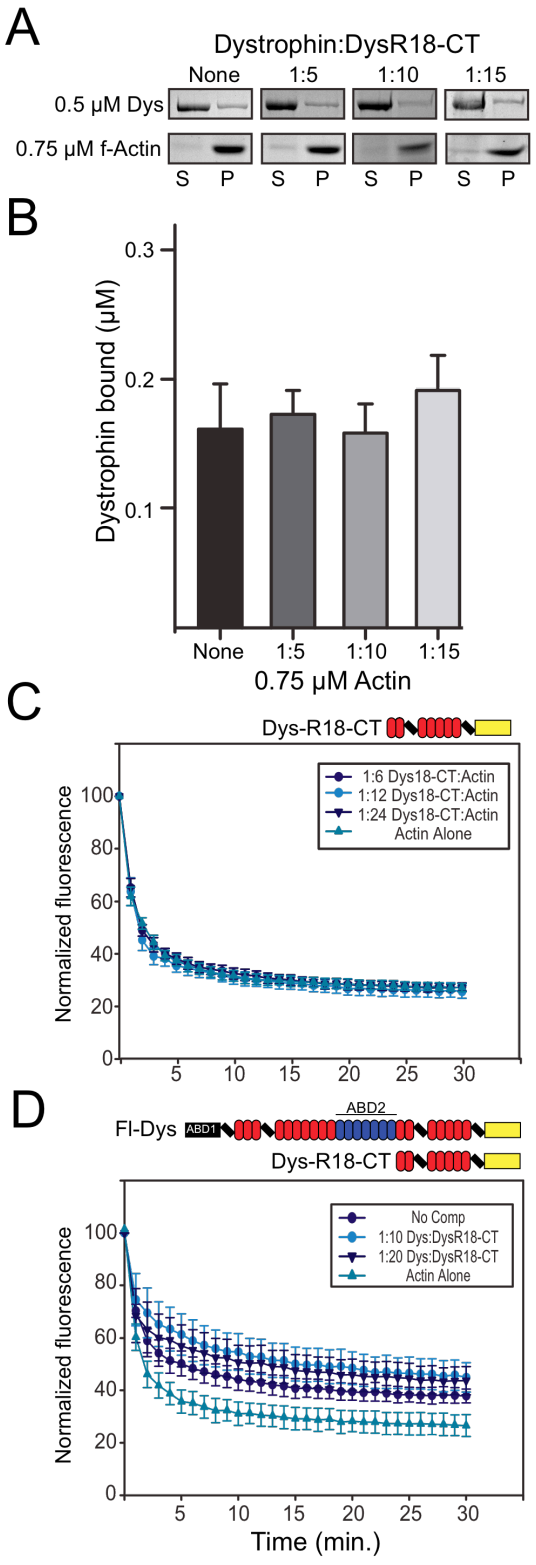
A
Dystrophin:DysR18-CT
None
1:5
1:10
1:15
0.5 μM Dys
0.75 μM f-Actin
S P S P S P S P
B
Dystrophin bound (μM)
0.3
0.2
0.1
None
1:5
1:10
1:15
0.75 μM Actin
C
Dys-R18-CT
1:6 Dys18-CT:Actin
1:12 Dys18-CT:Actin
1:24 Dys18-CT:Actin
Actin Alone
Normalized fluorescence
100
80
60
40
20
0
5
10
15
20
25
30
D
ABD2
Fl-Dys
ABD1
Dys-R18-CT
No Comp
1:10 Dys:DysR18-CT
1:20 Dys:DysR18-CT
Actin Alone
Normalized fluorescence
Time (min.)

Figure 2-5: **Dystrophin C-terminus competition.** (A) A single point dystrophin actin cosedimentation assay with a fixed concentration of actin of 0.75 μM and a concentration of 0.5 μM dystrophin. DysR18-CT was added at ratios of 1:5, 1:10, and 1:15 (Dystrophin:DysR18-CT) to compete for full-length dystrophin binding. Boxed images are coomassie stained polyacrylamide gels that display the amount of dystrophin and actin in the supernatant and pellet for each ratio of DysR18-CT added. (B) Bar graph depicting the quantitation of the cosedimentation assay in A. No significant difference in actin binding activity is observed with increasing amounts of DysR18-CT. (C) Actin depolymerization protection control experiment at molar ratios of 1:6, 1:12, and 1:24 for DysR18-CT:actin. (D) Actin depolymerization protection assay with full-length dystrophin alone at a molar ratio of 1:12 (Dystrophin:actin) and DysR18-CT added as a competitor at molar ratios of 1:10 and 1:20 (Dystrophin:DysR18-CT). No significant competition was observed for the amounts of DysR18-CT tested. (B-D) Error bars represent SEM.

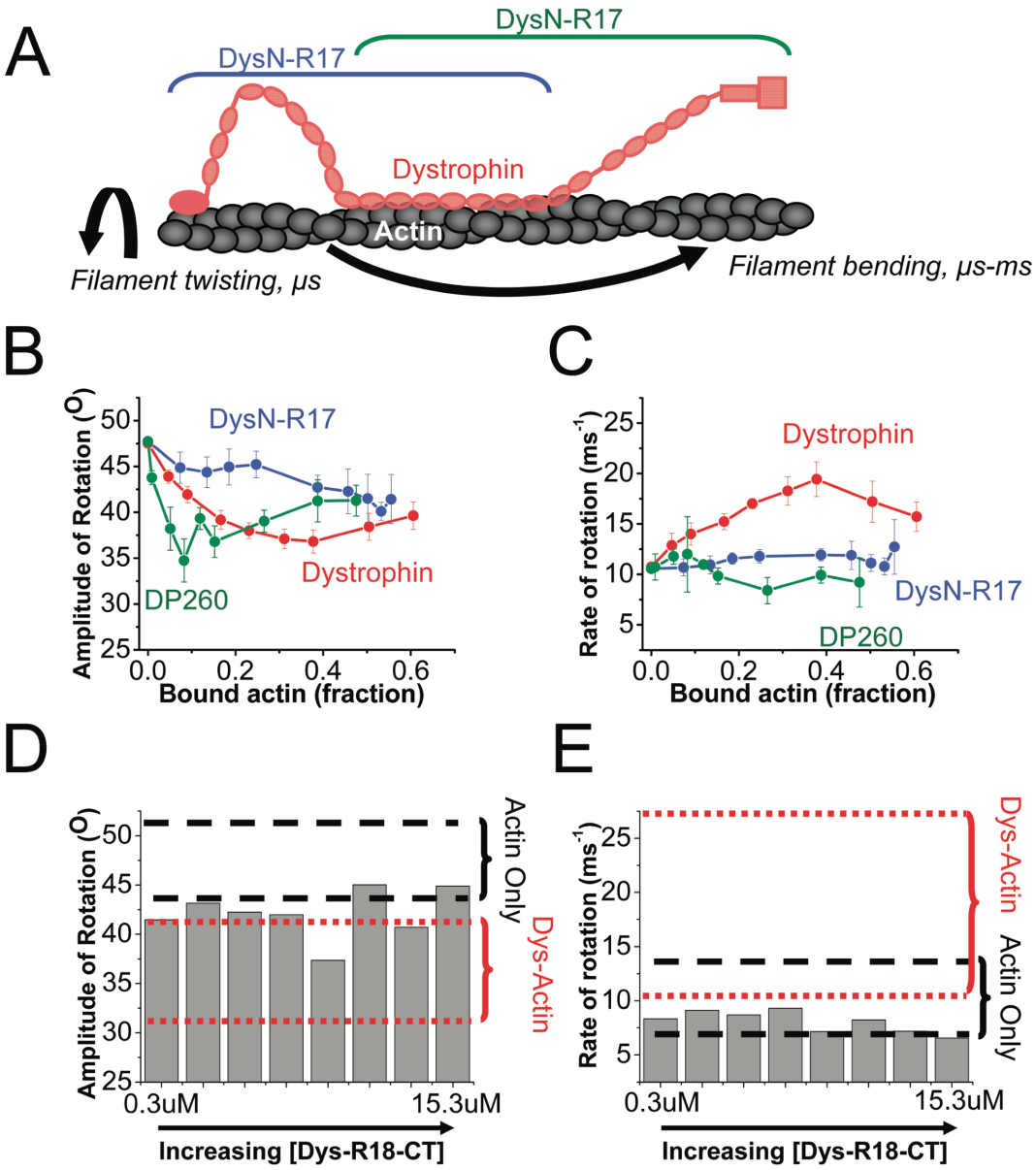

Figure 2-6. **Actin rotational dynamics by TPA.** (A) Diagram of actin rotational dynamics evaluated by time-resolved phosphorescence anisotropy (TPA) when bound to full length dystrophin (red), DysN-R17 (blue) or DP260 (green). Effects on amplitudes (B) and rates (C) of actin rotational motion are plotted against the fraction of bound actin protomers, $B_{max}[actin]/(K_d + [actin])$. Full length dystrophin

(red) restricts the amplitude and increases the rate of actin rotational motion (99). Deletion of the C-terminal region of dystrophin in DysN-R17 (blue) shows similar restriction of amplitude (B) at higher titrations compared with full length dystrophin, but there is loss in the cooperativity of the effect. DP260 (green), containing the C-terminal tail regains the cooperative effect on restricting actin rotational amplitude. However, either loss of the C-terminal or N-terminal regions in DysN-R17 or DP260 fails to produce any increase on the rate of rotational motion in actin (C). Dys-R18-CT has negligible effect in restricting the amplitude (D) or increasing the rate (E). In D and E, the ranges of values from actin only (dash lines, black) and when 40% of the actin is decorated with dystrophin (dotted line, red) are shown.

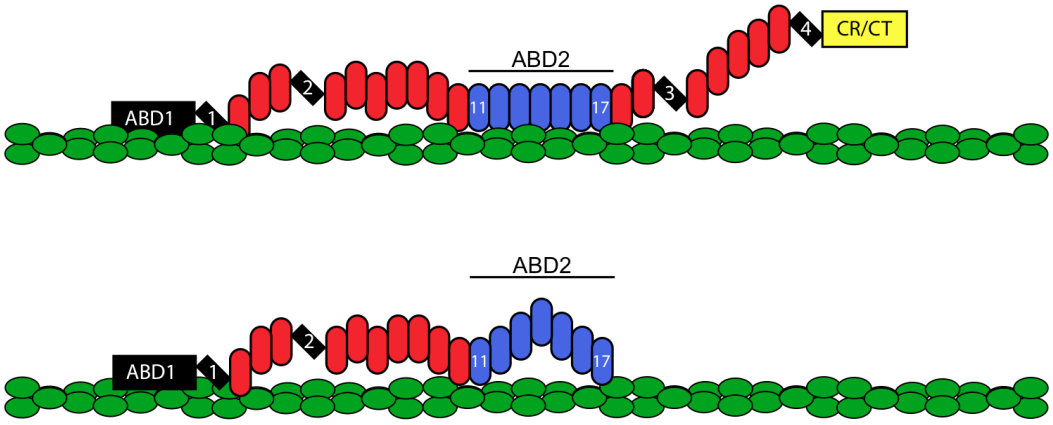

Figure 2-7: **Model of disrupted actin binding conformation.** The C-terminus of dystrophin helps to stabilize a high affinity actin binding conformation in the full-length dystrophin protein

Chapter 3: Disease-Causing Missense Mutations in Actin Binding Domain 1 of Dystrophin Induce Thermodynamic Instability and Protein Aggregation

Davin Henderson generated all constructs except WT-dystrophin and performed all experiments except for those found in Figure 3-3A which were performed by Ann Lee. The WT-dystrophin construct was previously generated in Rybakova et al. JBC, 2006.

Reprinted with permission from The Proceedings of the National Academy of Sciences USA (PNAS)

Henderson, D.M., Lee, A. and Ervasti, J.M. (2010). *Proc Natl Acad Sci U S A*, **107**, 9632-9637.

Chapter Summary

Mutations in the dystrophin gene cause Duchenne muscular dystrophy (DMD) most commonly through loss of protein expression. In a small sub-population of patients, missense mutations can cause DMD, Becker muscular dystrophy (BMD) or X-linked cardiomyopathy (XLCM). Nearly one-half of disease-causing missense mutations are located in actin-binding domain 1 (ABD1) of dystrophin. To test the hypothesis that ABD1 missense mutations cause disease by impairing actin binding activity, we engineered the K18N, L54R, D165V, A168D, L172H and Y231N mutations into the full-length dystrophin cDNA and characterized the biochemical properties of each mutant protein. The K18N and L54R mutations are associated with the most severe diseases in humans and each caused a small but significant 4-fold decrease in actin binding affinity, while the affinities of the other four mutant proteins were not significantly different from WT dystrophin. More interestingly, WT dystrophin was observed to unfold in a single-step, highly cooperative manner. In contrast, all six mutant proteins were significantly more prone to thermal denaturation and aggregation. Our results suggest that missense mutations in ABD1 may all cause loss of dystrophin function via protein instability and aggregation rather than through loss of ligand binding function. However, more severe disease progressions may be due to the combinatorial effects of some mutations on both protein aggregation and impaired actin binding activity.

Introduction

Duchenne muscular dystrophy (DMD) is a severe muscle wasting disease that affects 1/3500 males born and is caused by mutations in the dystrophin gene (1,2). Dystrophin is a 427 kDa protein that localizes to costameres, large subsarcolemmal protein assemblies that are thought to transmit force radially from the Z-line of the contractile apparatus to neighboring muscle fibers (2-6). At costameres, dystrophin interacts with the cortical actin cytoskeleton, composed primarily of γ-actin and the transmembrane heterodimer dystroglycan (6,7) which in turn binds to the extacellular matrix protein laminin (8,9). Through interactions with γ-actin, dystroglycan and other proteins, dystrophin forms the dystrophin glycoprotein complex (DGC), which establishes a mechanically strong link between the intracellular cortical actin cytoskeleton and the extracellular matrix that provides stability to the fragile sarcolema during muscle contraction (9-11). Loss of dystrophin expression destabilizes the DGC, which results in sarcolemmal damage and muscle cell necrosis (9,11-13).

Dystrophin is a large, multi-domain protein containing a tandem calponin homology (CH) actin-binding domain (ABD1) at its amino terminus (2,9). The largest domain of dystrophin is composed of a series of 24 spectrin-like repeats and 4 hinge regions that are thought to allow dystrophin to adopt a flexible rod-like architecture (9,14). The rod domain was also shown to contain a second actin-binding site (ABD2) composed of a series of basic spectrin-like repeats that

interact electrostatically with acidic actin filaments (15). The combined actin binding activities of the amino-terminal tandem CH and central rod domain enable dystrophin to bind laterally along actin filaments with sub-micro molar affinity (7,16). The carboxyl terminus of dystrophin is a globular domain containing a cysteine rich domain, a WW domain, a ZZ domain and two EF hand modules (9,17,18) that interact with the cytoplasmic domain of β-dystroglycan as well as other members of the DGC (9).

Three actin-binding sequences (ABS 1-3, Fig. 1 and S1) within the dystrophin tandem CH domain were initially thought to directly interact with actin filaments (19,20). ABS1 and 2 were identified through analysis of peptide binding to actin filaments using NMR spectroscopy (19,20). ABS3 was proposed based on its homology with actin-binding sequences identified in other tandem CH domain containing proteins (21). Subsequent studies showed that only the first 90 amino acids of the dystrophin tandem CH domain were critical for actin binding *in vitro* (22,23) while a KTFT motif in ABS1 proposed to contact actin filaments directly was not required (22). Most recently, a micro-gene replacement study demonstrated that an intact tandem CH domain is required to rescue the phenotypes associated with dystrophin-deficiency in the *mdx* mouse (24).

While dystrophinopathies are most typically caused by mutations that lead to loss of protein expression or deletion of key ligand binding domains, missense mutations have been identified in a subset of patients (www.dmd.nl). Of the 35

disease-causing missense mutations identified to-date, 17 are located in ABD1 (www.dmd.nl). The first such mutation identified, L54R, is associated with DMD, other mutations in the tandem CH domain cause a less severe disease known as Becker muscular dystrophy (BMB) (25-27), while the K18N mutation is associated with X-linked cardiomyopathy (28). Since almost half of the missense mutations localize to ABD1, we have tested the hypothesis that one or more of these mutations would specifically disrupt the interaction between dystrophin and actin filaments. Using biochemical analysis of full-length recombinant proteins bearing six different missense mutations, we demonstrate that these ABD1 mutations had only modest effects on actin binding activity. Instead, the most noteworthy biochemical change we observed for every mutation studied was significantly decreased protein stability and solubility. These results suggest that several different single amino acid changes in ABD1 all may cause a loss of function through protein aggregation.

Results

Expression of disease-causing dystrophin mutations:

Several amino acids in the tandem CH domain of ABD1 are conserved between dystrophin and its autosomal homolog utrophin. Furthermore, these residues are also conserved from flies to humans (Figure 3-1), suggesting that they are critical to protein structure and/or function. Consistent with this idea, mutations in the tandem CH domain of ABD1 account for 50% of the known disease causing missense mutations in the dystrophin gene even though the domain only comprises 6.7% of the dystrophin sequence (Figure 3-1).

The eight ABD1 missense mutations known at the initiation of this study are associated with myopathies of varying degrees of severity and are either buried in hydrophobic alpha helices or reside on solvent-exposed surface regions of alpha helices (Figure 3-2A and B). To understand how single amino acid changes cause disease in such a large protein, we introduced each mutation into the full length dystrophin cDNA by site directed mutagenesis and expressed each protein in Sf9 insect cells using the baculovirus system. All mutants expressed to high levels and purified as single bands that co-migrated with WT dystrophin on SDS-polyacrylamide gels (Figure 3-2C).

Circular Dichroism:

To examine the effect of each mutation on the secondary structure of dystrophin, we analyzed WT and mutant proteins using circular dichroism (CD) spectroscopy. At concentrations between 0.2 and 1 mg/ml, WT dystrophin

displayed CD spectra typical of highly alpha helical proteins (Figure 3-3). Mutant dystrophin proteins over the same range of concentrations exhibited CD spectra similar to WT protein (Figure 3-3). In order to determine if disease causing mutations rendered the protein less stable, we performed a melting point analysis of WT and mutant dystrophin proteins. For WT dystrophin, we observed a sharp two state transition with a melting temperature of 59.6° C (Figure 3-3). Surprisingly, none of the disease causing mutant proteins exhibited sharp transitions and appeared to unfold in a non-cooperative fashion. The linear melting curves of the mutant proteins were consistent for multiple preparations and reproducible at multiple concentrations.

Solubility of dystrophin mutants:

To determine whether disease-causing missense mutations affected the solubility of dystrophin, we measured the fraction of insoluble WT and mutant protein when overexpressed in Sf9 insect cells. While only 5% of WT dystrophin protein was found in the insoluble fraction, K18N, L172H and Y231N mutations all had more than 25% of the total protein associated with the insoluble fraction of insect cell lysates (Figure 3-4A and Figure 3-5A). The L54R, D165V and A168D mutations caused 40-50% of dystrophin to shift to the insoluble fraction (Figure 3-4A). In addition to analyzing cell lysates, we measured the solubility of purified WT and mutant dystrophin using high-speed centrifugation. Equal concentrations of WT and mutant protein were spun at 100,000 x *g* and protein levels determined for the supernatant and pellet. Our previous experiments

showed that WT dystrophin was predominantly associated with the soluble supernatant. Therefore, the fraction of WT or mutant protein found in the pellet was considered insoluble or aggregated. For WT dystrophin, less than 15% of the protein was in the insoluble or aggregated fraction (Figure 3-4B and Figure 3-5B). In contrast, the K18N, L54R, A168D and L172H mutations caused a significant increase in the amount of aggregated protein as compared to WT dystrophin (Figure 3-4B). The fraction of aggregation for the D165V and Y231N mutants was greater than WT protein, but the difference was not statistically significant (Figure 3-4B).

Actin binding properties of missense mutant dystrophins:

Despite the greater insolubility of mutant dystrophins, we were able to purify sufficient protein to characterize their actin binding properties. We previously measured the affinity of full-length dystrophin for F-actin at 0.2 μM (16,29) using an actin cosedimentation assay where the concentration of dystrophin was varied against a constant actin concentration. Since a substantial fraction of each mutant protein self-pelleted under conditions used in the actin binding assay we varied the concentration of actin and corrected all binding data by subtracting the amount of self-pelleting dystrophin measured in the absence of actin. When actin cosedimentation assays were performed with increasing concentrations of F-actin and a fixed concentration of 0.5 μM WT dystrophin, we measured a K_d value of 0.22 ± 0.081 μM (Figure 3-6A and 3-8), which is in good

agreement with our previous studies (16,29). Surprisingly, D165V, A168D, L172H and Y231N mutant dystrophins showed no significant differences in F-actin affinity compared with WT protein (Figure 3-6D, 3-7 and 3-8). K18N and L54R mutant dystrophins bound F-actin with affinities of 0.76± 0.40 μM and 0.85± 0.21 μM for K18N and L54R, respectively (Figure 3-6B and C and 3-8), which were 4-5 fold lower than and significantly different from WT dystrophin ($p \leq 0.5$). Additionally, we observed significant increases in B_{max} values for the binding of L54R, D165V, A168D and L172H mutants to F-actin (Figure 3-6 and 3-7).

Dystrophin binds laterally along actin filaments with a stoichiometry of 1 dystrophin per 24 actin monomers and protects actin filaments from forced depolymerization *in vitro* (16,30). At dystrophin:actin molar ratios of 1:12 and 1:24, we found that WT dystrophin and all mutants slowed pyrene-labeled actin filaments from forced depolymerization with similar efficacies (Figure 3-9 A and B). Finally, dystrophin binding to actin filaments is inhibited by increasing salt concentrations, predominantly due to the disruption of the electrostatic interaction between ABD2 and actin filaments (15,16). We reasoned that the effects of mutations in ABD1 may render the full-length protein even more sensitive to increasing ionic concentration. To correct for the small differences between WT and mutant dystrophins in binding affinity, experiments were performed at a fixed concentration of 0.5 μM WT or mutant dystrophin and concentrations of actin corresponding to each protein's measured K_d. We found that binding of mutant

dystrophin to actin filaments with increasing salt concentration (up to 700 mM) followed the same trend as WT, suggesting that the mutations did not affect the electrostatic binding component of dystrophin (Figure 3-9C).

Discussion

Genetic studies have demonstrated that a disproportionately high percentage of disease causing missense mutations are located in ABD1 of dystrophin (www.dmd.nl). Based on the crystal structure of ABD1, Norwood et al., predicted that disease-causing missense mutations would greatly destabilize ABD1 and disrupt folding (31). Our results demonstrate that the actin binding activity of dystrophin is remarkably robust as six different ABD1 mutations only modestly decreased actin binding affinity. More interestingly, we observed significantly more aggregation of the mutant dystrophins compared to WT protein. Mutant dystrophin protein formed large aggregates which pelleted when centrifuged at 100,000 *x g* and were found in insoluble cellular extracts (Figure 3-5). Additionally, the L54R, D165V, A168D and Y231N mutants showed significantly higher B_{max} values than WT protein in actin cosedimentation assays (Figure 3-6 and 3-7). The increased B_{max} values may be due to the formation of micro-aggregates that did not pellet at 100,000 *x g* but cosedimented with actin filaments. Previously, two micro-dystrophin constructs deleted for either CH1 or CH2 showed a greater propensity to form aggregates when expressed in dystrophin-deficient *mdx* muscle (24). While cellular localization studies on patient specimens bearing missense mutations are rare, immunofluorescence microscopic analysis of dystrophin localization in a biopsy from the original L54R DMD patient revealed the presence of increased cytoplasmic staining with bright puncta (25). Our results extend these previous studies by showing that six

different single amino-acid changes in ABD1 can dramatically induce aggregation *in vitro.*

Recently a study from Legardinier et al. (32) reported on the effects of two disease-causing missense mutations in a recombinant protein fragment encoding spectrin-like repeat 23 of dystrophin. Distinct from the effects of ABD1 mutations on full-length dystrophin, the mutant spectrin-like repeat fragments remained fully soluble *in vitro.* While mutations in the isolated spectrin-like repeat resulted in decreased thermal stability, the sharp transition from folded to denatured was primarily left-shifted compared to WT (32). In contrast, we found that ABD1 mutants of full-length dystrophin yielded CD spectra similar to WT dystrophin at room temperature, but all mutations in ABD1 abolished the sharp transition at approximately 60^{o} C and mutant proteins unfolded in a linear fashion as a function of increasing temperature. In order for a protein to undergo a cooperative unfolding transition, the protein must be in a compact, well-folded state. A broad or non-cooperative unfolding, as seen for mutated dystrophin proteins, suggests that the protein sample is loosely folded or exists in numerous folded states. The mutated residue may disrupt the compact fold of the amino-terminal CH domain or the mutation may cause the domain to adopt multiple folding conformations. Our results suggest that disease-causing missense mutations in ABD1 of dystrophin lead to dramatic destabilization of the full-length dystrophin protein.

While 35 missense mutations and their corresponding disease phenotypes have been cataloged for the dystrophin gene, much less information is available on the tissue expression levels associated with each mutation. The L54R mutant protein was measured at 20% of normal dystrophin levels (25). A more recent study by Hamed et al. (26) reported that the L172H and R82P mutations reduced protein levels by western blot to 20% and 50% of normal levels, respectively. Based on studies in transgenic *mdx* mice, 20% of WT dystrophin protein levels is sufficient to rescue the dystrophic phenotype (33). Our data on the L54R and L172H mutations suggest that both mutations cause the full-length protein to be markedly less soluble than WT dystrophin but only the L54R mutation binds to actin filaments with 4-fold lower affinity. These data fit well with previous studies (22,23) identifying CH1 as the predominant actin binding module in ABD1 of dystrophin. The L172H mutation, which causes the milder BMD, exhibits a similar propensity to aggregate as the L54R mutation but displayed near WT actin affinity for actin filaments. Perhaps the L54R mutation results in a more severe disease phenotype through the combined effects of protein aggregation and decreased actin-binding activity. In light of the limited characterization of rare patients bearing disease causing missense mutations, we cannot exclude the possibility that pathogenesis may also be driven by premature degradation or toxic gain-of-function by misfolded or aggregated protein. Mutations in many muscle proteins result in protein aggregate myopathies (PAMs) where misfolded proteins resist degradation and aggregate resulting in impaired muscle function

(34). Further *in vivo* analysis is required to determine whether ABD1 missense mutant dystrophins also classify as PAMs.

Despite substantial thermodynamic instability and protein aggregation, disease-causing ABD1 mutants of dystrophin retained near WT affinity for actin filaments. A similar scenario has been observed for the Δ508F mutation in the cystic fibrosis transmembrane conductance regulator (CFTR) (35). The Δ508F CFTR mutation retains function, but is improperly processed leading to premature degradation of the protein rather than trafficking to the plasma membrane (35). Pharmacological modulation of heat shock proteins by 4-phenylbutyrate was shown to increase the functional levels of the Δ508F CFTR protein in the plasma membrane (36) and trials are underway to examine how protein levels in CFTR patients can be increased by pharmacologically manipulating the folding and degradation pathway (35,36). Based on our results, drugs that block protein aggregation may hold promise for the treatment of DMD patients carrying missense mutations in ABD1.

Finally, our CD spectroscopic analysis of WT full-length dystrophin speaks to the potential for structural heterogeneity within the rod domain. Several studies have reported that different spectrin repeats in the rod domain display widely-varying thermal stabilities when characterized in isolation (32,37-41). These data have led to the suggestion that the dystrophin rod domain cannot function as a monolithic single unit (40). However, our studies demonstrate that

full-length dystrophin melted in a highly cooperative, one-step process (Figure 3-3). We conclude that the thermal stability of individual spectrin-like repeats is strongly influenced by neighboring sequences so that the entire protein functions as a single unit regardless of the different intrinsic stabilities of its isolated parts.

Experimental Procedures

Site directed mutagenesis: Disease-causing missense mutations (Figure 3-2A and 3-S1) were introduced into the first 1.2 kb of mouse dystrophin cDNA containing an amino-terminal FLAG tag in the pFastBac™ vector (Invitrogen, Carlsbad, CA) using overlapping primers in (Figure 3-10) and the quick-change mutagenesis kit (Stratagene, La Jolla, CA) following the manufacturer's instructions. Mutant full-length FLAG-dystrophin cDNAs were engineered into pFastBac™ vector (Invitogen) by ligating the remaining 12.5 kb of the dystrophin cDNA into the vector containing the mutant 1.2 kb construct using a SpeI site common to the dystrophin sequence and pFastBac™.

Protein expression and purification: WT and mutant dystrophin proteins were expressed using the Bac-to-Bac Baculovirus System (Invitrogen, Carlsbad, CA) in Sf9 insect cells as previously described (42). After verifying protein expression, P1 viruses were amplified and used to infect Sf9 cells at 1-liter scale by Kinnakeet Biotechnology (Midlothian, VA). WT and mutant proteins were purified by FLAG affinity chromatography (Sigma-Aldrich, St. Louis, MO) and dialyzed against two changes of phosphate-buffered saline pH 7.5 (PBS). Proteins were concentrated using Amicon Ultra centrifuge based cartridge concentrators (Millipore, Billerica, MA) and protein concentration determined with the BioRad D_c Protein Assay using a BSA standard curve (Bio-Rad, Hercules, CA).

Solubility Assay: Purified protein was centrifuged at 100,000 x g for 25 minutes and the amount present in the supernatant and pelleted fractions was quantified by densitometric analysis of Coomassie blue-stained SDS polyacrylamide gels. To measure protein solubility in live cells, Sf9 insect cells infected with baculoviruses encoding WT or mutant dystrophins were lysed and total protein levels were compared to protein remaining in the supernatant after centrifugation at 16,000 x g for 15 minutes. At least 3 experiments for each condition were averaged and compared to the WT values using student's t-test.

Circular Dichroism Measurements: WT and mutant full-length proteins were prepared for CD measurements in an identical fashion as all other experiments except 0.5% Triton X100 was omitted from the elution buffer. Proteins were centrifuged at 16,000 x g to remove large light scattering particles. CD spectra were acquired on a J-815 spectopolarimeter (JASCO Inc., Easton, MD) fitted with a Peltier temperature regulator. Spectrum for WT and mutant dystrophins were acquired from 260 nm to 200 nm at 20º C and at a range of concentrations between 0.5 and 0.2 mg/ml at pH 7.5. The melt curves for full-length WT dystrophin and dystrophin mutants were collected by varying the temperature from 20º C to 85º C collecting a spectrum from 235 nm to 200 nm every 1 degree Celsius. Data from the 222 nm reading was fit by regression analysis in Sigma Plot (Systat Software, Inc. Chicago, IL) using an equation for a two state unfolding model reported by Legardinier et al (32).

Actin binding assay: The binding of WT and mutant dystrophins to actin filaments was measured using a previously described high-speed cosedimentation assay (16) except that the actin concentration was varied between 0.2 μM and 15 μM around a fixed concentration of 0.5μM dystrophin. Regression analysis was performed using Sigma Plot software (Systat Software) using the equation

$$Y=B_{max} * [X]/ (K_d + X)$$

corresponding to one site saturation kinetics. F-actin binding in the presence of increasing NaCl concentration (100-700mM) was also measured using the high-speed cosedimentation assay at a fixed concentration of 0.5 μM dystrophin and an actin concentration corresponding to WT or each mutant's measured Kd.

Actin depolymerization assay: WT or mutant dystrophins were incubated for 30 minutes with 2 μM pyrene labeled actin (Cytoskeleton, Inc. Denver, CO) filaments at ratios of 1:12 or 1:24 dystrophin molecules bound per actin monomer. Actin filaments were induced to depolymerize by dilution below critical concentration in low salt buffer (G-buffer: 5mM Tris pH 8.0, 0.2mM $CaCl_2$ 0.2 mM ATP and 0.5 mM DTT) and the fluorescence decay was monitored every minute for 30 minutes using a Gemini plate reader system (Molecular Devices, Toronto, Canada). Fluorescence was normalized to initial fluorescent signal for each condition and plotted as a function of time.

Figures

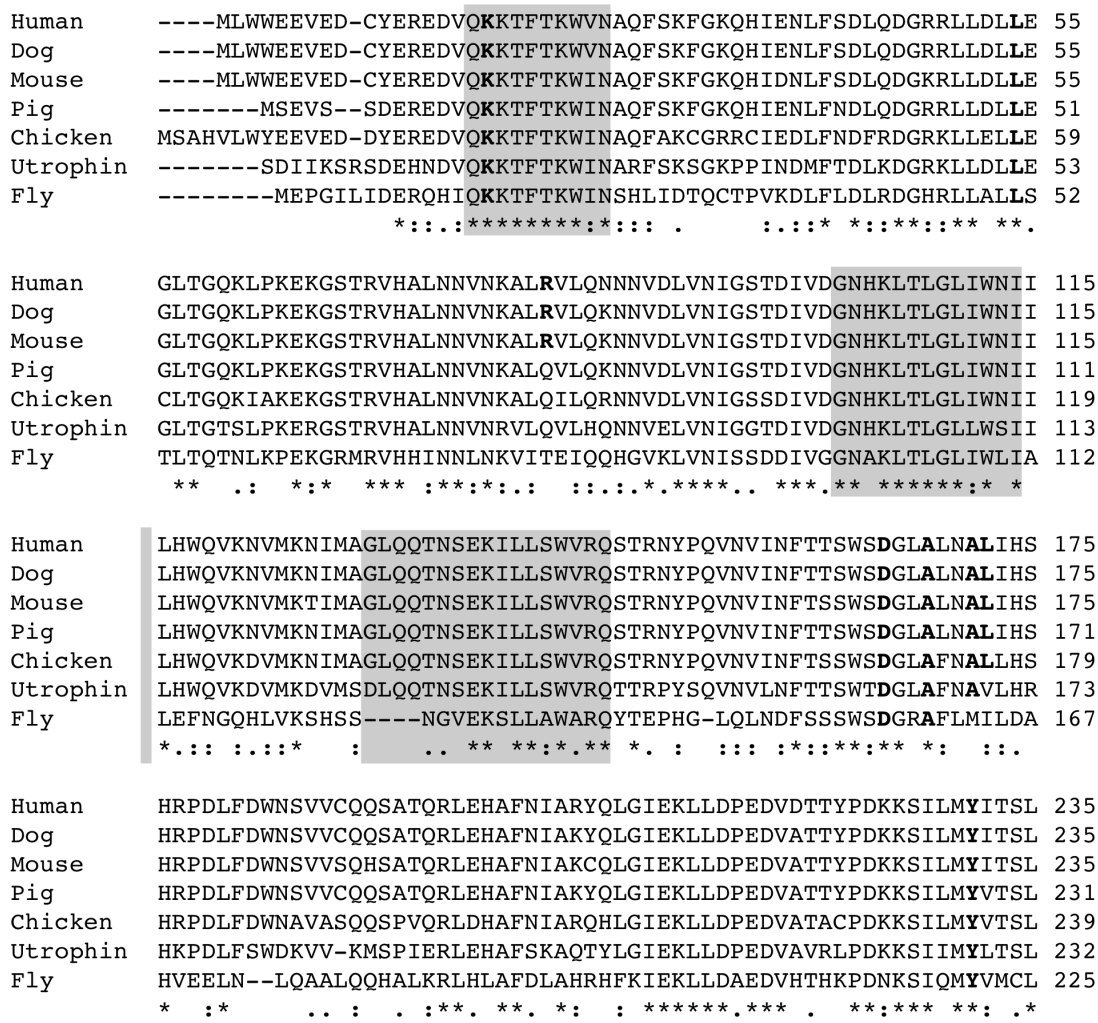

Figure 3-1: **Sequence alignment of the dystrophin tandem CH domain.** Conserved residues across all species are marked with an asterisk. Disease-causing mutations in human dystrophin are bolded. Actin binding sites 1-3 are highlighted in grey.

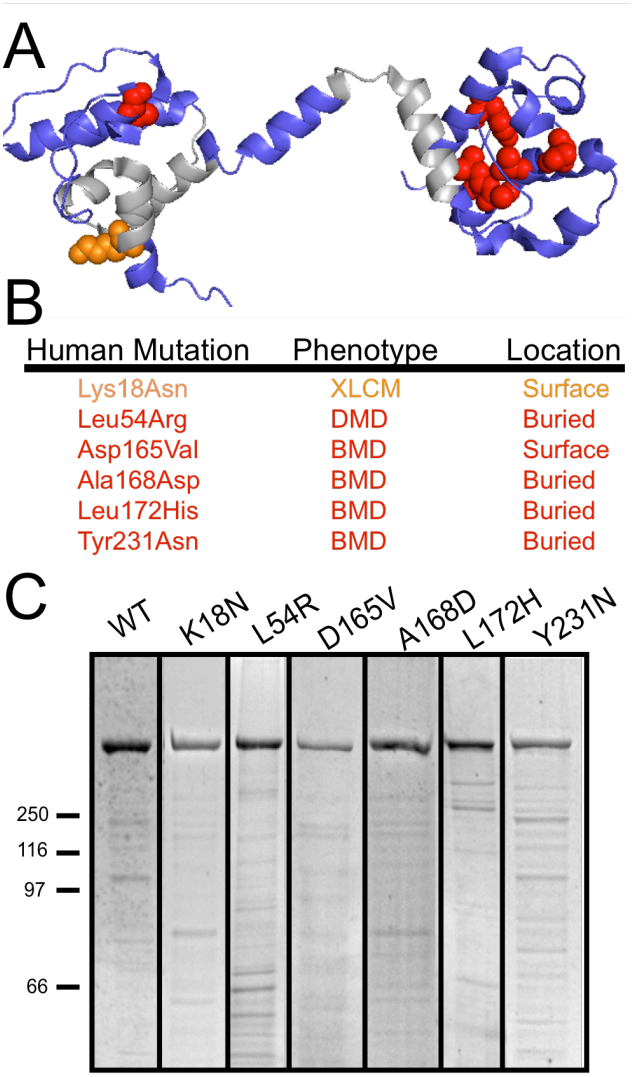

Figure 3-2: **Disease state and expression of mutant dystrophin proteins.** (A) A ribbon diagram of the dystrophin tandem CH domain structure (38). Grey shaded region denotes proposed actin interacting regions (19,20). Residues marked in red represent disease-causing mutations not located in a proposed actin binding region. The K18N mutation lies in ABS1 and is orange. (B) Disease phenotype and molecular location of missense mutations studied. DMD, Duchenne muscular dystrophy; BMD, Becker muscular dystrophy; XLCM, X-

linked cardiomyopathy. The molecular location of each mutation was classified as buried in a hydrophobic core or surface exposed based on the location of the residue in the crystal structure of wild-type protein (38). (C) Coomassie blue-stained SDS-polyacrylamide gels of purified WT and mutant dystrophins. Molecular weight standards are shown on the left.

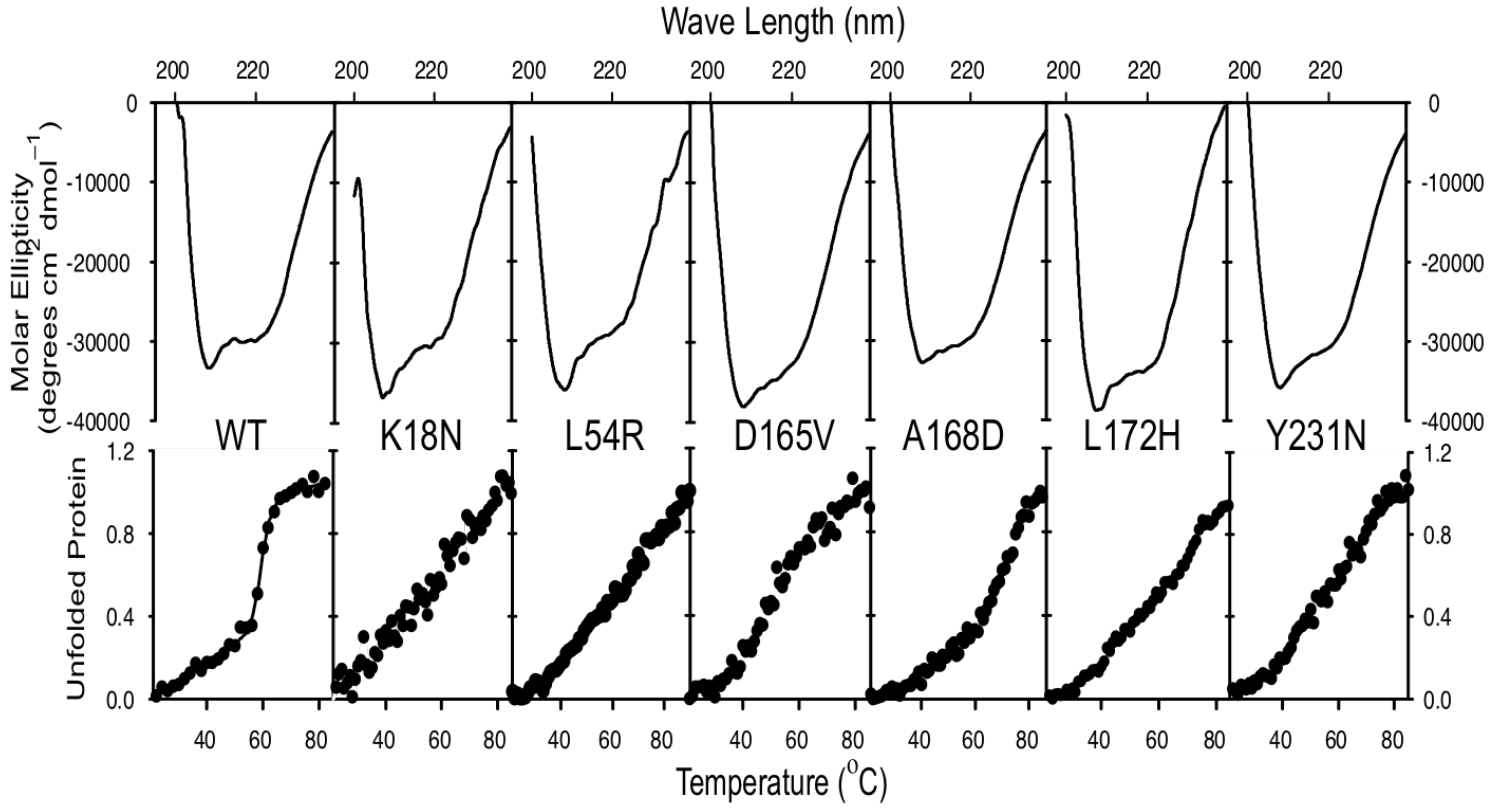
Wave Length (nm)
200
220
Molar Ellipticity (degrees cm^2 dmol^{-1})
0
-10000
-20000
-30000
-40000
WT
K18N
L54R
D165V
A168D
L172H
Y231N
Unfolded Protein
1.2
0.8
0.4
0.0
40
60
80
Temperature (^{O}C)

Figure 3-3: **Circular Dichroism measurements of WT and mutant dystrophin.** WT and mutant dystrophin proteins display characteristic alpha-helical CD signature between 200 and 260 nm. Full-length WT dystrophin unfolds cooperatively and has melting temperature of 59.6 °C. Mutant dystrophin proteins unfold non-cooperatively.

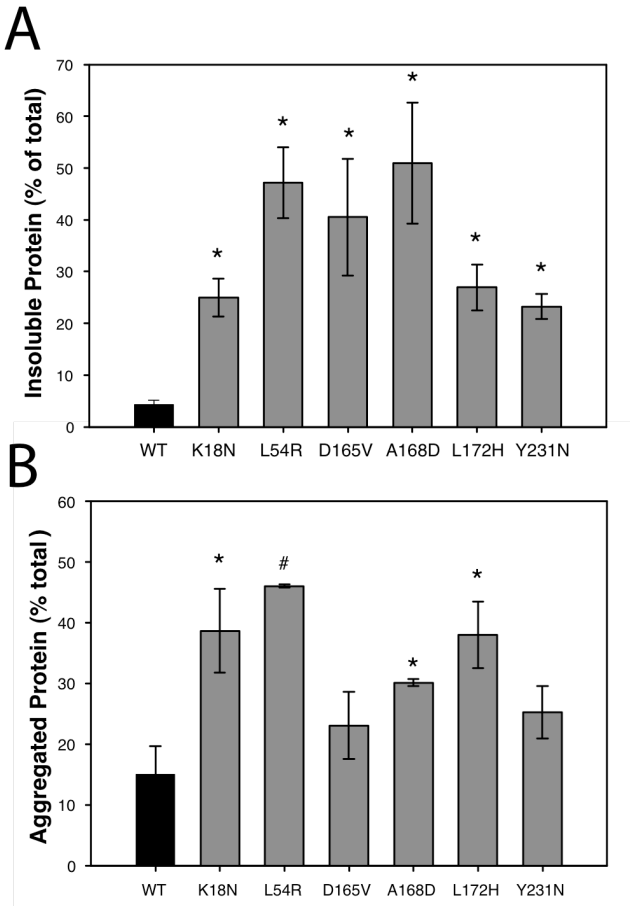

Figure 3-4: **Relative solubility of cellular and purified dystrophin proteins.** (A) Significantly more of each dystrophin mutant in SF9 insect cell lysates pelleted at 14,000 x *g* compared to WT (*, $p < 0.05$; n = ≥3). (B) Significantly more purified K18N, L54R, A168D and L172H mutants pelleted at 100,000 x *g* compared to WT (*, $p < 0.05$; #, $p < 0.01$; n = ≥3). (A and B) Error bars represent S.E.M.

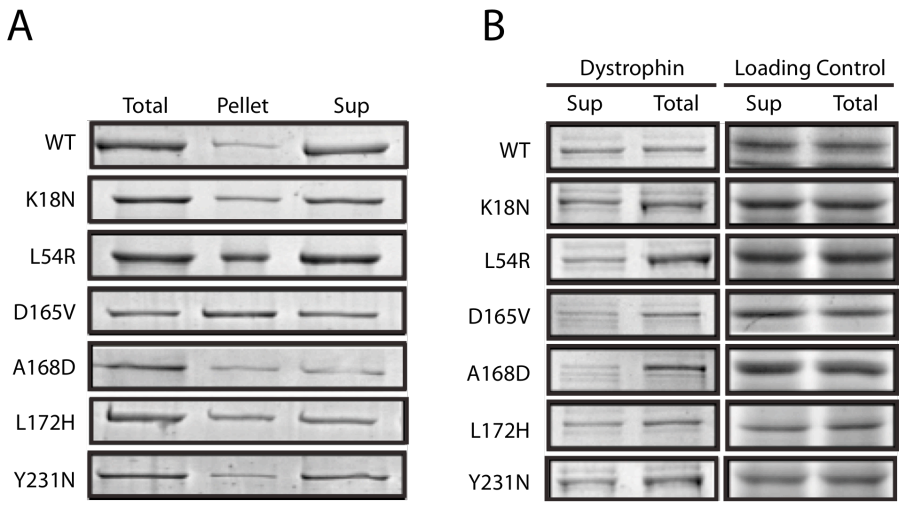

Figure 3-5: **Raw data for figure 3-3.** Representative Coomassie blue stained gels for each of the aggregation experiments. (A) In vitro Aggregation assay. (B) Insect cell protein solubility assay.

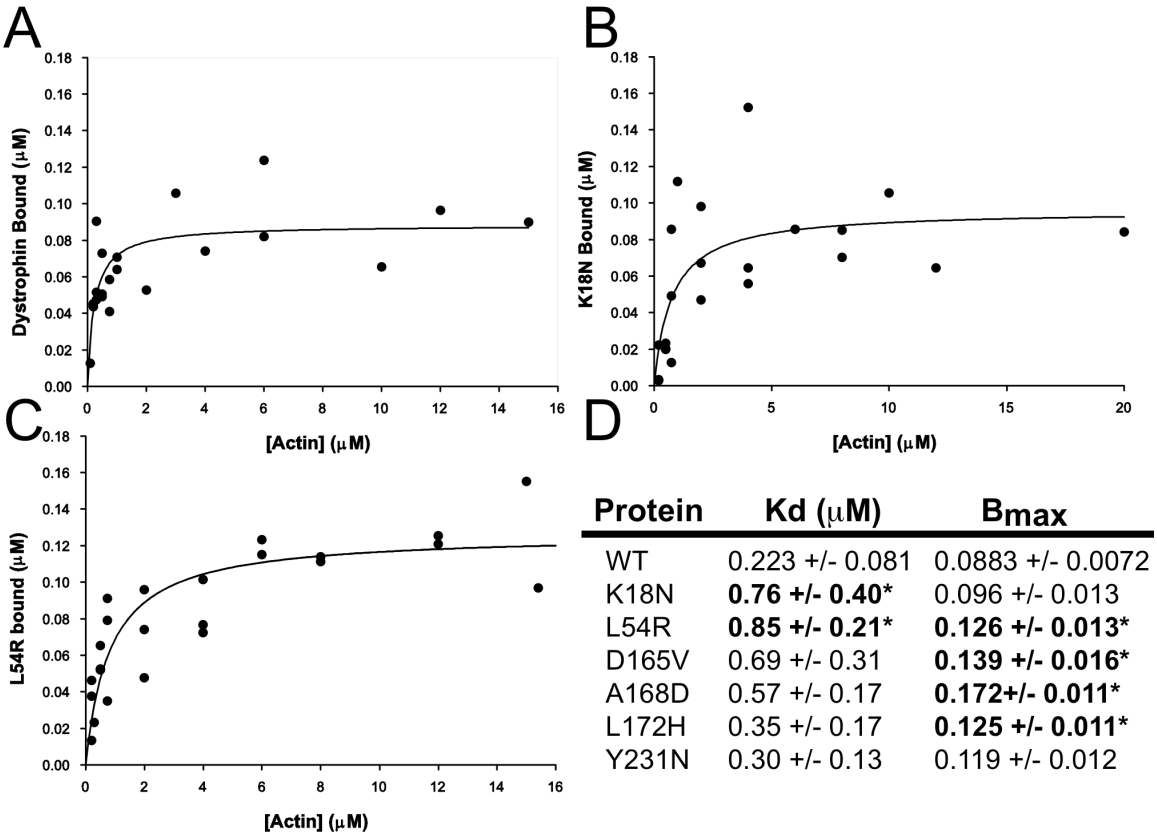

Protein	Kd (μM)	B_{max}
WT	0.223 +/- 0.081	0.0883 +/- 0.0072
K18N	**0.76 +/- 0.40***	0.096 +/- 0.013
L54R	**0.85 +/- 0.21***	**0.126 +/- 0.013***
D165V	0.69 +/- 0.31	**0.139 +/- 0.016***
A168D	0.57 +/- 0.17	**0.172+/- 0.011***
L172H	0.35 +/- 0.17	**0.125 +/- 0.011***
Y231N	0.30 +/- 0.13	0.119 +/- 0.012

Figure 3-6: **Actin binding properties of WT and mutant dystrophins**. F-actin binding isotherms for 0.5 μM WT (A), K18N (B), and L54R (C) dystrophins measured by high-speed cosedimentation with increasing amounts of F-actin. Symbols represent three independent experiments plotted on the same graph and curves represent the best fit of the aggregate cosedimentation data. (D) The Kd's obtained from fitted data for WT and each mutant protein were significantly different for K18N and L54R ($p < 0.05$). The B_{max} values obtained from the same data set were significantly different ($p < 0.05$) for L54R, D165V A168D, AND L172H.

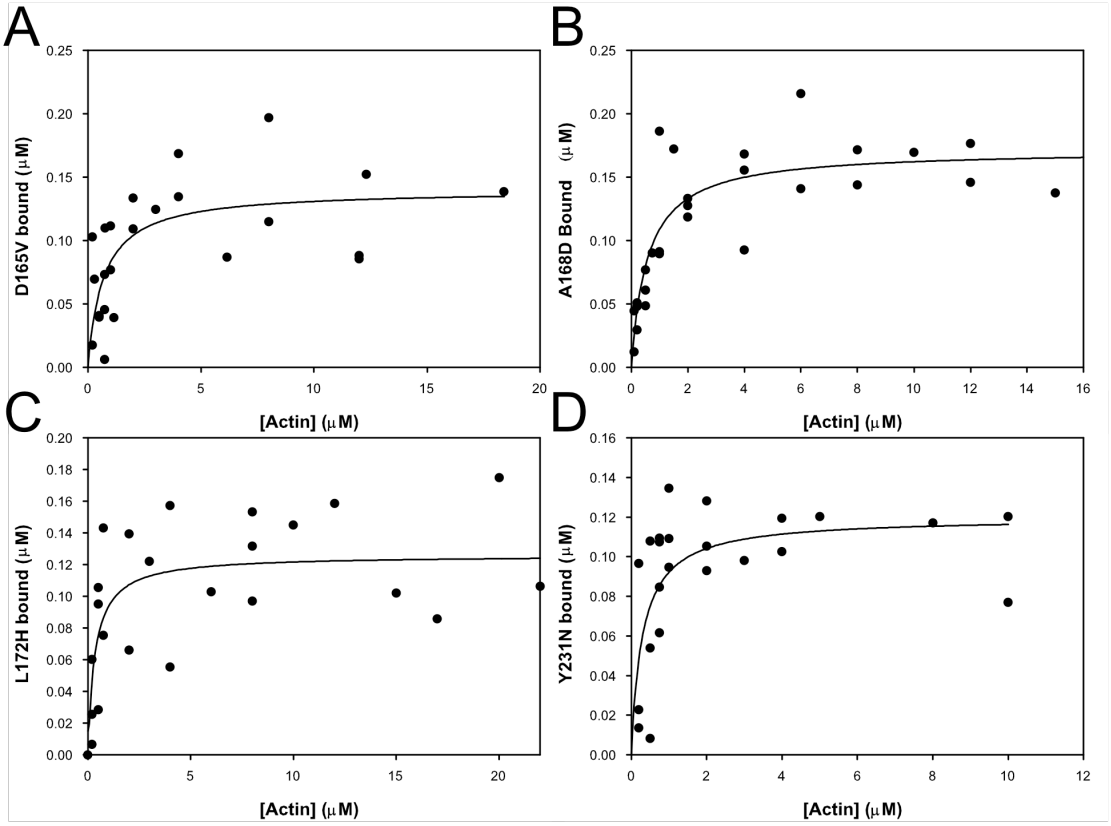

Figure 3-7: **Actin binding properties of mutant dystrophins**. F-actin binding isotherms for 0.5 mM D165V (A), A168D (B), L172H (C) and Y231N (D) dystrophins measured by high-speed cosedimentation with increasing amounts of F-actin. Symbols represent data from three independent experiments. Lines represent best fit by regression analysis. Actin binding is not significantly different than WT.

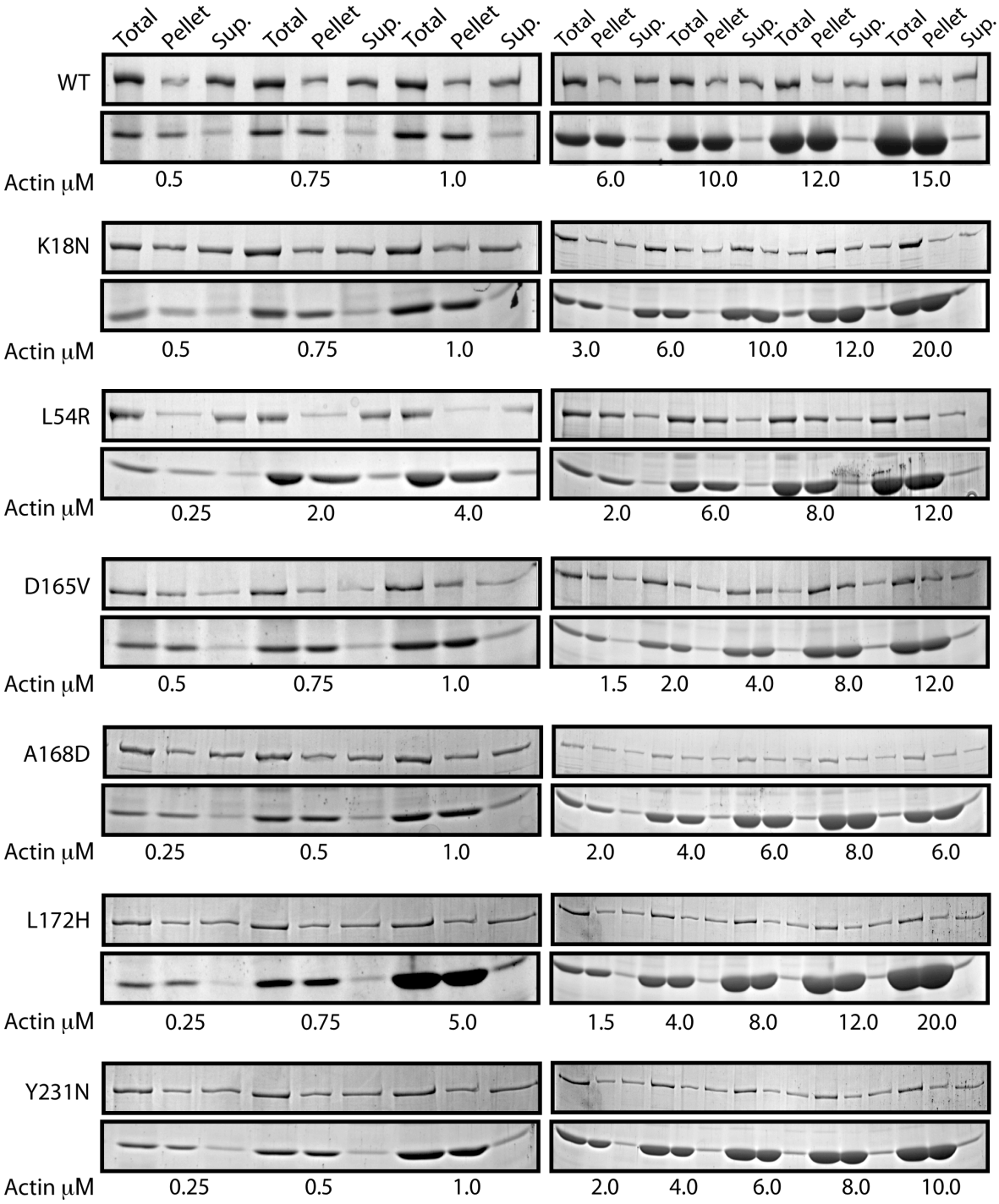
Total
Pellet
Sup.
WT
Actin μM
0.5
0.75
1.0
6.0
10.0
12.0
15.0
K18N
3.0
20.0
L54R
0.25
2.0
4.0
8.0
D165V
1.5
A168D
L172H
5.0
Y231N

Figure 3-8: **Raw data for figure 3-4 and 3-9.** Representative Coomassie blue stained gels for each of the actin cosedimentation assays.

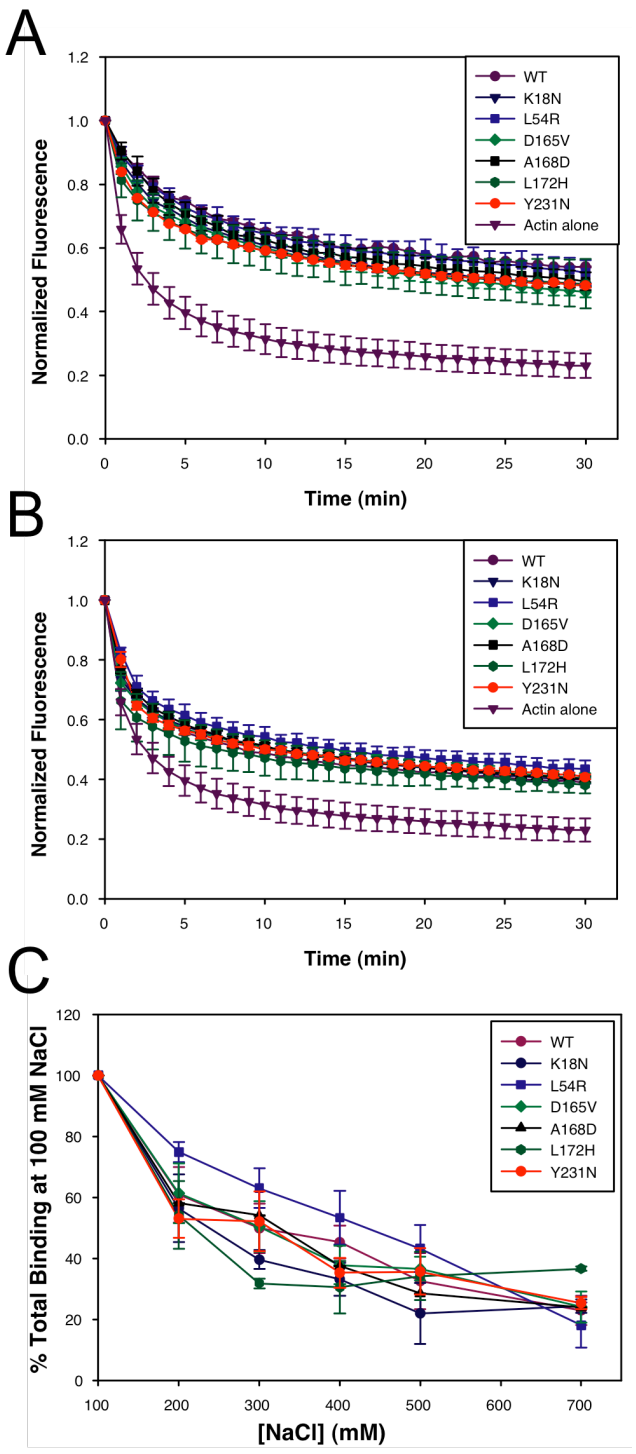

Figure 3-9: **Effect of WT and mutant dystrophin on actin depolymerization.**

(A and B) WT and mutant dystrophins were co-incubated with actin filaments at

dystrophin:actin ratios of 1:12 (A) and 1:24 (B). Filament depolymerization was induced by dilution and monitored by decay of pyrene-actin fluorescence. Normalized fluorescence is plotted as a function of time (minutes). (C) Effect of NaCl concentration on WT and mutant dystrophin binding to actin. WT and mutant dystrophins at a concentration of 0.5 μM were subjected to high-speed cosedimentation with K_d concentrations of F-actin at the indicated concentration of NaCl. The data are expressed as the percent of each protein pelleted in the presence of 100 mM NaCl. (A-C) Error bars represent S.E.M.

Mutation	Primers
K18N	5'-GAAAGAGAAGATGTTCAAAACAAAACATTCAC-3' 5'-CCATTTTGTGAATGTTTTGTTTTGAACATC-3'
L54R	5'-CCTAGACCTCCGGGAAGGCCTTACAG-3', 5'-CTTCCCGGAGGTCTAGGAGGCGTTTT-3'
D165V	5'-ACCTCTAGCTGGTCCGTCGGGTTGGCTTTG-3' 5'-GCATTCAAAGCCAACCCGACGGACCAGC-3'
A168D	5'-TGGTCCGACGGGTTGGATTTGAATGCTC-3' 5'-GGATAAGAGCATTCAAATCCAACCCGTCG-3'
L172H	5'-GTTGGCTTTGAATGCTCATATCCATAGTC-3' 5'- CCTGTGACTATGGATATGAGCATTCAA-3'
Y231N	5'-GAAGTCCATCTTAATGAACATCACATC-3' 5'-GAAAGAGTGATGTGATGTtCATTAAGATG-3'

Figure 3-10: **Primers used to generate mutant dystrophin cDNA.** Primers used to generate the K18N, L54R, D165V, A168D, L172H and Y231N mutations.

Chapter 4: Internal Deletion Compromises the Stability of Dystrophin

Davin Henderson performed all experiments, generated all constructs and purified all proteins besides the following. Bin Li helped perform circular dichroism experiments and helped purify proteins. Joe Belanto generated the mini-dystrophin constructs and Utr-R11-CT. Hanke Heun-Johnson generated the mini-utrophin constructs and micro-utrophin construct.

Reprinted with permission from Human Molecular Genetics, Oxford University Press

Davin M. Henderson, Joseph J. Belanto, Bin Li, Hanke Heun-Johnson, and James M. Ervasti. Internal deletion compromises the stability of dystrophin *Hum. Mol. Genet. (2011) first published online May 10, 2011*

Chapter Summary

Duchenne muscular dystrophy (DMD) is a deadly and common childhood disease caused by mutations that disrupt dystrophin protein expression. Several miniaturized dystrophin/utrophin constructs are utilized for gene therapy, and while these constructs have shown promise in mouse models, the functional integrity of these proteins is not well described. Here, we compare the biophysical properties of full-length dystrophin and utrophin with therapeutically-relevant miniaturized constructs using an insect cell expression system. Full-length utrophin, like dystrophin, displayed a highly cooperative melting transition well above 37^{o}C. Utrophin constructs involving N-terminal, C-terminal, or internal deletions were remarkably stable, showing cooperative melting transitions identical to full-length utrophin. In contrast, large dystrophin deletions from either the N- or C-terminus exhibited variable stability, as evidenced by melting transitions that differed by 20^{o}C. Most importantly, deletions in the large central rod domain of dystrophin resulted in a loss of cooperative unfolding with increased propensity for aggregation. Our results suggest that the functionality of dystrophin therapeutics based on mini- or micro-constructs may be compromised by the presence of non-native protein junctions that result in protein misfolding, instability and aggregation

Introduction

Duchenne muscular dystrophy (DMD) is a common (1/3500 live male births) and deadly childhood disease that is characterized by a fragile muscle cell membrane and progressive rounds of muscle cell death and regeneration (1-3). To date, many potential therapies have shown promise in animal models but no cure or effective treatment for human patients currently exists (4).

DMD is primarily caused by the loss of dystrophin protein expression due to gene deletions, duplications or mutations (5). Dystrophin is a large, multi-domain protein that functions intracellularly in muscle to stabilize cell membranes (6,7). Dystrophin binds actin filaments through a tandem calponin homology (CH) domain at its N-terminus and through an electrostatic interaction between basic spectrin repeats 11-17 and acidic actin (8-11). In addition, a C-terminal domain of dystrophin interacts with the transmembrane protein b-dystroglycan, a component of the dystrophin glycoprotein complex (DGC) that in turn is anchored to the extracellular matrix (ECM) (12-14). Therefore, dystrophin forms a structural link between the intracellular cytoskeleton and the ECM that protects muscle from contraction-induced injury (7).

Multiple strategies have been explored to rescue dystrophin expression in animal models of DMD including exon-skipping to restore a functional reading frame, stop codon suppression and viral gene therapy. One of the most promising approaches has been the expression of miniaturized dystrophin genes through adeno-associated viral (AAV) delivery (4,15). Since the packaging

capacity of AAV is significantly smaller than the large dystrophin cDNA (16), a portion of the dystrophin sequence was internally deleted to decrease its size while retaining critical ligand binding domains located at the N- and C-termini (15). Recently, a viral vector encoding such a miniaturized dystrophin construct was tested in a phase I clinical trial to determine efficacy and safety in DMD patients with large deletions of the dystrophin gene (17). Unfortunately, very few muscle fibers were found to express dystrophin long-term while, at the same time an immune response specific for peptides unique to the internally-deleted dystrophin protein was reported (17).

To circumvent possible immune reactions to exogenously delivered dystrophin, multiple studies have explored whether the closely related protein utrophin could serve as a surrogate in dystrophin-deficient muscle (18). Utrophin is an autosomal homolog of dystrophin that is upregulated in dystrophin-deficient muscle and has been shown to functionally substitute for dystrophin when transgenically overexpressed in dystrophic mouse models (19-23). Utrophin is expressed at high levels in muscle perinatally, but is restricted to the myotendinous and neuromuscular junctions in adult muscle (21). Additionally, utrophin has been shown to bind actin filaments and β-dystroglycan (24,25), but through modes of contact distinct from those employed by dystrophin (11). Multiple gene therapy studies have used internally deleted utrophin based constructs to rescue the dystrophic phenotype in *mdx* mice (18,26). Importantly, utrophin is expressed in adult muscle of DMD patients and is therefore less likely

to stimulate an immune response. However, expression of utrophin may not substitute for all of dystrophin's functions, such as anchoring neuronal nitric oxide synthase (nNOS) to the sarcolemma (27).

A common theme of several proposed DMD treatments is the generation of proteins encoding non-native junctions between spectrin-like repeats in dystrophin (4). Two studies of small recombinant dystrophin fragments examined the stability of non-native junctions expected from exon skipping approaches for DMD (28,29). Ruszczak et al. (28) found that hybrid repeats generated from skipping of exons 43 and 44 were significantly less stable, while skipping exons 44 and 45 had almost no affect on protein stability. Carag-Kreiger et al. (29) measured forced unfolding for non-native repeat junctions generated by exon skipping, or resulting from in-frame deletions of the dystrophin gene found in patients with Becker muscular dystrophy. The authors reported variable mechanical stability as well as aggregation in the proteins that were tested (29). These studies highlight the potential for decreased stability or protein aggregation when non-native repeat junctions are created in the dystrophin protein. Similar to exon skipping strategies, the success of a gene therapy approach is also dependent on the stability of internally deleted dystrophin or utrophin mini genes with non-native spectrin-like repeat junctions. A study by Banks et al. (30) reported that viral delivery of an internally-truncated dystrophin micro gene led to skeletal muscle abnormalities. A number of human patient studies have documented missense mutations or small deletions that lead to a

loss of dystrophin protein levels causing disease (31-36). Our previous work (37), recently confirmed and expanded by Singh et al. (38), demonstrated that disease-causing missense mutations in dystrophin can lead to marked loss of protein stability and increased aggregation. In order to optimize therapeutic constructs for the treatment of dystrophinopathies in humans, it is imperative to characterize the biophysical consequences of internal deletions within dystrophin and utrophin. Here, we report that full-length utrophin exhibits a lower intrinsic thermal stability compared to dystrophin and displays a uniform thermal stability from N- to C-terminus. Additionally, internal deletion of spectrin-like repeats in utrophin is highly tolerated. In sharp contrast, we show that the thermal stability of dystrophin varies from N- to C-terminus, and internal deletion of hinge 2 though repeat 19 causes significant loss of protein stability.

Results

Biophysical analysis of utrophin and internally deleted utrophin proteins:

In the first biophysical comparison of dystrophin and utrophin, we performed circular dichroism spectroscopy on full-length utrophin and two large fragments encoding the N-terminus through spectrin-like repeat 10 and repeat 11 through C-terminus (Figure 4-1A). All three proteins exhibited similar alpha helical content (Figure 4-2A) as previously published for full-length dystrophin (105). Analysis of thermal denaturation revealed that all three utrophin proteins exhibited highly cooperative unfolding transitions at nearly identical melting points ($T_m \approx 49^{\circ}C$), which were 10 degrees lower than the T_m of full-length dystrophin (Figure 4-2B and Table 4-1).

We also performed circular dichroism analysis on four different utrophin constructs that we are investigating as a potential protein replacement therapy for DMD (39), each tagged with an 11 amino acid protein transduction domain of the HIV-1 TAT protein (TAT). All four proteins yielded highly alpha helical spectra similar to full-length utrophin (Figure 4-3). Full-length TAT-utrophin yielded a spectrum nearly identical to non-TAT-utrophin suggesting the TAT tag did not grossly affect protein structure. Despite differences in large internal deletions, all of the TAT-utrophin constructs displayed highly cooperative unfolding at very similar melting temperatures (Figure 4-3 and Table 4-1), which indicates that utrophin folding and thermal stability is uniform and unaffected by internal deletion.

In addition to thermal stability, we examined how the presence of non-native spectrin-like repeat junctions affected sensitivity to protease digestion. We subjected each protein, at a constant concentration, to increasing concentrations of the non-specific protease, proteinase K (28,40). Proteins with well-structured and compact folding are typically degraded at a slower rate than proteins with compromised folding or unstructured regions (41,42). We suspected that either the large deletions or non-native junctions would lead to a less stable protein and cause an increased rate of degradation compared to the native protein as previously reported by Ruszczak et al. (28) for small recombinant fragments of dystrophin. In contrast, we observed that each of the internally deleted utrophin proteins showed similar sensitivities to protease digestion compared to native protein (Figure 4-4, 4-5 and Table 4-1), which again suggests that internal deletions and resulting non-native junctions had little effect on utrophin stability. We conclude that utrophin exhibits a lower intrinsic thermal stability compared to dystrophin, but is uniformly stable from N- to C-terminus and is highly tolerant to internal deletion.

Biophysical analysis of truncated dystrophin proteins:

In stark contrast to the invariant biophysical properties of all analyzed utrophin constructs (Figures 4-4, 4-5, Table 4-I), truncated dystrophin proteins (Figure 4-1B) showed more marked differences in biophysical properties. Two recombinant fragments encoding the N-terminus through the first 10 or 17 spectrin-like repeats (Dys-N-R10, Dys-N-R17) exhibited significantly lower

melting transitions compared to full-length dystrophin, while the C-terminal retinal isoform DP260 and a construct encoding spectrin repeat 18 through C-terminus (Dys-R18-CT) melted at 10˚C higher than the full-length protein (Figure 4-6B and Table 4-1). Consistent with the results of Mirza et al. (40), we observed a double transition in DP260 at 50˚C and 70˚C (Figure 4-6C and Table 4-1), which is also apparent upon closer inspection of data previously reported for full-length dystrophin (37). Our data demonstrate that the thermal stabilities of dystrophin fragments are context-dependent. Note that despite differences in T_m between N- and C-terminal fragments of dystrophin, all displayed highly cooperative denaturation transitions (Figure 4-6B) indicative of well-folded proteins.

In order to better understand how the differential thermal stabilities of the N- and C-terminal regions affected the structural stability of the protein we compared the proteinase K resistance of full-length dystrophin protein with that of N- and C- terminally -deleted fragments. We found that the protease sensitivity of the C-terminal fragments of dystrophin, DP260 and Dys-R18-CT, were similar to the stability of the full-length protein. In contrast we found that a construct containing the N-terminus and the first 17 spectrin-like repeats was significantly ($p=<0.01$) more susceptible to PK degradation than either the full-length protein, DP260 or Dys-R18-CT, suggesting that the folding in N-terminal region is less compact (Figure 4-7 and Table 4-1) than the C-terminal region of the protein. Since the protease stability of full-length dystrophin aligned closely with Dys-R18-CT and DP260 (Figure 4-7, Table 4-1) but has a lower thermal stability compared

to the same C- terminal fragments, (Figure 4-6, Table 4-1) we conclude that the correlation between protease sensitivity and thermal stability for full length protein and large protein fragments is not as robust as previously observed for smaller dystrophin fragments (28,40).

Analysis of internally deleted dystrophin proteins:

Finally, we characterized two internally truncated mini-dystrophin constructs containing non-native junctions (Fig 4-1B). hDys-DH2-R19DCT is the cDNA that demonstrated the greatest efficacy in rescuing the dystrophic phenotype when transgenically over-expressed in *mdx* mice (15). mDysDH2-R19 is the corresponding mouse construct generated for the current study, which differs from hDys-DH2-R19DCT in that it encodes an intact C-terminus. Circular dichroism analysis revealed that the mouse construct with an intact C-terminus was highly alpha helical while the human construct lacking a portion of the C-terminus showed a stronger minimum at 209 nm (Figure 4-8A), suggesting an alternative fold had been adopted. Most surprisingly, we failed to detect a cooperative melting transition for either of the mini dystrophin proteins (Figure 4-8B). In fact, the unfolding isotherms (Figure 4-8B) were most similar to those exhibited by full-length dystrophin mutants bearing a variety of disease-causing missense mutations in the tandem CH domain (37). Despite the loss of cooperative unfolding with thermal denaturation (Figure 4-8B), both hDys-DH2-R19DCT and mDys-DH2-R19 displayed wild type sensitivities to proteinase K digestion, suggesting they were as stable as full-length dystrophin (Figure 4-8C

and D and Table 4-1).

To assess whether the protease stability of hDys-DH2-R19DCT and mDys-DH2-R19 was caused by aggregation, we measured the fraction of hDys-DH2-R19DCT and mDys-DH2-R19 pelleted by high-speed sedimentation compared to several well-folded, highly soluble controls (Figure 4-9A). We found that hDys-DH2-R19DCT but not mDys-DH2-R19 exhibited a significantly higher percentage of aggregated protein after purification compared to all other proteins tested (Figure 4-9B), which may help to explain the robust stability to protease challenge (Figure 4-8C and D). In addition to the solubility of proteins after purification, we examined the propensity of hDys-DH2-R19DCT and mDys-DH2-R19 to aggregate immediately after lysis of infected insect cells. Previously, we demonstrated that disease-causing missense mutations in ABD1 cause a large percentage of the mutant protein to be redistributed to the insoluble fraction of insect cells (37). We performed a similar analysis with hDys-DH2-R19DCT and mDys-DH2-R19 compared to full-length utrophin and internally deleted Tat-micro-utrophin ΔR4-21 (Figure 4-9C). Both utrophin and TAT-Utr-ΔR4-21 were found predominantly in the soluble fraction while both mini-dystrophin proteins were equally distributed between the insoluble and soluble fractions (Figure 4-9C). Thus, while prior studies clearly demonstrate that hDys-DH2-R19DCT can fully rescue the dystrophic phenotype of *mdx* mice when overexpressed (15), our *in vitro* biophysical analyses suggest that its thermal stability and solubility is compromised in comparison to full-length dystrophin, utrophin and numerous

truncated constructs. Furthermore, because N- and C-terminal fragments of dystrophin were all highly soluble (Figure 4-9A, B) and displayed highly cooperative unfolding transitions (Figure 4-6B), we suggest that the compromised stability/solubility of mini-dystrophins may be due to the presence of non-native protein junctions.

Discussion

Dystrophin and utrophin are related proteins that share multiple common structural domains (7,21). Not surprisingly, the highest level of sequence identity occurs in the N-terminal actin binding and the C-terminal dystroglycan binding domains. The central rod regions of dystrophin and utrophin display the lowest sequence identity with one another. Multiple studies have investigated the biophysical properties of dystrophin rod domain fragments and demonstrated marked heterogeneity in the stability of individual spectrin-like repeats (28,40). Despite these intrinsic differences between isolated modules, we recently demonstrated that full-length dystrophin unfolds in a highly cooperative, two-state manner (37). To assess whether the low level of sequence identity between dystrophin and utrophin translates into differences in protein stability, we performed the first biophysical characterization of full-length utrophin as well as an array of N-terminal, C-terminal, and internal truncated dystrophin and utrophin proteins. We report that like dystrophin, utrophin unfolds in a highly cooperatively manner, but with a lower melting temperature. Although utrophin exhibits lower thermal stability compared to dystrophin, it must be noted that utrophin is nonetheless a highly stable protein as it only unfolds at a temperature well above 37˚C.

We recently reported that dystrophin displays a melting point of approximately 60˚C (36), but here we show that this value is an amalgamation of the differing thermal stabilities of the N- and C-terminal portions (Figure 4-6) of

the full-length protein. The N-terminal half of dystrophin exhibits a cooperative transition at approximately 50˚C while the C-terminal half exhibits a cooperative transition at over 70˚C. In contrast, utrophin showed little change in stability from N- to C-terminus and we observed nearly identical unfolding transitions for several internally deleted utrophin constructs. Most notable from the perspective of therapeutic development, we observed no cooperative transition during thermal denaturation and significant protein aggregation for two internally deleted dystrophin mini-gene constructs (Figures 4-8 and 4-9). One of the mini-dystrophin constructs analyzed here has previously shown to effectively prevent dystrophy in the *mdx* mouse, albeit at expression levels that greatly exceeded dystrophin expression in normal skeletal muscle (15). Because our analyses relied on proteins expressed in insect cells, it remains possible that mini-dystrophin folding may be more efficient in mammalian cells, or muscle cells in particular. Equally notable, however, our findings with mini-dystrophins expressed in insect cells were analyzed in parallel with an array of 11 dystrophin and utrophin constructs that displayed full solubility and highly cooperative unfolding transitions. Therefore, we believe that our biophysical analyses of recombinant dystrophin and utrophin constructs provides the basis for a rapid and highly sensitive assay of protein stability that may be useful in optimizing mini- or micro-gene constructs prior to extensive testing in animals.

Our results establish the importance of protein stability as a new factor to consider in the design of therapeutic vectors for the treatment of DMD. While our

results on a limited number or internally deleted dystrophin and utrophin constructs immediately suggest that utrophin is more amenable to the sequence deletions necessary for AAV-mediated gene therapy approaches, we believe they also provide the basis for a functional assay to engineer more stable miniaturized dystrophin constructs as well. Finally, further analysis of junctions within internally truncated dystrophins modeling exonic deletions in Becker muscular dystrophy patients may provide a basis for the variability in protein expression and phenotype seen in these patients (43,44).

Experimental Procedures

Cloning: TAT-Flag-Utrophin protein coding sequences were assembled using PCR as described in (39). The construction and characterization of DP260 was previously described by Prins et al. (45). Flag DysR18-CT was also assembled using PCR and cloned into pFastBac Dual. The human mini-dystrophin cDNA was obtained from the Chamberlain lab and cloned into pFastBac using PCR and restriction digest. Mouse mini-dystrophin was assembled by PCR from full-length cDNA and cloned into pFastBac using restriction digest.

Expression and Purification: All proteins for this study were expressed by Kinnakeet Biosciences in Sf9 insect cells using the Bac-to-Bac expression system (Invitrogen). Expressed proteins were purified using Flag affinity chromatography (Sigma-Aldrich) and dialyzed in two changes of phosphate buffered saline at pH 7.5. After purification proteins were concentrated using either 50 kDa or 100 kDa cut-off centrifuge-based concentrators (Millipore). Protein concentration was determined by D_c protein assay (Bio-Rad) with a bovine serum albumin standard curve.

Circular Dichroism: CD spectra and melt curves were acquired as previously described (37). Briefly, measurements were acquired on a Jasco J-815 spectropolarimeter. Temperature was varied from 20 to 90˚C using an attached Peltier thermal regulator. Each protein was assayed with at least two different purifications and at least two different concentrations between 0.15 and 0.5 mg/ml. CD spectra were collected between 200 and 260 nm at 20˚C at pH 7.5 in

PBS. Melting point analysis was assayed by collecting spectra between 200 and 240 nm for every degree of temperature change and displayed by plotting the change at 222 nm. Data was fit using regression analysis in Sigma Plot (Systat Software) using a two state unfolding model to obtain a melting point (46).

Protease Sensitivity Assay: Each protein was assayed at constant concentration of 0.15 mg/ml for sensitivity to a non-specific protease, proteinase K, similar to Ruszczak et al. (28). Samples were subjected to no PK and a range of PK from 1.5 ng to 0.003 ng. Every other sample represents a 1:10 dilution. Each series was incubated at 37˚C for 30 minutes then subjected to SDS-PAGE. Poly-acrylamide gels were stained with Coomassie blue and remaining full-length protein was quantitated using software from UVP Bioimaging Systems. Values were fit using first order exponential decay regression analysis in Sigma Plot to obtain a value that represents the PK concentration (ng) where ½ of the full-length protein is still present (PK_{50}).

Analysis of aggregates and insoluble protein: For sedimentation analysis of purified proteins each protein was subjected to ultracentrifugation at 100,000 x *g* to separate large molecular weight aggregates from soluble protein. The resulting supernatant and pellet fractions were separated by SDS-PAGE and the coomassie-stained gels were quantitated using densitometry. Analysis of soluble and insoluble proteins was performed in Sf21 insect cells by baculovirus expression. An identical viral load to large-scale expressions was used to standardize expression levels. Cells were infected and incubated for 72 hours.

The resulting cell pellets were lysed and solubilized identically to large-scale purifications as before (37). Each sample was centrifuged at 14,000 x *g* for 20 minutes to separate the soluble and insoluble fraction of the lysed insect cells. The pellet was resuspended in 6 M urea in PBS and incubated at 50˚C to solubilize aggregated protein. 5x SDS protein sample buffer was then used to solubilize any remaining protein. The soluble and insoluble fractions were then separated by SDS-PAGE and transferred to PVDF membranes. Membranes were then immunoblotted using a monoclonal anti-Flag® antibody (Sigma) as recommended by the manufacturer. Goat anti-mouse Li-cor secondary antibody was used to detect primary antibodies and resulting membranes were imaged on a Li-cor Odyssey infrared scanner.

Figures

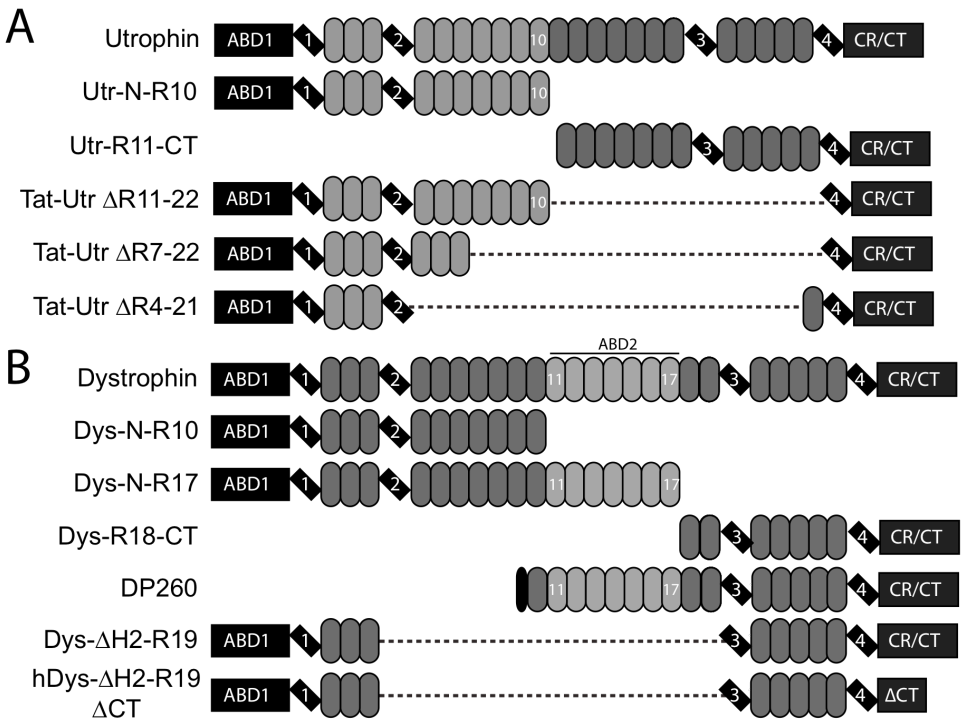

Figure 4-1: **Domain structure of proteins analyzed.** (A and B) Tilted rectangles represent hinge regions, ovals represent spectrin-like repeats, lighter shaded ovals represent spectrin-like repeats that participate in actin binding and dashed lines represent deleted region. (A) Utrophin proteins analyzed. (B) Dystrophin proteins analyzed.

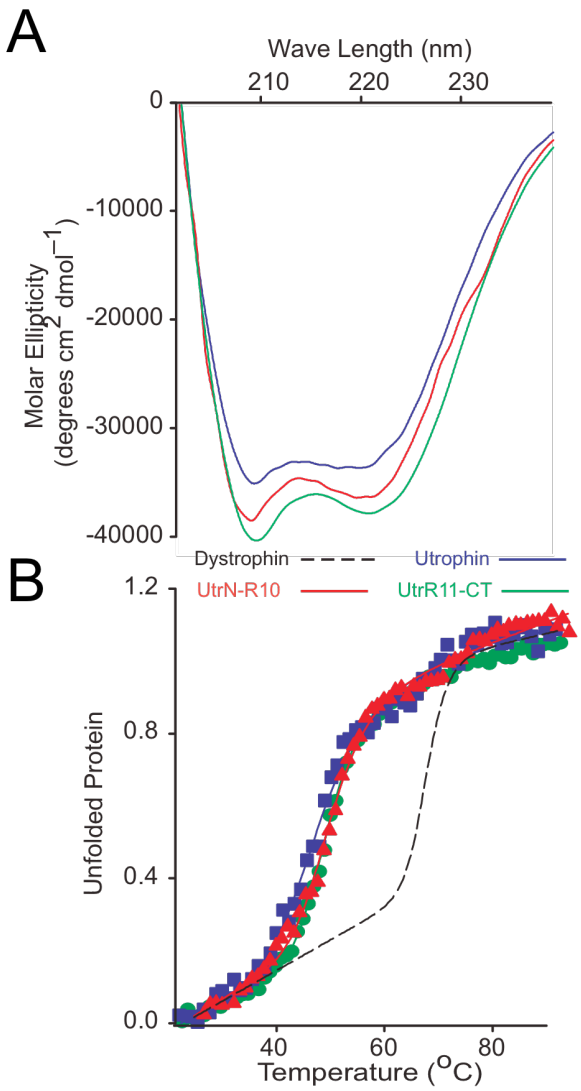

Figure 4-2: **Circular dichroism analysis of utrophin.** (A) Far UV spectra of full-length utrophin (blue line), Utr-N-R10 (red line) and Utr-R11-CT (green line). (B) Thermal unfolding of utrophin, Utr-NT-R10 and Utr-R11-CT from 20 to 90 ˚C. Dashed line represents previously published full length dystrophin thermal unfolding provided for reference.

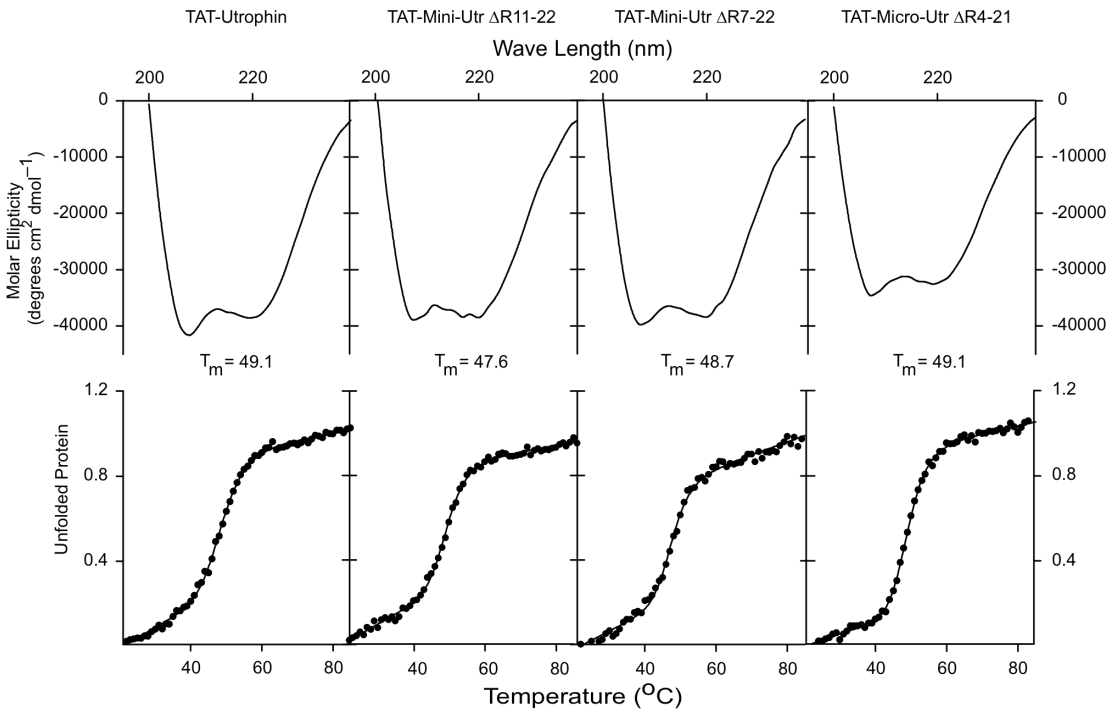

Figure 4-3: **Circular dichroism analysis of TAT-utrophin proteins.** (Top) Far UV spectra of TAT-utrophin and internally deleted TAT-utrophin proteins. (Bottom) Thermal unfolding of TAT-utrophin and internally deleted TAT-utrophin proteins.

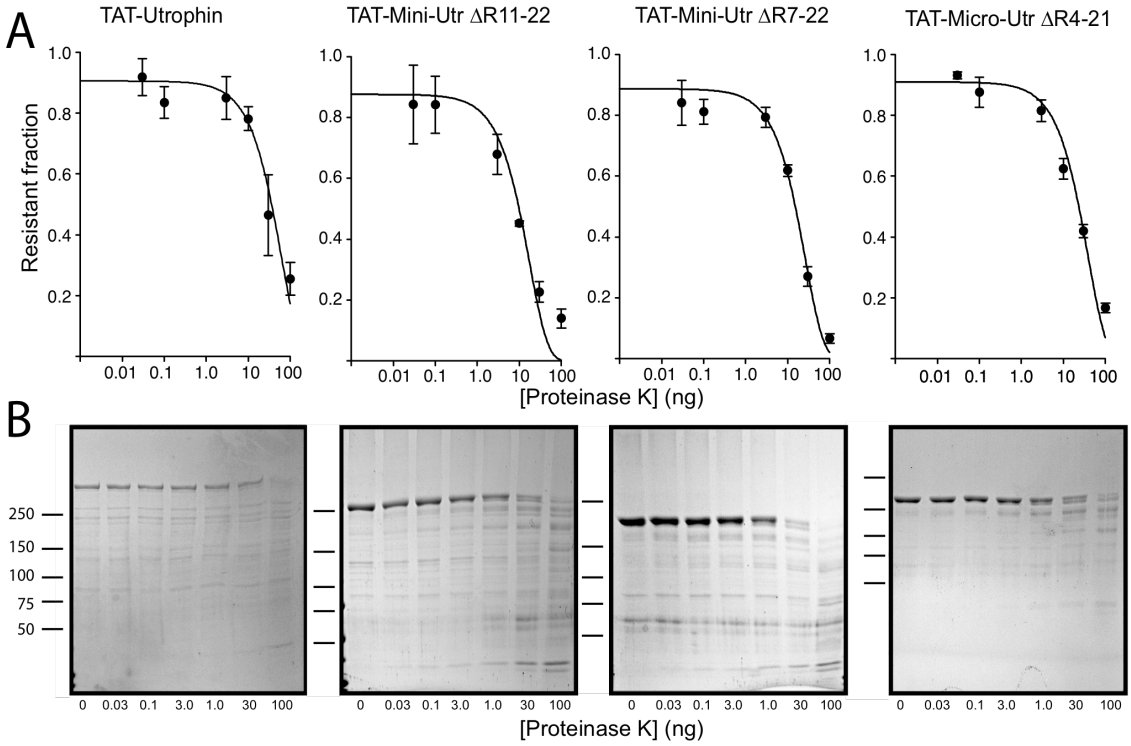

Figure 4-4: **Protease sensitivity analysis of TAT-utrophin proteins.** (A) Exponential decay plots representing the fraction (ng) of TAT-utrophin protein remaining over a range of proteinase K concentrations. Data were plotted using a log scale and fit to a first order exponential decay function using regression analysis. Error bars represent standard error of the mean (SEM). (B) Representative Coomassie stained SDS polyacrylamide gels.

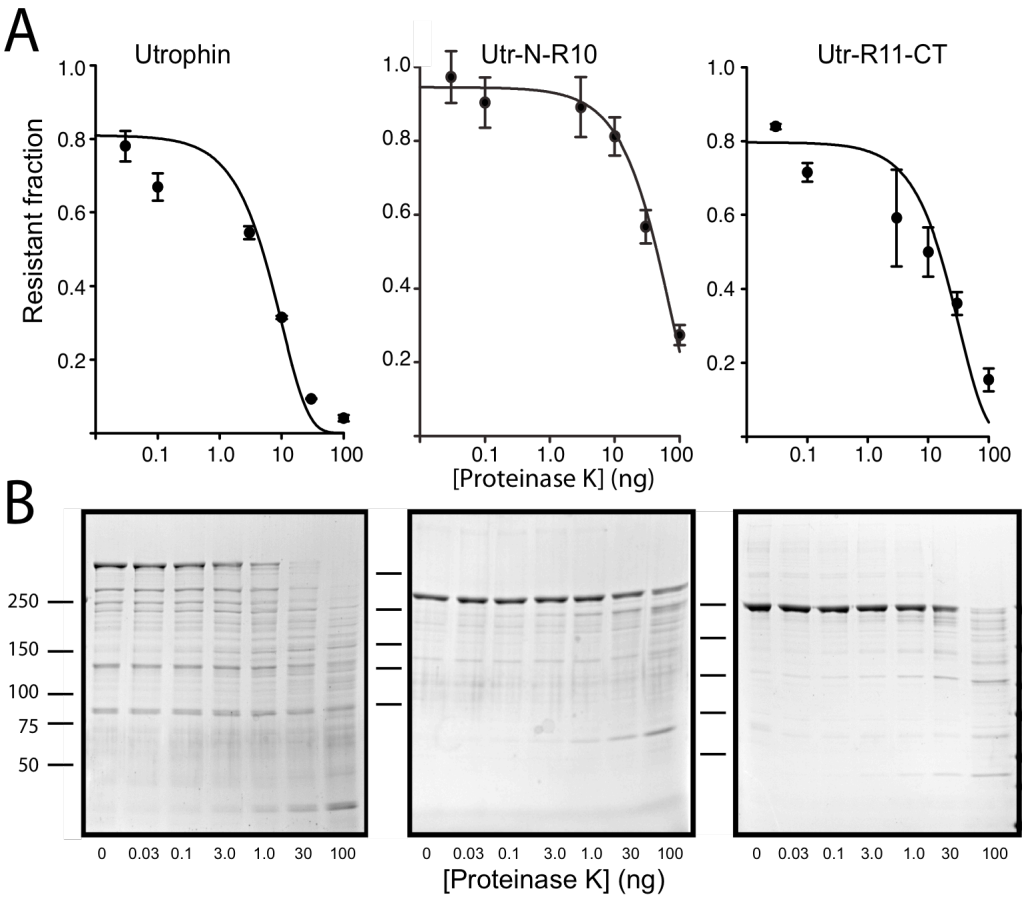

Figure 4-5: **Protease sensitivity analysis of Utrophin proteins.** (A) Exponential decay plots representing the fraction (ng) of utrophin protein remaining over a range of proteinase K concentrations. Data were plotted using a log scale and fit to a first order exponential decay function using regression analysis. Error bars SEM (B) Representative Coomassie stained SDS polyacrylamide gels of a protease sensitivity assay.

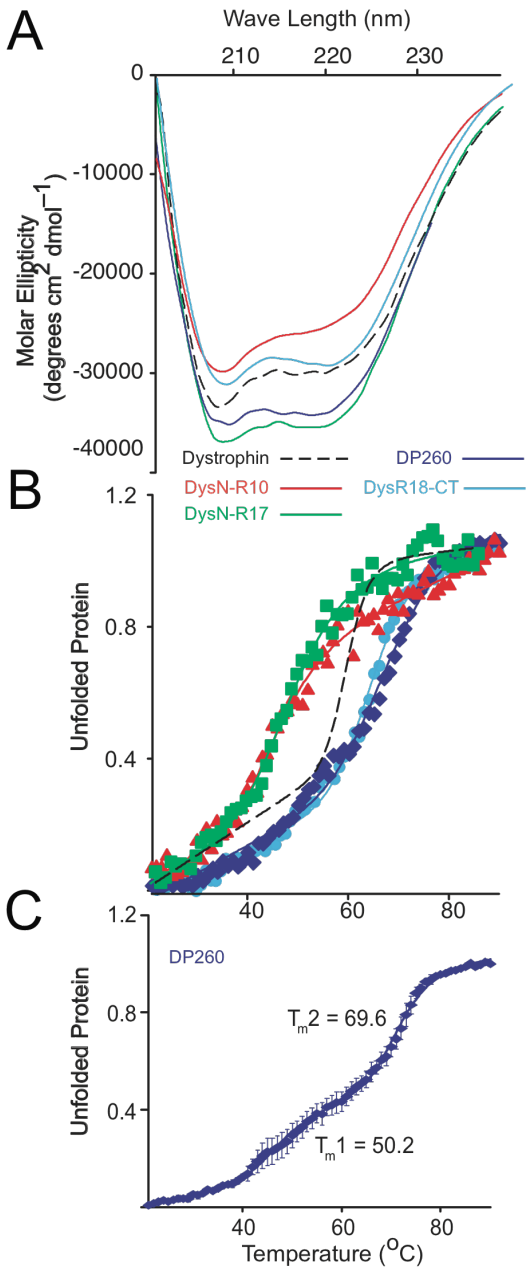

Figure 4-6: **Circular Dichroism Analysis of dystrophin proteins.** (A) Far UV spectra of Dys-N-R10 (red), Dys-N-R17 (green), DP260 (blue) and DYS-R18-CT (light blue). (B) Thermal unfolding analysis of Dys-N-R10, Dys-N-R17, DP260 and Dys-R18-CT. (A and B) Dashed line represents previously published data for full-length dystrophin for reference. (C) Detailed thermal unfolding of DP260 showing two transitions states.

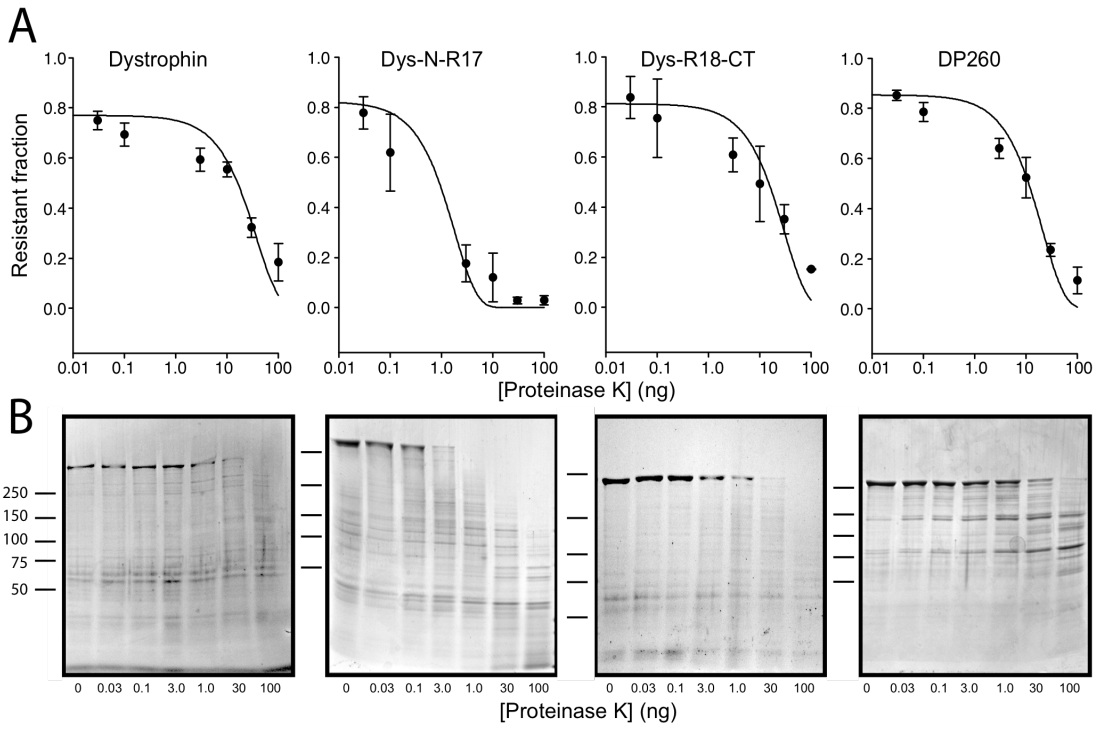

Figure 4-7: **Protease sensitivity analysis of dystrophin proteins.** (A) Exponential decay plots representing the fraction (ng) of dystrophin protein remaining over a range of proteinase K concentrations. Data were plotted using a log scale and fit to a first order exponential decay function using regression analysis. Error bars represent SEM. (B) Coomassie stained SDS polyacrylamide gels of a representative protease sensitivity assay.

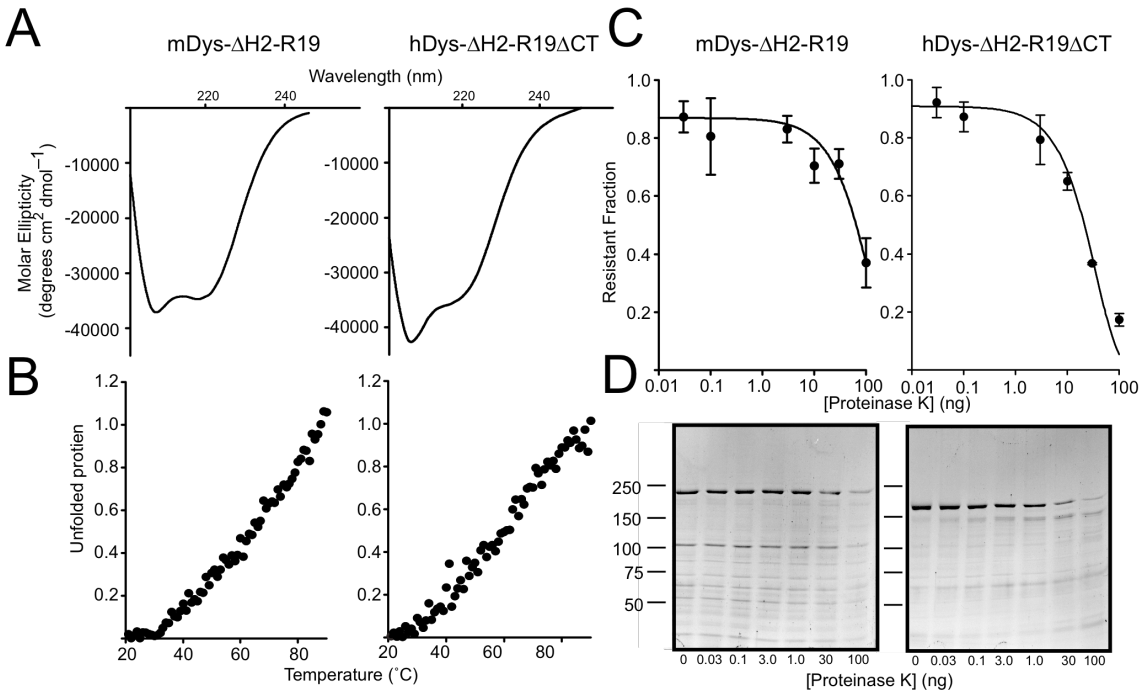

Figure 4-8: **Analysis of mini-dystrophin proteins.** (A) Far UV spectra of mouse and human mini-dystrophin proteins. (B) Thermal unfolding of mouse and human mini dystrophin. No cooperative transition is observed for either protein. (C) Protease sensitivity decay isotherm for human and mouse mini-dystrophin proteins. Error bars represent SEM. (D) SDS polyacrylamide gels representing typical protease sensitivity assays for human and mouse mini-dystrophin.

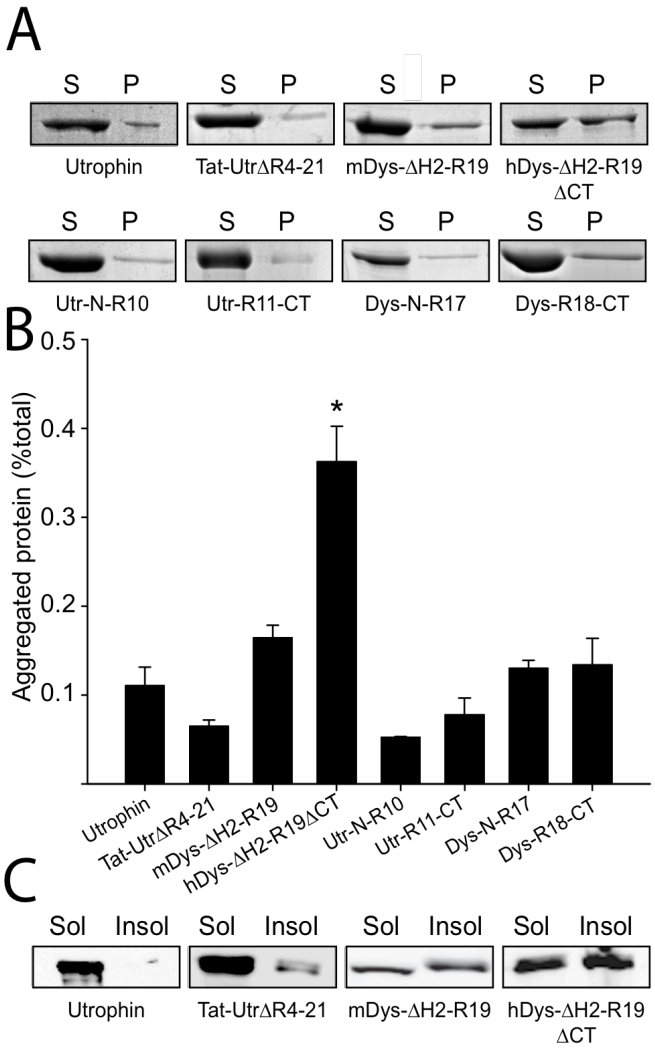

Figure 4-9: **Aggregation and solubility of mini-dystrophins.** (A) High speed sedimentation assessment of purified protein aggregation levels. Supernatant and pellet fractions for each protein tested. (B) Densitometry analysis of SDS gels in A. Analysis was performed on 3-5 independent experiments. Error bars represent SEM. (C) Anti-Flag immunoblots of the soluble and insoluble fractions of Sf21 insect cells expressing utrophin, TAT-UtrΔR4-21, mDysΔH2-R19 or hDysΔH2-R19ΔCT.

Table 4-1: **Melting point and Pk_{50} values for each protein assayed**.

	T_m (˚C)	PK (ng)
Utrophin	48.7 ± 0.64	7.0 ± 0.08
Utr-N-R10	48.2 ± 0.40	51.1 ± 8.4
Utr-R11-CT	48.2 ± 0.40	22.8 ± 7.7
TAT-Utrophin	49.1 ± 0.19	43.4 ± 11.6
TAT-UtrΔR11-22	48.6 ± 0.28	12.8 ± 1.49
TAT-UtrΔR7-22	47.6 ± 0.18	18.9 ± 2.38
TAT-UtrΔR4-21	49.1 ± 0.12	27.7 ± 0.92
Dystrophin	59.6 ± 0.29 [38]	25.1 ± 2.09
Dys-N-R10	46.1 ± 1.13	nd
Dys-N-R17	50.9 ± 1.37	0.19 ± 0.10
DysR18-CT	65.5 ± 0.76	29.5 ± 4.9
DP260	50.2 ± 1.63, 69.6 ± 2.73	15.1 ± 3.39
DysΔH2-R19	na	89.4 ± 22.7
hDysΔH2-R19ΔCT	na	25.25 ± 0.79

Chapter 5: Conclusions and Discussion

My major findings are: (1) that the dystrophin-actin interaction is not affected by actin isoform, (2) that the C-terminus of dystrophin contributes to the full actin binding activity of dystrophin even though it does not itself bind directly to actin, (3) that disease causing missense mutations in dystrophin cause protein instability and aggregation and (4) that internal sequence deletion of dystrophin results in protein instability and aggregation. In the following sections, I will discuss how my findings enhance our understanding of dystrophin structure/function and its role in muscular dystrophy.

Actin Binding Properties of Dystrophin

Early dystrophin-actin binding studies reported conflicting results when testing whether the affinity for different actin isoforms varied (13, 82). However, previous claims that dystrophin preferentially bound one actin isoform over another relied on fragments encoding the isolated ABD1 and comparisons between studies performed by different laboratories. My results in chapter 2 demonstrate that full-length dystrophin protein exhibits no measureable difference in affinity for three of the actin isoforms expressed in skeletal muscle.

While it seems that the high affinity interaction between dystrophin and actin filaments is a simple and straightforward biochemical process, my thesis research details several cases for more complex activity than was expected. Chapter 2 examined in parallel the contributions of each dystrophin ABD to the activity of the full-length protein. We showed that a fragment with both ABDs but lacking the C-terminal third of the protein did not fully recapitulate the actin binding properties of the full-length protein. The C-terminal third did not interact directly with actin filaments but may serve to stabilize an optimal actin binding conformation. When a portion of the C-terminus was linked to the N-terminal ABD in the internally deleted DysΔH2-R19 protein, no increased affinity was measured compared to a protein containing ABD1 with no C-terminus. Additionally, no increase in affinity was seen when the C-terminal third of the protein was linked to ABD2 in DP260. DP260 interacted with actin filaments with a similar affinity as the previously published value for isolated ABD2 (50).

Therefore, both ABDs and the C-terminal third of dystrophin must be present in cis for full actin binding activity (Figure 2-6 p. 39).

One of the main differences between dystrophin and utrophin is that the dystrophin ABDs are separated by a long flexible linker of 10 spectrin-like repeats. Additionally, the C-terminal third of dystrophin is significantly more thermally stable than the rest of the molecule and is more stable than utrophin. The stability of the C-terminal region also influences the overall stability of the full length protein. One would expect that the 50˚C melting point of the N-terminal half of dystrophin and the 70˚C stability of the C-terminal half of dystrophin would manifest as two distinct thermal transitions in the full length protein. Instead, we observed one cooperative melting point exactly half way between the values observed for the N- and C-terminal halves, which indicates that the C-terminal region of dystrophin allosterically influences the stability of the whole molecule. Perhaps, the allosteric influence of the C-terminal region stabilizes a conformation that allows for maximal actin binding affinity in addition to increasing stability. Moreover, further experiments looking at the distinct biochemical features of the dystrophin C-terminal region and differing mode of contact to actin may help us to understand why utrophin expression is restricted to specialized regions later in life. Altogether, it seems that dystrophin has evolved a more complex domain structure and possibly higher order function than utrophin.

Pathomechanism of Dystrophin Disease Causing Mutations

The primary focus of this thesis was to understand how a single amino acid change in a very large protein might lead to disease as severe as a null. We chose to examine 6 mutations localized to ABD1 of dystrophin and hypothesized that we would observe a decrease in actin binding activity. However, we found that only two mutations produced a modest loss of actin binding activity, while the remaining 4 mutations had no significant effect on actin binding activity. As it turned out, all of the mutations we investigated induced thermodynamic instability and increased protein aggregation. We know from work in other fields that mutations that lead to protein aggregation or mislocalization due to instability lead to a number of severe diseases such as cystic fibrosis and Huntington's disease. The well characterized ΔF508 mutation in the cystic fibrosis transmembrane conductance regulator (CFTR) prevents trafficking from the ER to the plasma membrane where the channel normally functions and also triggers premature degradation of the protein. Destabilizing mutations in dystrophin may have a similar effect in that misfolded dystrophin cannot escape the chaperone machinery and is either degraded or becomes aggregated in the cytosol. Our results are the first to implicate aggregation as a possible mechanism for dystrophinopathies.

It is clear from our results comparing the native dystrophin protein and a multitude of dystrophin fragments that disease causing mutations in ABD1 lead to instability and aggregation. However, it would be informative to examine the fate

of mutant dystrophins expressed in mammalian cells or as transgenes in the *mdx* mouse. We feel it is likely that these mutant dystrophin proteins would have a decreased protein half-life and/or disrupted sub-cellular localization and understanding which of these mechanisms leads to disease would point the way for treatments or therapy.

Importantly, the results in Chapter 3 establish that disease-causing missense mutations retain a high level of biochemical function despite having mutations in a critical ligand binding domain. Therefore, drugs that increase the protein levels of mutated dystrophin in patients could result in a milder or disease free phenotype. Many drugs that target the protein quality control machinery in the cell have shown promise in increasing the levels of proteins, such as CFTR, that are unstable due to mutation. Given the results presented here, this class of drugs could also be beneficial to DMD, BMD or XLCM patients with destabilizing missense mutations in dystrophin.

Instability of internally deleted dystrophin proteins

The finding that internal deletion of the dystrophin (Dys-ΔH2-R19) protein led to thermodynamic instability and aggregation was surprising to us due to the success of gene therapy studies which used the same construct. However, after carful review of the literature we noted that the expression level of the miniaturized dystrophin protein (DysΔH2-R19) was substantially higher than that of the native protein in muscle. We concluded from our research in Chapter 4 that the non-native junction created between repeat 3 and hinge 3 in the DysΔH2-R19 construct was the cause of protein instability. Thus, the ligand binding domains are likely still functional. High levels of DysΔH2-R19 expression would allow a substantial portion of the protein produced to evade quality control machinery and facilitate proper localization and incorporation into the DGC. At low levels of expression, which would eventually result from loss or mutation of viral DNA, it seems likely that the protein would not retain the proper localization to stabilize the membrane but instead be sequestered by protein quality control machinery in the cell. Determining the stability and half-life of the protein products expressed in gene therapy is key to long-term success and, to date, has only been performed on a handful of constructs now in use.

A major consideration for gene therapy protein products is their potential immunogenicity. Immune responses to exogenously expressed dystrophin proteins have been observed in clinical trials investigating the functionality of miniaturized dystrophin proteins. Since DMD patients do not express dystrophin,

the observed immune responses may simply be due to the introduction of a non-self protein. However, a more robust immune response may be seen if the miniaturized dystrophin protein introduced has the potential to aggregate or is partially misfolded. Misfolded or aggregated proteins can stimulate an innate immune response (111). Innate immune cells such as macrophages are found at high levels in DMD patients due to the high rate of tissue damage and clearance caused by contraction-induced injury (112). A recent study (87) of DMD patients that received a virally delivered, miniaturized dystrophin construct reported very limited protein expression combined with a robust immune response to the therapeutic protein. Misfolded proteins typically aggregate to minimize solvent exposure of hydrophobic portions that are normally buried (113). A possible mechanism for low miniaturized dystrophin protein expression in clinical trials is that macrophages and other innate immune cells target hydrophobic regions of misfolded protein and present them to the active immune system, which in turn activates a long-term immune response to the hydrophobic peptide created by the non-native protein junction (111).

Another mechanism for the immune response seen in patients expressing a miniaturized dystrophin protein (87) is recognition of the dystrophin protein as a non-self antigen. MHC class I receptors display peptides of degraded intracellular proteins extracellularly to immune cells, which recognize antigens that are non-self. Presented peptides are predominantly sourced from newly synthesized proteins that have been targeted for degradation due to misfolding

(114, 115). Approximately 18-37% of newly synthesized proteins are degraded due to stalling as folding intermediates (114, 115). In cases where folding is complex or unusually inefficient, the proteins involved are over-represented as MHC class I antigens (114). In the recent study of DMD patients (17), virally-delivered, miniaturized dystrophin protein was recognized by CD8+ T-cells as a non-self antigen. Since dystrophin proteins bearing non-native protein junctions may be unstable it is reasonable to assume there would be an increased amount of stalled or improperly folded protein produced which would lead to an over-representation of dystrophin peptides in MHC Class I peptide display. It remains possible that the observed CD8+ T-cell response and loss of therapeutic protein expression may be due in part to over-representation of mini-dystrophin protein in MHC class I antigen display.

In addition to implications for gene therapy the finding that internally deleted dystrophin proteins can be unstable relates to the disease severity of BMD patients. BMD is typically caused by the splicing out of exons during mRNA maturation that leads to an in-frame but internally deleted dystrophin protein. During the construct design for gene therapy the phasing and domain boundaries for internal deletion are carefully considered. When exons are spliced together the phasing and domain organization are often not ideal. Exon boundaries in the dystrophin gene typically do not correlate well with protein domain phasing. Therefore, when aberrant splicing occurs, unorganized and possibly misfolded protein domains are created. It is clear from variable BMD patient disease

severity that deletions can result in phasing that leads to a range of outcomes from minimal protein perturbation to highly unstable proteins. Correlating disease severity with the degree of protein instability will help to explain how internal deletion of dystrophin in BMD patients leads to disease and may point the way to new therapies for BMD patients.

Exon skipping to treat DMD also relies on the presumed functionality of proteins bearing non-native junctions. The premise of exon skipping is that the deleterious mutation in a DMD patient will be excluded from the mRNA by introduction of an oligo-nucleotide that blocks splice acceptors or donors of the exon containing the mutation. Of course, more than one exon must be skipped if the reading frame is disrupted with only the disease harboring exon skipped. Here too, it is important to determine the stability of the protein products expressed once proper skipping is achieved. Screening the possible protein products of exon skipping would identify a skipping strategy that would benefit the largest number of patients and create the most stable protein possible. Additionally, one cocktail of oligo-nucleotides could be identified that creates a stable protein and would help the largest number of patients. The successful cocktail could be brought to clinical trials as a single drug instead of bringing multiple drugs, targeting many exon combinations, through the expensive and time consuming clinical trial process.

Based on sequence similarity, dystrophin and utrophin share a remarkably similar domain structure and it was surprising to observe that the thermal stability

of the full-length proteins differed by 10˚C (60˚C for dystrophin and 50˚C for utrophin). Even more striking, the cooperative transition of dystrophin at 60˚C turned out to be an amalgamation of the 50˚C transition for N-terminal half of the protein and the 70˚C transition for the C-terminal half. In contrast, each utrophin protein tested for thermal stability whether it was the full-length protein, a N-terminal fragment, a C-terminal fragment, or an internally deleted protein had a cooperative transition at 50˚C. In sharp contrast to the instability of the internally deleted dystrophin proteins we tested, the three utrophin internal deletions examined were remarkably stable and soluble.

It is possible that the stability of internally deleted utrophin proteins is due to the homogeneity of the utrophin protein. In contrast, the instability of the dystrophin protein may be due to the heterogeneity of the repeats joined together to create an internally deleted dystrophin protein. To date, all constructs designed with internal deletions of dystrophin retain spectrin-like repeats from the N- and C-terminal halves of the protein. The joining of repeats from the N-terminal region of the protein, which has a moderate thermal stability, to repeats in the C-terminal region, which has a high thermal stability may be incompatible. Perhaps, including only N-terminal or only C-terminal repeats in conjunction with the essential ligand binding domains would result in more stable internally truncated proteins.

A recent study by Suarez et al. may help us to understand the mechanical forces that lead to protein destabilization in internally deleted dystrophin proteins.

Suarez and colleagues expands and refines the currently accepted model of how cofilin severs actin filaments. Cofilin is an actin severing protein that serves to increase actin polymerization through increasing available filament ends for monomers to add on to. The model postulates that cofilin binds to actin filaments and increases their flexibility and mobility at a localized region of the filament. Due to the cooperative nature of cofilin binding an incoming cofilin molecule always binds next to a bound cofilin. This cooperativity creates boundaries of cofilin bound f-actin and cofilin free f-actin. The mechanical contrast between the flexible and mobile cofilin bound filament and the naked filament builds up shear stress and increases the likelihood of severing occurring at that boundary. Perhaps the contrasting mechanical properties of the linked SLRs in the internally deleted dystrophin proteins also build up shear stress though a similar mechanism. The dissimilar mechanical properties of juxtaposed N- and C-terminal SLRs could result in localized unfolding. Therefore, mechanical stress may be a possible mechanism for the aggregation and loss of cooperative thermal transition we observed with internally deleted dystrophin proteins. Understanding the mechanism by which the non-native boundary in these proteins leads to instability is paramount in creating a stable protein product for DMD gene therapy.

Going Forward

My thesis research raises new questions and the following section sets forth a course of action to address them

How does the C-terminus of dystrophin increase affinity for actin filaments?

We know that the C-terminal third of dystrophin increases the effectiveness of ABD1 and ABD2 when joined in cis to these domains. The C-terminal region is also significantly more thermally stable than the N-terminal region of dystrophin. It seems likely that the C-terminal third of dystrophin would most dramatically alter the effectiveness of ABD2 since they are directly in contact with one another. Therefore, measuring the dynamic nature and mobility of ABD2 when bound to actin filaments alone or joined to the C-terminus may provide some hint of the structural conformation that facilitates full actin binding activity. To accomplish this measurement, cysteines could be engineered into strategic locations in ABD2 and labeled with a dye that would participate in Förster resonance energy transfer with another dye labeling actin filaments. The resulting distance measurements could establish a model for how ABD2 interacts with actin filaments and give clues as to how the C-terminal third of dystrophin affects ABD2. Presumably, cysteines localized, and possibly labeled in the non-actin binding C-terminus of dystrophin would not interfere with the measurement because they would be too far away from the bound filament. On the other hand, if there were inference then that would also give us an idea of how the C-terminal region of dystrophin enhances actin binding activity.

What is the fate of dystrophin bearing a missense mutation in vivo?

Current research in our laboratory is striving to answer this question using many techniques. Establishing the sub-cellular localization of dystrophin harboring disease-causing mutations in a relevant cell line would help us understand how aggregation-prone dystrophin protein is trafficked. Additionally, protein levels with and without a proteasome inhibitor would establish the level of protein turnover occurring when aggregation-inducing mutations are present. These experiments could also facilitate the screening of compounds aimed at increasing functional protein levels in patients with protein destabilizing dystrophin mutations. Moreover, there are many disease-causing mutations found in other ligand binding domains of dystrophin that may also lead to instability or affect ligand binding function. Studies are underway to evaluate the effects of mutations localized to the beta-dystroglycan binding domain of dystrophin and mutations that localize to the recently discovered microtubule-binding domain of dystrophin. To date, only a handful of mutations have been examined and all have led to protein destabilization to some degree. In the future, further investigation may uncover mutations that exert their pathogenesis though loss of function instead of loss of protein stability and could help us to better understand the key residues required to support actin and beta-dystroglycan binding.

How does internal deletion lead to dystrophin instability?

Our finding that internal deletion of dystrophin leads to instability was surprising, since each of the utrophin constructs tested in a similar manner behaved normally and because the same coding sequence was successful in rescuing disease. The level at which the internally deleted dystrophin protein was expressed helps us understand how it can rescue disease, but it does not explain the striking difference between the stability of utrophin derived internal deletions. The spectrin-like repeats in dystrophin were thought to be interchangeable due to a presumed similar structure. However, no structure has been solved for a dystrophin or utrophin spectrin-like repeat. It is clear from stability studies in my thesis, as well as by others, that repeats in the C-terminal third of the dystrophin protein are more stable than those localized to the N-terminal region. Additionally, we know from this thesis that utrophin repeats have a uniform stability and internal deletion is well tolerated. Thus, the joining of repeats in dystrophin with differing stabilities may be the cause of the decreased stability. In any case, the therapy constructs derived from the dystrophin cDNA should be optimized for increased stability, which can be accomplished in multiple ways.

First, and most obviously, more internally deleted dystrophin proteins should be screened for stability. These data would help organize an approach to design the most stable combination of repeats to test in animal models and clinical trials.

Once a candidate construct has been selected, it can be optimized to produce a highly stable and soluble protein. Stability optimization can be focused in a number of ways but is dependent on knowing whether a particular region of the internally deleted protein causes instability. We know that dystrophin fragments lacking a N- or C-terminus are stable but when two ends are joined instability may ensue. If the junction is to blame, a relatively small region of about 15 to 30 amino acids can be randomly changed to make a library of candidate proteins to be screened for increased stability. If the problem resides in the joining of repeats that are not optimized to work together then a library encompassing random changes throughout the rod region of the construct should be screened to achieve an increase in stability. Screening can be performed in multiple ways, but using an *in vivo* split GFP solubility and expression level reporter assay would be fast and require little hands-on time.

Does differential thermal stability of the N- and C-terminal domains of dystrophin correlate with extensibility and/or flexibility?

Understanding the mechanism(s) by which dystrophin and utrophin protect the membrane from contraction induced injury may help in the design of better gene therapy proteins in the future. Utrophin has one continuous ABD stretching from the tandem CH domain to spectrin-like repeat 10. The entire utrophin protein has a consistent thermal stability of 50˚C. If flexibility and extensibility of the protein correlate with stability then the whole rod domain would act as a uniform spring extending as membrane stress increases during contraction. If

repeats 1-10 of utrophin, which are required for high affinity actin binding, become stretched during contraction they may adopt an extended conformation that decreases utrophin's affinity for actin. It would be interesting to measure the affinity of utrophin for actin filaments using isothermal calorimetery where binding could be measured at varying temperatures.

Dystrophin on the other hand has two ABDs separated by a spacer of 10 spectrin-like repeats. We know from Chapter 4 of this thesis that the 10 repeat spacer is more sensitive to protease challenge, suggesting a more breathable conformational state. Additionally, it has a lower thermal stability and contains multiple repeats that are unstable without the presence of a neighboring repeat. Moreover, the C-terminal region of dystrophin is very thermally stable. If decreased thermal stability and increased protease sensitivity correlate with increased flexibility then the 10 repeat spacer may act as an extensible spring between the important ABDs. To answer these questions, atomic force microscopy experiments testing the extensibility of rod domains of dystrophin and utrophin are now underway.

References

1 S, O.O. and Saitou, N. (1999) Phylogenetic relationship of muscle tissues deduced from superimposition of gene trees. *Mol. Biol. Evol.*, **16**, 856-867.

2 Verma, S., Anziska, Y. and Cracco, J. (2010) Review of Duchenne muscular dystrophy (DMD) for the pediatricians in the community. *Clin. Pediatr. (Phila).* **49**, 1011-1017.

3 Hoffman, E.P., Brown, R.H., Jr. and Kunkel, L.M. (1987) Dystrophin: the protein product of the Duchenne muscular dystrophy locus. *Cell Tissue Res.*, **51**, 919-928.

4 Koenig, M., Hoffman, E.P., Bertelson, C.J., Monaco, A.P., Feener, C. and Kunkel, L.M. (1987) Complete cloning of the Duchenne muscular dystrophy (DMD) cDNA and preliminary genomic organization of the DMD gene in normal and affected individuals. *Cell*, **50**, 509-517.

5 Chamberlain, J.S. (1992) X-linked dystrophies: from gene localization to gene therapy. *Curr. Opin. Neurol. Neurosurg.*, **5**, 610-614.

6 Kunkel, L.M., Hejtmancik, J.F., Caskey, C.T., Speer, A., Monaco, A.P., Middlesworth, W., Colletti, C.A., Bertelson, C., Muller, U., Bresnan, M. *et al.* (1986) Analysis of deletions in DNA from patients with Becker and Duchenne muscular dystrophy. *Nature*, **322**, 73-77.

7 Hoffman, E.P. (1993) Genotype/phenotype correlations in Duchenne/Becker dystrophy. *Mol. Cell Biol. Hum. Dis. Ser.*, **3**, 12-36.

8 Ervasti, J.M. and Campbell, K.P. (1993) A role for the dystrophin-glycoprotein complex as a transmembrane linker between laminin and actin. *The Journal of Cell Biology*, **122**, 809-823.

9 Ervasti, J.M. and Sonnemann, K.J. (2008) Biology of the striated muscle dystrophin-glycoprotein complex. *Int. Rev. Cytol.*, **265**, 191-225.

10 Rybakova, I.N., Patel, J.R. and Ervasti, J.M. (2000) The dystrophin complex forms a mechanically strong link between the sarcolemma and costameric actin. *The Journal of Cell Biology*, **150**, 1209-1214.

11 Ervasti, J.M. (2007) Dystrophin, its interactions with other proteins, and implications for muscular dystrophy. *Biochim. Biophys. Acta*, **1772**, 108-117.

12 Levine, B.A., Moir, A.J., Patchell, V.B. and Perry, S.V. (1990) The interaction of actin with dystrophin. *FEBS Lett.*, **263**, 159-162.

13 Way, M., Pope, B., Cross, R.A., Kendrick-Jones, J. and Weeds, A.G. (1992) Expression of the N-terminal domain of dystrophin in E. coli and demonstration of binding to F-actin. *FEBS Lett.*, **301**, 243-245.

14 Rybakova, I.N. and Ervasti, J.M. (1997) Dystrophin-glycoprotein complex is monomeric and stabilizes actin filaments in vitro through a lateral association. *The Journal of Biological Chemistry*, **272**, 28771-28778.

15 Ibraghimov-Beskrovnaya, O., Ervasti, J.M., Leveille, C.J., Slaughter, C.A., Sernett, S.W. and Campbell, K.P. (1992) Primary structure of dystrophin-

associated glycoproteins linking dystrophin to the extracellular matrix. *Nature*, **355**, 696-702.
16 Ervasti, J.M. and Campbell, K.P. (1991) Membrane organization of the dystrophin-glycoprotein complex. *Cell Tissue Res.*, **66**, 1121-1131.
17 Suzuki, A., Yoshida, M., Yamamoto, H. and Ozawa, E. (1992) Glycoprotein-binding site of dystrophin is confined to the cysteine-rich domain and the first half of the carboxy-terminal domain. *FEBS Lett.*, **308**, 154-160.
18 Godfrey, C., Foley, A.R., Clement, E. and Muntoni, F. (2011) Dystroglycanopathies: coming into focus. *Curr. Opin. Genet. Dev.*
19 Finsterer, J. (2004) Limb girdle muscular dystrophies. *Der Nervenarzt*, **75**, 1153-1166.
20 Laval, S.H. and Bushby, K.M. (2004) Limb-girdle muscular dystrophies--from genetics to molecular pathology. *Neuropathol. Appl. Neurobiol.*, **30**, 91-105.
21 Moore, S.A., Shilling, C.J., Westra, S., Wall, C., Wicklund, M.P., Stolle, C., Brown, C.A., Michele, D.E., Piccolo, F., Winder, T.L. *et al.* (2006) Limb-girdle muscular dystrophy in the United States. *J. Neuropathol. Exp. Neurol.*, **65**, 995-1003.
22 Bunnell, T.M., Jaeger, M.A., Fitzsimons, D.P., Prins, K.W. and Ervasti, J.M. (2008) Destabilization of the dystrophin-glycoprotein complex without functional deficits in alpha-dystrobrevin null muscle. *PLoS One*, **3**, e2604.
23 Kameya, S., Miyagoe, Y., Nonaka, I., Ikemoto, T., Endo, M., Hanaoka, K., Nabeshima, Y. and Takeda, S. (1999) alpha1-syntrophin gene disruption results in the absence of neuronal-type nitric-oxide synthase at the sarcolemma but does not induce muscle degeneration. *J. Biol. Chem.*, **274**, 2193-2200.
24 Lebakken, C.S., Venzke, D.P., Hrstka, R.F., Consolino, C.M., Faulkner, J.A., Williamson, R.A. and Campbell, K.P. (2000) Sarcospan-deficient mice maintain normal muscle function. *Mol. Cell. Biol.*, **20**, 1669-1677.
25 Zubrzycka-Gaarn, E.E., Bulman, D.E., Karpati, G., Burghes, A.H., Belfall, B., Klamut, H.J., Talbot, J., Hodges, R.S., Ray, P.N. and Worton, R.G. (1988) The Duchenne muscular dystrophy gene product is localized in sarcolemma of human skeletal muscle. *Nature*, **333**, 466-469.
26 Porter, G.A., Dmytrenko, G.M., Winkelmann, J.C. and Bloch, R.J. (1992) Dystrophin colocalizes with beta-spectrin in distinct subsarcolemmal domains in mammalian skeletal muscle. *The Journal of Cell Biology*, **117**, 997-1005.
27 Straub, V., Bittner, R.E., Leger, J.J. and Voit, T. (1992) Direct visualization of the dystrophin network on skeletal muscle fiber membrane. *The Journal of Cell Biology*, **119**, 1183-1191.
28 Ervasti, J.M. (2003) Costameres: the Achilles' heel of Herculean muscle. *The Journal of Biological Chemistry*, **278**, 13591-13594.
29 Han, R., Kanagawa, M., Yoshida-Moriguchi, T., Rader, E.P., Ng, R.A., Michele, D.E., Muirhead, D.E., Kunz, S., Moore, S.A., Iannaccone, S.T. *et al.* (2009) Basal lamina strengthens cell membrane integrity via the laminin G

domain-binding motif of alpha-dystroglycan. *Proc. Natl. Acad. Sci. U. S. A.*, **106**, 12573-12579.
30 Hoffman, E.P. (1989) Human molecular genetics and the elucidation of the primary biochemical defect in Duchenne muscular dystrophy. *Cell Motil. Cytoskeleton*, **14**, 163-168.
31 Hartwig, J.H. (1995) Actin-binding proteins. 1: Spectrin super family. *Protein Profile*, **2**, 703-800.
32 Koenig, M., Monaco, A.P. and Kunkel, L.M. (1988) The complete sequence of dystrophin predicts a rod-shaped cytoskeletal protein. *Cell Tissue Res.*, **53**, 219-228.
33 Tinsley, J.M., Blake, D.J., Roche, A., Fairbrother, U., Riss, J., Byth, B.C., Knight, A.E., Kendrick-Jones, J., Suthers, G.K. and Love, D.R. (1992) Primary structure of dystrophin-related protein. *Nature*, **360**, 591-593.
34 Levine, B.A., Moir, A.J., Patchell, V.B. and Perry, S.V. (1992) Binding sites involved in the interaction of actin with the N-terminal region of dystrophin. *FEBS Lett*, **298**, 44-48.
35 Ishikawa-Sakurai, M., Yoshida, M., Imamura, M., Davies, K.E. and Ozawa, E. (2004) ZZ domain is essentially required for the physiological binding of dystrophin and utrophin to beta-dystroglycan. *Hum. Mol. Genet.*, **13**, 693-702.
36 Huang, X., Poy, F., Zhang, R., Joachimiak, A., Sudol, M. and Eck, M.J. (2000) Structure of a WW domain containing fragment of dystrophin in complex with beta-dystroglycan. *Nat. Struct. Biol.*, **7**, 634-638.
37 Rentschler, S., Linn, H., Deininger, K., Bedford, M.T., Espanel, X. and Sudol, M. (1999) The WW domain of dystrophin requires EF-hands region to interact with beta-dystroglycan. *Biol. Chem.*, **380**, 431-442.
38 Koenig, M. and Kunkel, L.M. (1990) Detailed analysis of the repeat domain of dystrophin reveals four potential hinge segments that may confer flexibility. *The Journal of Biological Chemistry*, **265**, 4560-4566.
39 Broderick, M.J. and Winder, S.J. (2005) Spectrin, alpha-actinin, and dystrophin. *Adv. Protein Chem.*, **70**, 203-246.
40 Winder, S.J., Gibson, T.J. and Kendrick-Jones, J. (1995) Dystrophin and utrophin: the missing links! *FEBS Lett.*, **369**, 27-33.
41 Djinovic-Carugo, K., Gautel, M., Ylanne, J. and Young, P. (2002) The spectrin repeat: a structural platform for cytoskeletal protein assemblies. *FEBS Lett.*, **513**, 119-123.
42 Saadat, L., Pittman, L. and Menhart, N. (2006) Structural cooperativity in spectrin type repeats motifs of dystrophin. *Biochim. Biophys. Acta*, **1764**, 943-954.
43 Legardinier, S., Raguenes-Nicol, C., Tascon, C., Rocher, C., Hardy, S., Hubert, J.F. and Le Rumeur, E. (2009) Mapping of the lipid-binding and stability properties of the central rod domain of human dystrophin. *J. Mol. Biol.*, **389**, 546-558.

44 Lai, Y., Thomas, G.D., Yue, Y., Yang, H.T., Li, D., Long, C., Judge, L., Bostick, B., Chamberlain, J.S., Terjung, R.L. *et al.* (2009) Dystrophins carrying spectrin-like repeats 16 and 17 anchor nNOS to the sarcolemma and enhance exercise performance in a mouse model of muscular dystrophy. *The Journal of Clinical Investigation*, **119**, 624-635.
45 Le Rumeur, E., Fichou, Y., Pottier, S., Gaboriau, F., Rondeau-Mouro, C., Vincent, M., Gallay, J. and Bondon, A. (2003) Interaction of dystrophin rod domain with membrane phospholipids. Evidence of a close proximity between tryptophan residues and lipids. *J. Biol. Chem.*, **278**, 5993-6001.
46 Rybakova, I.N. and Ervasti, J.M. (2005) Identification of spectrin-like repeats required for high affinity utrophin-actin interaction. *The Journal of Biological Chemistry*, **280**, 23018-23023.
47 Amann, K.J., Renley, B.A. and Ervasti, J.M. (1998) A cluster of basic repeats in the dystrophin rod domain binds F-actin through an electrostatic interaction. *The Journal of Biological Chemistry*, **273**, 28419-28423.
48 Prins, K.W., Humston, J.L., Mehta, A., Tate, V., Ralston, E. and Ervasti, J.M. (2009) Dystrophin is a microtubule-associated protein. *The Journal of Cell Biology*, **186**, 363-369.
49 Legardinier, S., Hubert, J.F., Le Bihan, O., Tascon, C., Rocher, C., Raguenes-Nicol, C., Bondon, A., Hardy, S. and Le Rumeur, E. (2008) Sub-domains of the dystrophin rod domain display contrasting lipid-binding and stability properties. *Biochim. Biophys. Acta*, **1784**, 672-682.
50 Amann, K.J., Guo, A.W. and Ervasti, J.M. (1999) Utrophin lacks the rod domain actin binding activity of dystrophin. *The Journal of Biological Chemistry*, **274**, 35375-35380.
51 Rybakova, I.N., Humston, J.L., Sonnemann, K.J. and Ervasti, J.M. (2006) Dystrophin and utrophin bind actin through distinct modes of contact. *The Journal of Biological Chemistry*, **281**, 9996-10001.
52 Rybakova, I.N., Amann, K.J. and Ervasti, J.M. (1996) A new model for the interaction of dystrophin with F-actin. *The Journal of Cell Biology*, **135**, 661-672.
53 Mirza, A. and Menhart, N. (2008) Stability of dystrophin STR fragments in relation to junction helicity. *Biochim. Biophys. Acta*, **1784**, 1301-1309.
54 Bhasin, N., Law, R., Liao, G., Safer, D., Ellmer, J., Discher, B.M., Sweeney, H.L. and Discher, D.E. (2005) Molecular extensibility of mini-dystrophins and a dystrophin rod construct. *J. Mol. Biol.*, **352**, 795-806.
55 Ruszczak, C., Mirza, A. and Menhart, N. (2006) Hybrid spectrin type repeats produced by exon-skipping in dystrophin. *Biochim. Biophys. Acta*, **1764**, 993-999.
56 Legardinier, S., Legrand, B., Raguenes-Nicol, C., Bondon, A., Hardy, S., Tascon, C., Le Rumeur, E. and Hubert, J.F. (2009) A Two-amino Acid Mutation Encountered in Duchenne Muscular Dystrophy Decreases Stability of the Rod Domain 23 (R23) Spectrin-like Repeat of Dystrophin. *The Journal of Biological Chemistry*, **284**, 8822-8832.

57 Mirza, A., Sagathevan, M., Sahni, N., Choi, L. and Menhart, N. (2010) A biophysical map of the dystrophin rod. *Biochim. Biophys. Acta*, **1804**, 1796-1809.
58 Selden, L.A., Estes, J.E. and Gershman, L.C. (1983) The tightly bound divalent cation regulates actin polymerization. *Biochem. Biophys. Res. Commun.*, **116**, 478-485.
59 Milligan, R.A., Whittaker, M. and Safer, D. (1990) Molecular structure of F-actin and location of surface binding sites. *Nature*, **348**, 217-221.
60 Pollard, T.D. and Borisy, G.G. (2003) Cellular motility driven by assembly and disassembly of actin filaments. *Cell*, **112**, 453-465.
61 Small, J.V., Isenberg, G. and Celis, J.E. (1978) Polarity of actin at the leading edge of cultured cells. *Nature*, **272**, 638-639.
62 Firtel, R.A. (1981) Multigene families encoding actin and tubulin. *Cell*, **24**, 6-7.
63 Rubenstein, P.A. (1990) The functional importance of multiple actin isoforms. *Bioessays*, **12**, 309-315.
64 Perrin, B.J. and Ervasti, J.M. (2011) The actin gene family: function follows isoform. *Cytoskeleton (Hoboken)*, **67**, 630-634.
65 Prins, K.W., Call, J.A., Lowe, D.A. and Ervasti, J.M. (2011) Quadriceps myopathy caused by skeletal muscle-specific ablation of {beta}cyto-actin. *J. Cell Sci.*, **124**, 951-957.
66 Sonnemann, K.J., Fitzsimons, D.P., Patel, J.R., Liu, Y., Schneider, M.F., Moss, R.L. and Ervasti, J.M. (2006) Cytoplasmic gamma-actin is not required for skeletal muscle development but its absence leads to a progressive myopathy. *Developmental Cell*, **11**, 387-397.
67 Craig, S.W. and Pardo, J.V. (1983) Gamma actin, spectrin, and intermediate filament proteins colocalize with vinculin at costameres, myofibril-to-sarcolemma attachment sites. *Cell Motil.*, **3**, 449-462.
68 Bushby, K.M. (1992) Genetic and clinical correlations of Xp21 muscular dystrophy. *J. Inherit. Metab. Dis.*, **15**, 551-564.
69 Gillard, E.F., Chamberlain, J.S., Murphy, E.G., Duff, C.L., Smith, B., Burghes, A.H., Thompson, M.W., Sutherland, J., Oss, I., Bodrug, S.E. *et al.* (1989) Molecular and phenotypic analysis of patients with deletions within the deletion-rich region of the Duchenne muscular dystrophy (DMD) gene. *Am. J. Hum. Genet.*, **45**, 507-520.
70 Nicholson, L.V., Johnson, M.A., Bushby, K.M., Gardner-Medwin, D., Curtis, A., Ginjaar, I.B., den Dunnen, J.T., Welch, J.L., Butler, T.J., Bakker, E. *et al.* (1993) Integrated study of 100 patients with Xp21 linked muscular dystrophy using clinical, genetic, immunochemical, and histopathological data. Part 2. Correlations within individual patients. *J. Med. Genet.*, **30**, 737-744.
71 Hamed, S., Sutherland-Smith, A., Gorospe, J., Kendrick-Jones, J. and Hoffman, E. (2005) DNA sequence analysis for structure/function and mutation studies in Becker muscular dystrophy. *Clin. Genet.*, **68**, 69-79.

72 Roberts, R.G., Gardner, R.J. and Bobrow, M. (1994) Searching for the 1 in 2,400,000: a review of dystrophin gene point mutations. *Hum. Mutat.*, **4**, 1-11.
73 Prior, T.W., Papp, A.C., Snyder, P.J., Burghes, A.H., Bartolo, C., Sedra, M.S., Western, L.M. and Mendell, J.R. (1993) A missense mutation in the dystrophin gene in a Duchenne muscular dystrophy patient. *Nat. Genet.*, **4**, 357-360.
74 Feng, J., Yan, J., Buzin, C.H., Towbin, J.A. and Sommer, S.S. (2002) Mutations in the dystrophin gene are associated with sporadic dilated cardiomyopathy. *Mol. Genet. Metab.*, **77**, 119-126.
75 Tuffery-Giraud, S., Beroud, C., Leturcq, F., Yaou, R.B., Hamroun, D., Michel-Calemard, L., Moizard, M.P., Bernard, R., Cossee, M., Boisseau, P. *et al.* (2009) Genotype-phenotype analysis in 2,405 patients with a dystrophinopathy using the UMD-DMD database: a model of nationwide knowledgebase. *Hum. Mutat.*, **30**, 934-945.
76 Goldberg, L.R., Hausmanowa-Petrusewicz, I., Fidzianska, A., Duggan, D.J., Steinberg, L.S. and Hoffman, E.P. (1998) A dystrophin missense mutation showing persistence of dystrophin and dystrophin-associated proteins yet a severe phenotype. *Ann. Neurol.*, **44**, 971-976.
77 Lenk, U., Oexle, K., Voit, T., Ancker, U., Hellner, K.A., Speer, A. and Hubner, C. (1996) A cysteine 3340 substitution in the dystroglycan-binding domain of dystrophin associated with Duchenne muscular dystrophy, mental retardation and absence of the ERG b-wave. *Hum. Mol. Genet.*, **5**, 973-975.
78 Norwood, F.L., Sutherland-Smith, A.J., Keep, N.H. and Kendrick-Jones, J. (2000) The structure of the N-terminal actin-binding domain of human dystrophin and how mutations in this domain may cause Duchenne or Becker muscular dystrophy. *Structure*, **8**, 481-491.
79 Muir, L.A. and Chamberlain, J.S. (2009) Emerging strategies for cell and gene therapy of the muscular dystrophies. *Expert Reviews in Molecular Medicine*, **11**, e18.
80 Pichavant, C., Aartsma-Rus, A., Clemens, P.R., Davies, K.E., Dickson, G., Takeda, S., Wilton, S.D., Wolff, J.A., Wooddell, C.I., Xiao, X. *et al.* (2011) Current Status of Pharmaceutical and Genetic Therapeutic Approaches to Treat DMD. *Mol Ther*.
81 Blake, D.J., Weir, A., Newey, S.E. and Davies, K.E. (2002) Function and genetics of dystrophin and dystrophin-related proteins in muscle. *Physiol. Rev.*, **82**, 291-329.
82 Winder, S.J., Hemmings, L., Maciver, S.K., Bolton, S.J., Tinsley, J.M., Davies, K.E., Critchley, D.R. and Kendrick-Jones, J. (1995) Utrophin actin binding domain: analysis of actin binding and cellular targeting. *J. Cell Sci.*, **108 (Pt 1)**, 63-71.
83 Matsumura, K., Ervasti, J.M., Ohlendieck, K., Kahl, S.D. and Campbell, K.P. (1992) Association of dystrophin-related protein with dystrophin-associated proteins in mdx mouse muscle. *Nature*, **360**, 588-591.

84 Rybakova, I.N., Patel, J.R., Davies, K.E., Yurchenco, P.D. and Ervasti, J.M. (2002) Utrophin binds laterally along actin filaments and can couple costameric actin with sarcolemma when overexpressed in dystrophin-deficient muscle. *Mol. Biol. Cell*, **13**, 1512-1521.
85 Tinsley, J., Deconinck, N., Fisher, R., Kahn, D., Phelps, S., Gillis, J.M. and Davies, K. (1998) Expression of full-length utrophin prevents muscular dystrophy in mdx mice. *Nat. Med.*, **4**, 1441-1444.
86 Tinsley, J.M., Potter, A.C., Phelps, S.R., Fisher, R., Trickett, J.I. and Davies, K.E. (1996) Amelioration of the dystrophic phenotype of mdx mice using a truncated utrophin transgene. *Nature*, **384**, 349-353.
87 Mendell, J.R., Campbell, K., Rodino-Klapac, L., Sahenk, Z., Shilling, C., Lewis, S., Bowles, D., Gray, S., Li, C., Galloway, G. *et al.* (2010) Dystrophin immunity in Duchenne's muscular dystrophy. *The New England Journal of Medicine* **363**, 1429-1437.
88 Sonnemann, K.J., Heun-Johnson, H., Turner, A.J., Baltgalvis, K.A., Lowe, D.A. and Ervasti, J.M. (2009) Functional substitution by TAT-utrophin in dystrophin-deficient mice. *PLoS Medicine*, **6**, e1000083.
89 Welch, E.M., Barton, E.R., Zhuo, J., Tomizawa, Y., Friesen, W.J., Trifillis, P., Paushkin, S., Patel, M., Trotta, C.R., Hwang, S. *et al.* (2007) PTC124 targets genetic disorders caused by nonsense mutations. *Nature*, **447**, 87-91.
90 van Deutekom, J.C., Janson, A.A., Ginjaar, I.B., Frankhuizen, W.S., Aartsma-Rus, A., Bremmer-Bout, M., den Dunnen, J.T., Koop, K., van der Kooi, A.J., Goemans, N.M. *et al.* (2007) Local dystrophin restoration with antisense oligonucleotide PRO051. *N. Engl. J. Med.*, **357**, 2677-2686.
91 Fabbrizio, E., Bonet-Kerrache, A., Leger, J.J. and Mornet, D. (1993) Actin-dystrophin interface. *Biochemistry (Mosc).* **32**, 10457-10463.
92 Levine, B.A., Moir, A.J., Patchell, V.B. and Perry, S.V. (1990) The interaction of actin with dystrophin. *FEBS Lett.*, **263**, 159-162.
93 Renley, B.A., Rybakova, I.N., Amann, K.J. and Ervasti, J.M. (1998) Dystrophin binding to nonmuscle actin. *Cell Motil. Cytoskeleton*, **41**, 264-270.
94 Henderson, D.M., Belanto, J.J., Li, B., Heun-Johnson, H. and Ervasti, J.M. (2011) Internal deletion compromises the stability of dystrophin. *Hum. Mol. Genet.*
95 Ponting, C.P., Blake, D.J., Davies, K.E., Kendrick-Jones, J. and Winder, S.J. (1996) ZZ and TAZ: new putative zinc fingers in dystrophin and other proteins. *Trends Biochem. Sci.*, **21**, 11-13.
96 Hnia, K., Zouiten, D., Cantel, S., Chazalette, D., Hugon, G., Fehrentz, J.A., Masmoudi, A., Diment, A., Bramham, J., Mornet, D. *et al.* (2007) ZZ domain of dystrophin and utrophin: topology and mapping of a beta-dystroglycan interaction site. *Biochem. J.*, **401**, 667-677.
97 Bork, P. and Sudol, M. (1994) The WW domain: a signalling site in dystrophin? *Trends Biochem. Sci.*, **19**, 531-533.

98 Way, M., Pope, B., Cross, R.A., Kendrick-Jones, J. and Weeds, A.G. (1992) Expression of the N-terminal domain of dystrophin in E. coli and demonstration of binding to F-actin. *FEBS Lett.*, **301**, 243-245.
99 Prochniewicz, E., Henderson, D., Ervasti, J.M. and Thomas, D.D. (2009) Dystrophin and utrophin have distinct effects on the structural dynamics of actin. *Proc. Natl. Acad. Sci. U. S. A.*, **106**, 7822-7827.
100 McHugh, K.M., Crawford, K. and Lessard, J.L. (1991) A comprehensive analysis of the developmental and tissue-specific expression of the isoactin multigene family in the rat. *Dev. Biol.*, **148**, 442-458.
101 Lubit, B.W. and Schwartz, J.H. (1980) An antiactin antibody that distinguishes between cytoplasmic and skeletal muscle actins. *J. Cell Biol.*, **86**, 891-897.
102 Crawford, K., Flick, R., Close, L., Shelly, D., Paul, R., Bove, K., Kumar, A. and Lessard, J. (2002) Mice lacking skeletal muscle actin show reduced muscle strength and growth deficits and die during the neonatal period. *Mol. Cell. Biol.*, **22**, 5887-5896.
103 Renley, B.A., Rybakova, I.N., Amann, K.J. and Ervasti, J.M. (1998) Dystrophin binding to nonmuscle actin. *Cell Motil. Cytoskeleton*, **41**, 264-270.
104 Moores, C.A., Keep, N.H. and Kendrick-Jones, J. (2000) Structure of the utrophin actin-binding domain bound to F-actin reveals binding by an induced fit mechanism. *J. Mol. Biol.*, **297**, 465-480.
105 Henderson, D.M., Lee, A. and Ervasti, J.M. (2010) Disease-causing missense mutations in actin binding domain 1 of dystrophin induce thermodynamic instability and protein aggregation. *Proc. Natl. Acad. Sci. U. S. A.*, **107**, 9632-9637.
106 Tobacman, L.S. (2008) Cooperative binding of tropomyosin to actin. *Adv. Exp. Med. Biol.*, **644**, 85-94.
107 Prochniewicz, E., Zhang, Q., Howard, E.C. and Thomas, D.D. (1996) Microsecond rotational dynamics of actin: spectroscopic detection and theoretical simulation. *J. Mol. Biol.*, **255**, 446-457.
108 Prochniewicz, E., Walseth, T.F. and Thomas, D.D. (2004) Structural dynamics of actin during active interaction with myosin: different effects of weakly and strongly bound myosin heads. *Biochemistry*, **43**, 10642-10652.
109 Eads, T.M., Thomas, D.D. and Austin, R.H. (1984) Microsecond rotational motions of eosin-labeled myosin measured by time-resolved anisotropy of absorption and phosphorescence. *J. Mol. Biol.*, **179**, 55-81.
110 Prochniewicz, E. and Thomas, D.D. (1997) Perturbations of functional interactions with myosin induce long-range allosteric and cooperative structural changes in actin. *Biochemistry (Mosc).* **36**, 12845-12853.
111 Seong, S.Y. and Matzinger, P. (2004) Hydrophobicity: an ancient damage-associated molecular pattern that initiates innate immune responses. *Nature Reviews Immunology*, **4**, 469-478.

112 Spencer, M.J. and Tidball, J.G. (2001) Do immune cells promote the pathology of dystrophin-deficient myopathies? *Neuromuscul. Disord.*, **11**, 556-564.
113 Chiti, F., Taddei, N., Baroni, F., Capanni, C., Stefani, M., Ramponi, G. and Dobson, C.M. (2002) Kinetic partitioning of protein folding and aggregation. *Nat. Struct. Biol.*, **9**, 137-143.
114 Lehner, P.J. (2003) The calculus of immunity: quantitating antigen processing. *Immunity*, **18**, 315-317.
115 Yewdell, J. (2002) To DRiP or not to DRiP: generating peptide ligands for MHC class I molecules from biosynthesized proteins. *Mol. Immunol.*, **39**, 139-146.
116 Straub, V., Bittner, R.E., Leger, J.J. and Voit, T. (1992) Direct visualization of the dystrophin network on skeletal muscle fiber membrane. *J Cell Biol*, **119**, 1183-1191.
117 Ervasti, J.M. (2003) Costameres: the Achilles' heel of Herculean muscle. *J Biol Chem*, **278**, 13591-13594.
118 Puttini, S., Lekka, M., Dorchies, O.M., Saugy, D., Incitti, T., Ruegg, U.T., Bozzoni, I., Kulik, A.J. and Mermod, N. (2008) Gene-mediated Restoration of Normal Myofiber Elasticity in Dystrophic Muscles. *Mol Ther*.
119 Petrof, B.J., Shrager, J.B., Stedman, H.H., Kelly, A.M. and Sweeney, H.L. (1993) Dystrophin protects the sarcolemma from stresses developed during muscle contraction. *Proc Natl Acad Sci U S A*, **90**, 3710-3714.
120 Rybakova, I.N., Patel, J.R. and Ervasti, J.M. (2000) The dystrophin complex forms a mechanically strong link between the sarcolemma and costameric actin. *J Cell Biol*, **150**, 1209-1214.
121 Winder, S.J., Hemmings, L., Maciver, S.K., Bolton, S.J., Tinsley, J.M., Davies, K.E., Critchley, D.R. and Kendrick-Jones, J. (1995) Utrophin actin binding domain: analysis of actin binding and cellular targeting. *J Cell Sci*, **108 (Pt 1)**, 63-71.
122 Tinsley, J., Deconinck, N., Fisher, R., Kahn, D., Phelps, S., Gillis, J.M. and Davies, K. (1998) Expression of full-length utrophin prevents muscular dystrophy in mdx mice. *Nat Med*, **4**, 1441-1444.
123 Rybakova, I.N., Patel, J.R., Davies, K.E., Yurchenco, P.D. and Ervasti, J.M. (2002) Utrophin binds laterally along actin filaments and can couple costameric actin with sarcolemma when overexpressed in dystrophin-deficient muscle. *Mol Biol Cell*, **13**, 1512-1521.
124 Rybakova, I.N., Humston, J.L., Sonnemann, K.J. and Ervasti, J.M. (2006) Dystrophin and utrophin bind actin through distinct modes of contact. *J Biol Chem*, **281**, 9996-10001.
125 Ervasti, J.M. (2007) Dystrophin, its interactions with other proteins, and implications for muscular dystrophy. *Biochim Biophys Acta*, **1772**, 108-117.
126 Galkin, V.E., Orlova, A., VanLoock, M.S., Rybakova, I.N., Ervasti, J.M. and Egelman, E.H. (2002) The utrophin actin-binding domain binds F-actin in two

different modes: implications for the spectrin superfamily of proteins. *J Cell Biol*, **157**, 243-251.
127 Sutherland-Smith, A.J., Moores, C.A., Norwood, F.L., Hatch, V., Craig, R., Kendrick-Jones, J. and Lehman, W. (2003) An atomic model for actin binding by the CH domains and spectrin-repeat modules of utrophin and dystrophin. *J Mol Biol*, **329**, 15-33.
128 Prochniewicz, E., Zhang, Q., Howard, E.C. and Thomas, D.D. (1996) Microsecond rotational dynamics of actin: spectroscopic detection and theoretical simulation. *J Mol Biol*, **255**, 446-457.
129 Prochniewicz, E., Zhang, Q., Janmey, P.A. and Thomas, D.D. (1996) Cooperativity in F-actin: binding of gelsolin at the barbed end affects structure and dynamics of the whole filament. *J Mol Biol*, **260**, 756-766.
130 Prochniewicz, E., Janson, N., Thomas, D.D. and De la Cruz, E.M. (2005) Cofilin increases the torsional flexibility and dynamics of actin filaments. *J Mol Biol*, **353**, 990-1000.
131 Rybakova, I.N., Amann, K.J. and Ervasti, J.M. (1996) A new model for the interaction of dystrophin with F-actin. *J Cell Biol*, **135**, 661-672.
132 Prochniewicz, E., D.J.Spakowicz and D.D.Thomas. (2008) Changes in actin structural transitions associated with oxidative inhibition of muscle contraction. *Biochemistry*.
133 Moores, C.A., Keep, N.H. and Kendrick-Jones, J. (2000) Structure of the utrophin actin-binding domain bound to F-actin reveals binding by an induced fit mechanism. *J Mol Biol*, **297**, 465-480.
134 Prochniewicz, E. and Thomas, D.D. (1999) Differences in structural dynamics of muscle and yeast actin accompany differences in functional interactions with myosin. *Biochemistry*, **38**, 14860-14867.
135 Thomas, D.D., Prochniewicz, E. and Roopnarine, O. (2002) Changes in actin and myosin structural dynamics due to their weak and strong interactions. *Results Probl Cell Differ*, **36**, 7-19.
136 Renley, B.A., Rybakova, I.N., Amann, K.J. and Ervasti, J.M. (1998) Dystrophin binding to nonmuscle actin. *Cell Motil Cytoskeleton*, **41**, 264-270.

Appendix: Dystrophin and Utrophin Have Distinct Effects on the Structural Dynamics of Actin

Davin Henderson performed actin binding assays for dystrophin and utrophin (Figure A1) and purified all proteins. All other experiments were performed by Ewa Prochniewicz.

Reprinted with permission from The Proceedings of the National Academy of Sciences USA (PNAS)

Prochniewicz, E., Henderson, D., Ervasti, J. M., and Thomas, D. D. (2009) *Proc. Natl. Acad. Sci. U. S. A.* **106**, 7822-7827

Chapter Summary

We have used time-resolved spectroscopy to investigate the structural dynamics of actin's interaction with dystrophin and utrophin, in relationship to the pathology of muscular dystrophy. Dystrophin and utrophin bind actin *in vitro* with similar affinities, but the molecular contacts of these two proteins with actin are different. It has been hypothesized that the presence of two low-affinity actin-binding sites in dystrophin allows more elastic response of the actin-dystrophin-sarcolemma linkage to muscle stretches, compared with utrophin, which binds via one contiguous actin-binding domain. We have directly tested this hypothesis by determining the effects of dystrophin and utrophin on the microsecond rotational dynamics of a phosphorescent dye attached to C374 on actin, as detected by transient phosphorescence anisotropy (TPA). Binding of dystrophin or utrophin to actin resulted in significant changes in the TPA decay, increasing the final anisotropy (restricting the rotational amplitude) and decreasing the rotational correlation time (increasing the rotational rate and thus the torsional flexibility).

This paradoxical combination of effects on actin dynamics (decreased amplitude but increased rate) has not previously been observed for other actin-binding proteins. At low levels of saturation, the binding of dystrophin and utrophin have similar effects, but at higher levels, utrophin caused much greater restrictions in amplitude and increases in rate. The effects of dystrophin and

utrophin on actin dynamics provide molecular insight into the pathology of muscular dystrophy.

Introduction

Dystrophin and utrophin are large cytoskeletal proteins. In skeletal muscle, dystrophin is located within a cytoskeletal lattice termed the costamere, which is proposed to transmit the contractile force from the myofibrils to the extracellular matrix and adjacent muscle fibers (116, 117). The absence of dystrophin in patients with Duchenne muscular dystrophy is associated with defects in sarcolemmal elasticity (118) and integrity (119). It has been demonstrated that dystrophin provides a direct mechanical link between costameric actin filaments, comprised of γ-actin, and the sarcolemma (120), which may be critical for stabilization of the sarcolemma against stress developed during muscle contraction (119).

Utrophin expression is developmentally regulated: it is distributed throughout the sarcolemma of fetal and regenerating muscle, but is down-regulated in normal adult muscle. Since utrophin binds to the same proteins as dystrophin, it has been proposed that utrophin performs the same role in developing muscle as dystrophin in mature muscle (121). In support of this hypothesis, transgenic overexpression of utrophin in dystrophin-deficient mdx mice prevents development of muscular dystrophy (122), most probably by rescuing the defective mechanical linkage between costameric actin and the sarcolemma (123).

While *in vivo* studies indicate that dystrophin and utrophin play similar physiological roles, *in vitro* studies suggest that they do not act through the same biochemical pathways. Both dystrophin and utrophin bind to actin with similar affinities and both stabilize actin filaments against depolymerization (124). However, dystrophin and utrophin differ in their effects on the extent of lateral association with actin and in the ionic strength dependence of actin binding, and they do not compete for the same binding sites on the actin filament (124). The two proteins also have similarities and differences in the structures of their actin-binding domains. Both contain N-terminal tandem calponin-homology actin-binding domains. In utrophin, the whole actin-binding domain is completed by the first ten spectrin-like repeats, while in dystrophin the first ten spectrin-like repeats do not bind actin; there is a second actin-binding domain involving spectrin repeats 11-17 (125). Structural analysis of the molecular contacts between dystrophin and utrophin with actin has been limited to the contacts with their N-terminal domains, Dys 246 and Ut261, respectively. Docking of crystal structures of each domain to the electron densities of its complex with actin indicated interaction with three regions of actin: the DNase binding loop in subdomain 2, the C-terminus in subdomain 1 and the helix in subdomain 4 (126), but the difference in the size and shape of bound Dys246 and Ut261 suggested that Dys246 forms more extensive contacts, which are proposed to be better suited for stabilization of the sarcolemma during muscle contraction (127).

Since utrophin has the potential to rescue the dystrophic phenotype, design of therapies requires more studies comparing the mechanisms of molecular interactions of utrophin and dystrophin, particularly of their effects on actin structure and dynamics. It has been proposed that the presence of two low-affinity actin-binding sites in dystrophin allows for a more elastic response of the actin-dystrophin-sarcolemma linkage to muscle stretches, compared with binding of utrophin via one contiguous actin-binding domain (124). The present study is designed to test this hypothesis directly by comparing the effects of the two proteins on actin's structural dynamics. Our previous studies established transient phosphorescence anisotropy (TPA) as a powerful method for analyzing the effects of diverse actin-binding proteins on the microsecond rotational dynamics within the actin filament (108, 110, 128-130). We showed that changes in actin dynamics are specific to the interacting protein (129, 130) and to the functional properties of the actomyosin complex (108, 110). The present study applies TPA to test the hypothesis that the molecular mechanism of function of these two proteins involves specific effects on the dynamic properties of actin.

Results

Binding of Utrophin and Dystrophin to ErIA-actin

Binding of full-length dystrophin and utrophin to ErIA-actin was determined under the same experimental conditions (6 μM actin, varying the concentration of the added protein) as previously used with unlabeled actin (124) (Fig. A-1). The best fits to (Eq. A-1) gave B_{max} = 0.064 ± 0.015 and K_d = 0.95 ± 0.46 μM for dystrophin; B_{max} = 0.10 ± 0.02 and K_d = 1.21 ± 0.50 μM for utrophin. These values, which are similar to those previously reported for unlabeled actin binding to dystrophin (124, 131)or utrophin (123, 124), are used below to obtain values for the fraction of actin protomers that are bound to dystrophin or utrophin, so the effects of the two proteins can be compared quantitatively.

Since ErIA-actin used in binding assays and spectroscopic experiments was stabilized with phalloidin, we performed control experiments testing the effect of phalloidin on actin binding. Due to instability of phalloidin-free ErIA-actin (108, 132), these experiments were performed using unlabeled actin. 12 μM phalloidin had no effect on the extent of binding 0.3 μM utrophin to 6 μM actin. We conclude that actin-bound phalloidin has no effect on binding to utrophin and that previously reported inhibitory effects of phalloidin on interaction with the N-terminus of utrophin (133) are not applicable to the interaction with the full-length protein.

Effects of Dystrophin and Utrophin on TPA of Actin

Both dystrophin and utrophin decrease the amplitude of actin's microsecond TPA decay, implying restriction of rotational dynamics, but utrophin's effects are much greater than dystrophin's (Fig. A-2)

TPA experiments were performed over a wide range of added utrophin or dystrophin, then analyzed in detail by fitting the data with (Eq. A-2) and plotting the resulting amplitudes and correlation times as a function of the fraction of actin protomers bound to dystrophin or utrophin. This fraction of bound actin was calculated as [dystrophin or utrophin bound, mol/mol of actin]/B_{max}, assuming B_{max} = 0.064 for dystrophin and 0.1 for utrophin, as determined in (Fig. A-1) The most dramatic change was an increase in final anisotropy (r), indicating decreased amplitude of microsecond flexibility, due to both bending and twisting of the actin filament (108, 110). At low concentrations of added proteins, where less than 10% of actin protomers are bound, dystrophin and utrophin had similar effects. However, as the fraction of bound actin increased, the increase in anisotropy in the presence of utrophin was substantially greater than in the presence of dystrophin, indicating that utrophin is more effective in restricting the amplitude of actin's microsecond rotational dynamics. When modeled as an isotropic wobble-in-cone motion (Eq. A-5), the amplitude of microsecond motion was 57^{o} for actin alone, 36^{o} for saturated dystrophin-actin, and 29^{o} for saturated utrophin-actin. Dystrophin and utrophin also had different effects on the initial anisotropy of actin: utrophin increased this parameter, indicating decreased

amplitude of submicrosecond dynamics, from 35^{o} to 33^{o} (Eq. A-3) while dystrophin had no significant effect.

TPA analysis showed that bound dystrophin and utrophin decreased the rotational correlation times ϕ_1 and ϕ_2, as well as the corresponding amplitudes r_1 and r_2. Again, the effects of utrophin were much greater than those of dystrophin. The most striking effect was a four-fold decrease in the long correlation time (ϕ_1) due to utrophin, while dystrophin decreased ϕ_1 by less than 30%. Both proteins had similarly small effects on the short correlation time ϕ_2. Dystrophin and utrophin had similar effects on the amplitude of the slower motion (r_1), while utrophin was more effective than dystrophin in decreasing the amplitude of the faster motion (r_2).

The effect of dystrophin and utrophin on TPA decay was further analyzed in terms of a specific model of actin's rotational dynamics, in which actin is a homogenous elastic rod undergoing intrafilament torsional twisting motions (Eq. A-6). We have previously shown that this model fits actin TPA decays well (128), with substantial effects on actin's torsional rigidity due to actin binding proteins such as gelsolin (129), myosin (110, 134) and cofilin (130). To accommodate the basic assumption of the model that actin is a homogenous elastic rod, the effects of dystrophin and utrophin on the torsional motions in actin were analyzed under conditions where about 60% of actin protomers were bound. The results showed that dystrophin and utrophin decrease the torsional rigidity of actin by 26 ± 8%

and 78 ± 3%, respectively. Once again, utrophin is much more effective than dystrophin in affecting actin dynamics.

The phosphorescence intensity decays of actin in the presence of saturating dystrophin and utrophin showed that the lifetimes and amplitudes of the actin-bound phosphorescent probe were not significantly affected by either protein. We conclude that bound proteins had negligible effects on the local environment of the probe, so TPA effects were due to changes in actin filament dynamics.

Discussion

Summary of Results

The binding of dystrophin or utrophin restricts the amplitudes of both submicrosecond and microsecond rotational dynamics of actin, while increasing the microsecond rates (decreasing the correlation times). At a low level of actin saturation (≤5%), both proteins induced similar changes in actin dynamics, but at higher levels utrophin was more effective than dystrophin, causing greater restrictions in amplitude and increases in rates (Figure A-3 and A-4)

Relationship to Models of Actin Rotational Dynamics

Actin's rotational dynamics involves multiple modes and time scales (Figure A-6): intraprotomer motions on the submicrosecond time scale, intrafilament torsional motions on the microsecond time scale, and filament bending motions on both microsecond and millisecond time scales (135). Our results indicate that utrophin affects all of these modes more profoundly than does dystrophin. Most of these effects are restrictions of actin's dynamics, which is consistent with a previous electron microscopic study suggesting that a utrophin fragment restricts actin's bending flexibility (126). A remarkable exception is the increased rate of rotational dynamics induced by both proteins (Figure A-4). When analyzed using the torsional twisting model (Eq. A-6) this indicates decreased torsional rigidity (increased torsional flexibility) by 26 ± 8% for dystrophin and 78 ± 3% for utrophin. These opposite effects on the amplitude

and rate of actin's microsecond dynamics have not previously been observed for other actin-binding proteins, which have been shown to either decrease (e.g., myosin or antibodies (110)) or increase (e.g., gelsolin (129) or cofilin (130)) both amplitude and rate. These qualitatively unique effects of dystrophin and utrophin on actin dynamics are probably related to their physiological roles. These proteins do much more than stabilize actin filaments from depolymerization (124) they also manage to decrease the large-amplitude bending flexibility of actin filaments while increasing the torsional flexibility.

All experiments in this study were performed using skeletal muscle α-actin. Although *in vivo* dystrophin and utrophin probably bind mainly to costameric γ-actin, it has been shown that the amino-terminal actin-binding domain of dystrophin, as well as intact dystrophin in the dystrophin-glycoprotein complex, bind α-and γ-actin with the same affinity (136). Binding of full-length utrophin also is essentially the same for muscle and non-muscle actin isoforms (123). Thus our results are relevant to interactions *in vivo*. Of course, future studies on the structural dynamics of γ actin will be illuminating.

Utrophin and Dystrophin Interact Differently with Actin

The different effects of dystrophin and utrophin on actin dynamics presumably result from distinct modes of contact between actin and these two proteins, as concluded from biochemical experiments (124). Detailed structural information about these contacts is currently limited to the actin-binding N-terminal domains of dystrophin and utrophin, Dys246 and Utr261. The analysis of

electron micrographs of actin fully decorated with Dys246 and Utr261 showed that both of these proteins form extensive contacts with actin subdomains 1, 2 and 4 (126, 127), and qualitative differences observed between the structures of bound Dys264 and Utr261 suggest similarities as well as differences at the binding interfaces. One of the similarities is binding of the N-terminal parts of both proteins to actin's C-terminus, as indicated by electron micrographs of the complexes (126) and proton NMR spectroscopy of peptides (34). While this suggests that at least part of the observed effects of full-length dystrophin and utrophin on actin dynamics could result from direct effects of their N-terminal fragments on the probe-binding site at the C-terminus, lack of substantial changes in the lifetime of the Cys374-bound ErIA does not support this hypothesis. The large differences in the effects of the two proteins on actin dynamics must be understood in terms of their full-length structures: dystrophin has two separate low-affinity actin-binding sites while utrophin appears to bind via one contiguous actin-binding domain, so that the effects on actin dynamics detected via the ErIA probe probably reflect long-range cumulative effects from interaction at multiple binding sites. Our results suggest that the contiguous actin-binding domain of utrophin is more potent in perturbing actin rotational dynamics.

Implications for Pathophysiology

The effects of dystrophin and utrophin on actin structural dynamics could have profound physiological and pathological significance. We report two remarkable findings about the effects of these proteins on the actin-mediated

linkage with the sarcolemma. First, dystrophin and utrophin both have a combination of effects not previously observed for actin-binding proteins – they restrict the amplitude of actin's bending flexibility while increasing the rate of its torsional flexibility. These changes in actin flexibility may be important for optimal function of the actin-sarcolemma linkage, allowing for appropriate elastic response to muscle stretches. Second, the two proteins have different effects on actin, both qualitatively and quantitatively, and these differences are more prominent at high actin saturation. Utrophin's greater potency in perturbing actin dynamics could make it an effective substitute even if expressed at lower levels than dystrophin in normal muscle. However, the different effects of utrophin at high levels suggest that the two proteins have different, as yet undetermined, functions *in vivo*. Future experiments using expressed fragments of dystrophin and utrophin and their functionally relevant mutants will determine which structural elements of these proteins are critical in determining the flexibility of actin filaments and what level of actin flexibility is physiologically optimal. The results of this research will provide new insight into important functions of dystrophin and utrophin and will be informative to several therapeutic approaches for muscular dystrophies.

Utrophin's greater potency in perturbing actin dynamics could make it an effective substitute even if expressed at lower levels than dystrophin in normal muscle. However, the different effects of utrophin at high levels suggest that the two proteins have different, as yet undetermined, functions *in vivo*. Future

experiments using expressed fragments of dystrophin and utrophin and their functionally relevant mutants will determine which structural elements of these proteins are critical in determining the flexibility of actin filaments and what level of actin flexibility is physiologically optimal. The results of this research will provide new insight into important functions of dystrophin and utrophin and will be informative to several therapeutic approaches for muscular dystrophies.

Experimental Procedures

Preparation of dystrophin and utrophin: Sf-9 insect cells were infected with high-titer recombinant baculoviruses encoding FLAG-tagged full length mouse dystrophin or utrophin (124), incubated 72 hours and expressed protein was purified by anti-FLAG M2 affinity chromatography as previously described (123). The concentration of purified proteins was measured with the Bradford protein assay using BSA as a standard.

Preparation and labeling of actin: Actin was prepared from rabbit skeletal muscle as previously described (108), extracting acetone powder in cold water, polymerizing with 30 mM KCl for 1 hr at room temperature, and centrifuging for 30 min at 300,000xg. The pellet was suspended in G-Ca buffer (5 mM Tris pH 7.5, 0.5 mM ATP, 0.2 mM $CaCl_2$), clarified by 10 min centrifugation at 300,000xg , then polymerized with 2 mM $MgCl_2$ in 20 mM Tris (pH 7.5).

For phosphorescence experiments, actin was labeled at Cys 374 with ErIA (AnaSpec) as described previously (108). The dye, freshly dissolved in DMF, was added at a concentration of 480 μM to 48 μM F-actin. After 2 hrs incubation at 25°C, the labeling was stopped by 10 mM DTT, actin was ultracentrifuged for 30 min at 300,000xg, pellets were suspended in Mg-G-buffer (5mM Tris pH 7.5, 0.2 mM $MgCl_2$, 0.5 mM ATP), clarified by 10 min centrifugation at 300,000xg, and

actin was polymerized (to F-actin) for 30 min at 25°C by adding 2 mM $MgCl_2$. After ultracentrifugation for 30 min at 300,000xg, pellets were suspended in UD-buffer (100 mM NaCl, 2 mM $MgCl_2$, 10 mM Tris, pH 7.5, 0.2 mM ATP, 1 mM DTT) and the labeled F-actin (ErIA- actin) was immediately stabilized against depolymerization and denaturation by adding 1 molar equivalent of phalloidin. The extent of labeling, determined by measuring dye absorbance and protein concentration, was 0.99 ± 0.13 mol dye/mol actin, respectively. For fluorescence experiments, the same procedure was applied for labeling actin with IAEDANS (5-((((2-iodoacetyl)amino)ethyl)amino)naphtalene-1-sulfonic acid) and FMal (fluorescein-5-maleimide). The extent of labeling with IAEDANS and FMal was 0.87 and 0.65 mol dye/mol actin, respectively. The concentration of unlabeled actin was measured using a molar extinction coefficient of 0.63 mg ml^{-1} cm^{-1} at 290 nm. The concentration of labeled actin was measured with the Bradford protein assay using unmodified actin as a standard; attached dyes had negligible effect on this assay.

Actin binding analysis: Dystrophin and utrophin binding to actin filaments was measured using a high-speed co-sedimentation assay (131). Varying concentrations of dystrophin and utrophin were added to 6μM skeletal muscle F-actin, incubated for 30 minutes at 20^{o} C and centrifuged at 100,000 x g for 20 minutes. The resulting pellets and supernatants were separated by SDS-PAGE and stained with Coomassie blue. The fractions of free and bound protein were

quantified by densitometry. K_d and B_{max} of binding were obtained by fitting data by the function

$$y = B_{max}*[P]/(K_d + [P]) \qquad \textbf{Eq. A-1}$$

where y = bound protein (mol/mol actin) and [P] = free protein (μM).

Phosphorescence: For TPA experiments, phalloidin-stabilized ErIA-actin was diluted in UD-buffer to 1.0 μM, and increasing concentrations of dystrophin or utrophin were added. To prevent photobleaching of the dye, oxygen was removed from the sample by 5 min incubation with glucose oxidase (55 *μ*g/ml), catalase (36 *μ*g/ml), and glucose (45 *μ*g/ml) (108, 109). Phosphorescence was measured at 25°C. Actin-bound ErIA was excited with a vertically polarized 1.2-ns pulse from a FDSS 532-150 laser (CryLas) at 532 nm, operating at a repetition rate of 100 Hz. Phosphorescence emission was selected by a 670 nm glass cut-off filter (Corion), detected by a photomultiplier (R928, Hamamatsu), and digitized by a transient digitizer (CompuScope 14100, GaGe) at a time resolution of 1 μs/channel. The time-resolved phosphorescence anisotropy decay was calculated as $r(t) = [I_v(t) - GI_h(t)]/[I_v(t) + 2GI_h(t)]$, where $I_v(t)$ and $I_h(t)$ are vertically and horizontally polarized components of the emission signal, detected at 90° with a single detector and a sheet polarizer that alternated between the two orientations every 500 laser pulses. G is an instrumental correction factor, determined by performing the measurement with horizontally

polarized excitation, for which the corrected anisotropy value is set to zero. The time-dependent anisotropy decays of free actin and its complexes with dystrophin and utrophin were obtained by recording 30 cycles of 1000 pulses (500 in each orientation of the polarizer).

TPA Data analysis: The TPA decay was fitted with the function

$$r(t) = r_1 \exp(-t/\phi_1) + r_2 \exp(-t/\phi_2) + r_\infty , \qquad \textbf{Eq. A-2}$$

varying rotational correlation times, ϕ_1 (slow) and ϕ_2 (fast), the corresponding amplitudes, r_1 and r_2, and the final anisotropy r_∞. The initial anisotropy was then calculated as $r_0 = r(0) = r_1 + r_2 + r_\infty$. This method of analysis was established previously (108, 110) and was validated by comparing residuals and χ^2 for fits with one, two and three exponential terms. These parameters were interpreted as follows: Increased initial anisotropy (r_0) indicates decreased amplitude of submicrosecond rotational dynamics, usually attributed to motion within the actin protomer. The angular amplitude of this submicrosecond motion, assuming a wobble in a cone with half-angle θ_c, is given by (128)

$$\theta_c(ns) = \cos^{-1}[-0.5 + 0.5(1+8\{r_0/0.205\}^{1/2})], \qquad \textbf{Eq. A-3}$$

Increased final anisotropy r_∞ (decreased r_1 and/or r_2) indicates decreased amplitude of microsecond rotational dynamics (actin filament flexibility), and decreased correlation times (ϕ_1 and/or ϕ_2) indicate increased rates of

microsecond rotation. The overall angular amplitude of microsecond motion, assuming a wobble in a cone, is given by (128)

$$\theta_c(\mu s) = \cos^{-1}[-0.5 + 0.5(1+8\{r_\infty/r_0\}^{1/2})], \qquad \textbf{Eq. A-5}$$

The torsional constant of actin was obtained by fitting the TPA decay by a model assuming that actin is a continuous flexible rod (128):

$$r(t) = A_0 + A_1\exp[-0.25(t/\Phi)^{1/2}] + A_2\exp[-(t/\Phi)^{1/2}] \qquad \textbf{Eq. A-6}$$

The amplitudes A_i depend on orientation of the bound probe, and Φ is proportional to the torsional rigidity C of the filament, which is defined as the torque required to twist a 1-cm filament by 1 radian; for a completely rigid filament, $C = \infty$.

The phosphorescence lifetimes τ_i of actin-bound ErIA and their amplitudes a_i were obtained by fitting total phosphorescence intensity decay $I = (I_v(t)+2GI_h(t))/3$ by the function

$$I = a_1 \exp(-t/\tau_1) + a_2 \exp(-t/\tau_2) \qquad \textbf{Eq. A-7}$$

Fluorescence resonance energy transfer: Time-resolved fluorescence was measured with pulsed laser excitation and transient digitizer detection, as described previously (108). Actin-bound IAEDANS (donor) was excited with a 1 ns pulse from a passively Q-switched YAG laser (10 kHz repetition rate) at 355 nm. Time-dependent IADDANS fluorescence emission $I(t)$ was detected at 465

nm, digitized (DS252, Aqiris) and analyzed by fitting to a sum of three exponentials terms plus a scattering component (Eq. 6).

$$I(t) = Scat*\delta(0) + A_1\exp(-t/\tau_1) + A_2\exp(-t/\tau_2) + A_3\exp(-t/\tau_3) \quad \textbf{Eq. A-8}$$

Scat is the amplitude of scattered light, $\delta(0)$ is the delta function, A_i are amplitudes of fluorescence intensity decay, and τ_i are fluorescence lifetimes. The expression was convoluted with an excitation function L(t) obtained from a light scattered from water. This convolution was then fit to the data using an iterative non-linear least-squares simulation using the Marquardt algorithm. The average lifetime $\langle\tau\rangle$ of donor (IAEDANS-labeled filaments) in the absence and presence of acceptor (FMal-labeled filaments) was determined as:

$$\langle\tau\rangle = (\Sigma A_i \tau_i)/ \Sigma A_i \text{ , } i = 1,2,3 \quad \textbf{Eq. A-9}$$

The efficiency of energy transfer E was calculated from the average lifetime of donor in the presence (τ_{DA}) and the absence (τ_D) of acceptor:

$$E = 1-(\tau_{DA}/ \tau_D) \quad \textbf{Eq. A-10}$$

Each result is reported as mean ± SEM ($n > 4$), unless indicated otherwise.

Figures

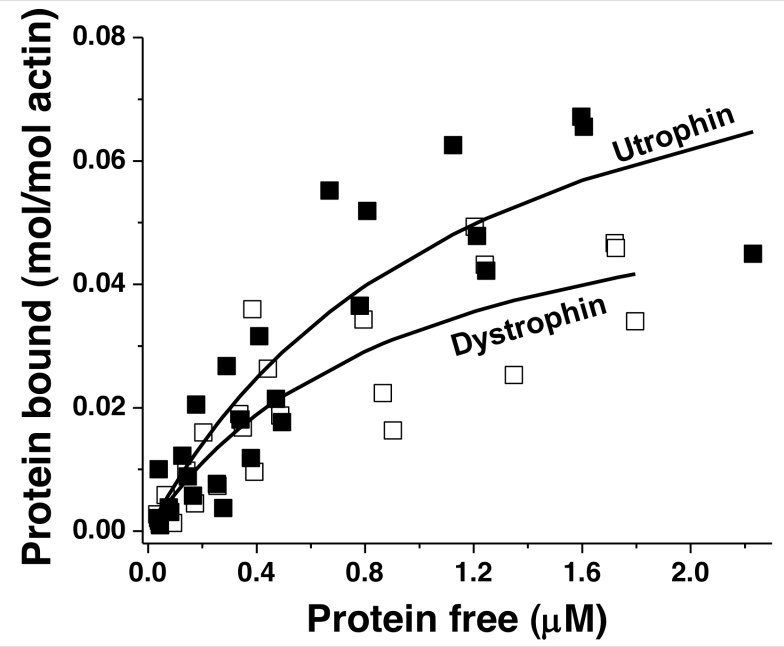

Figure A-1: Binding of dystrophin (open symbols) and utrophin (closed symbols) to ErIA F-actin. Solid lines represent best fits of (Eq. 1) to the experimental data.

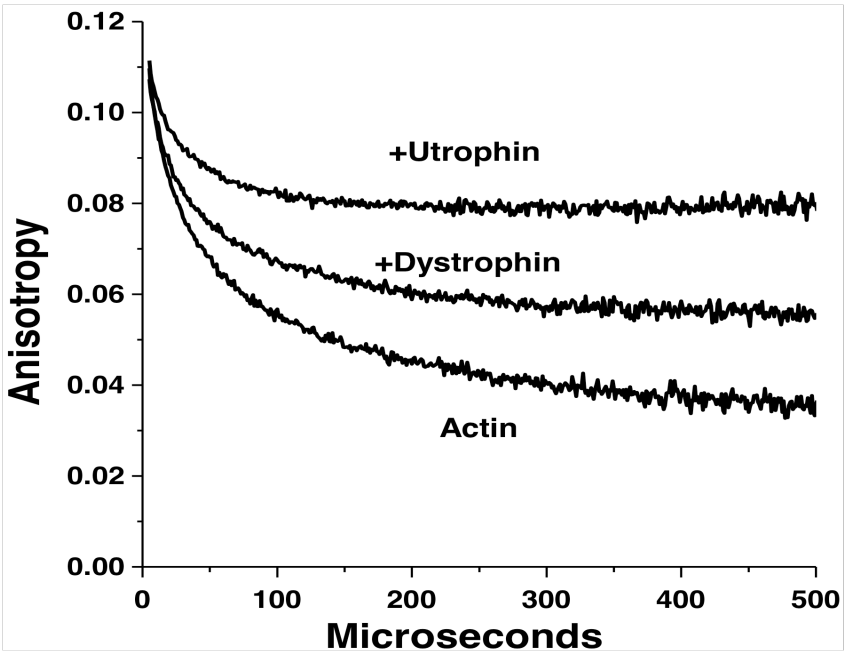

Figure A-2: The effect of 1.5 μM dystrophin and 2 μM utrophin on TPA decay of 1 μM ErIA-actin.

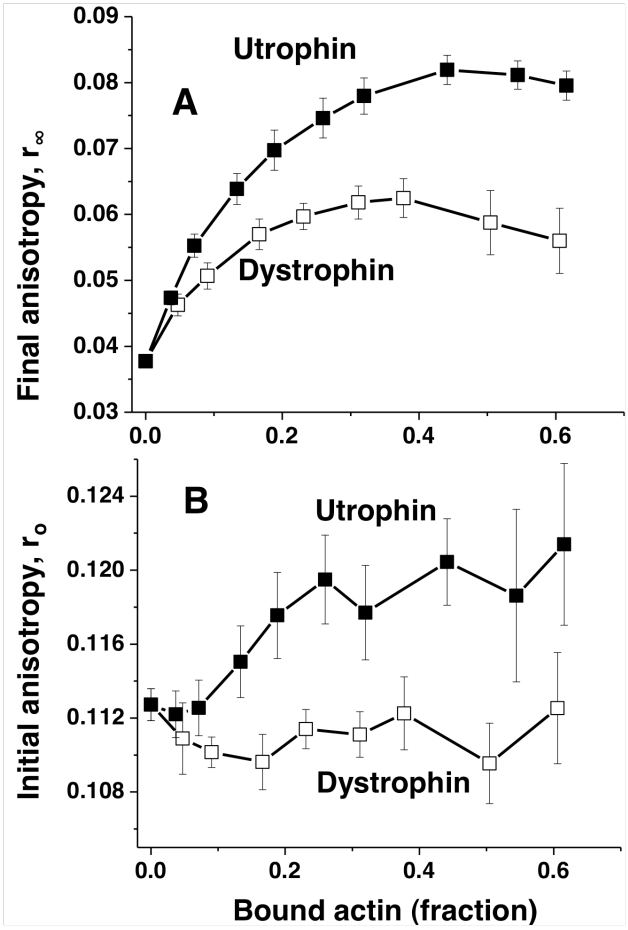

Figure A-3: The effect of dystrophin (open symbols) and utrophin (closed symbols) binding on the TPA of actin, as indicated by (A) final anisotropy (r_∞) and (B) initial anisotropy (r_0) (Eq. 2)

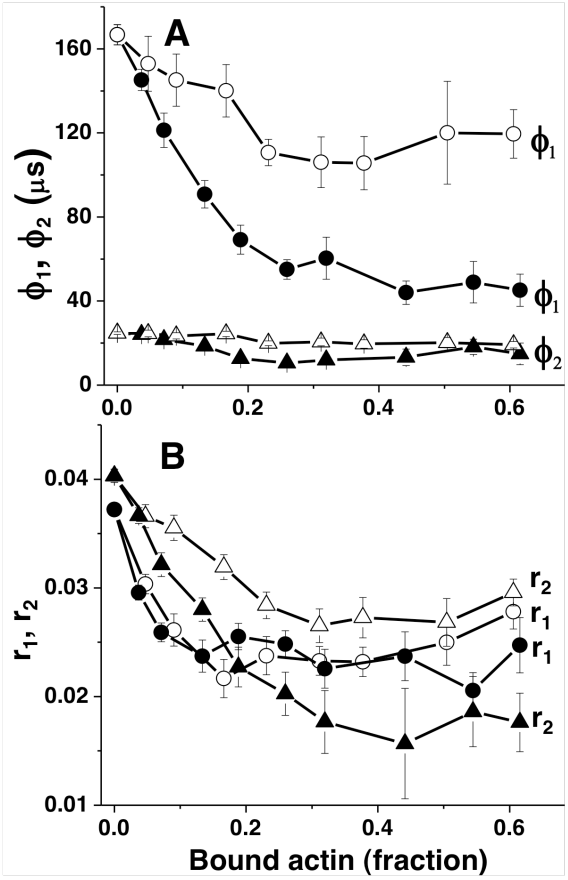

Figure A-4: The effect of dystrophin (open symbols) and utrophin (closed symbols) binding on the TPA of actin, as indicated by (A) correlation times and (B) amplitudes of rotational motions in actin (Eq. 2) Circles and triangles correspond to the slower (ϕ_1 , r_1) and faster (ϕ_2, r_2) motions

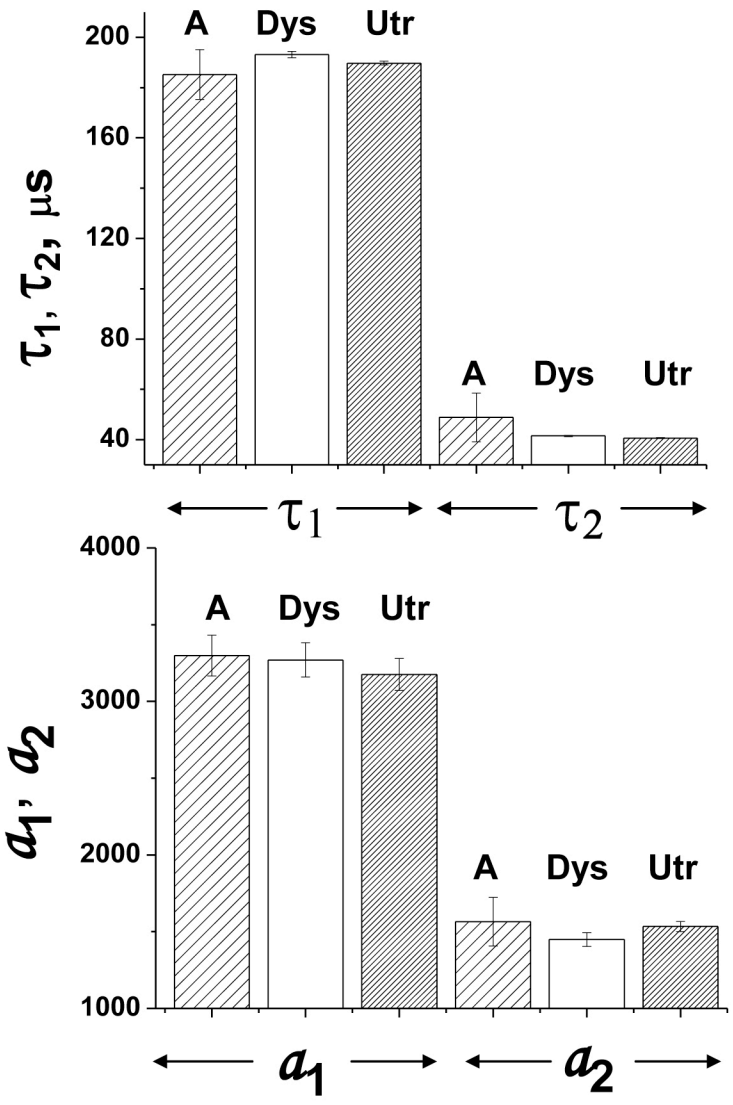

Figure A-5: The effect of dystrophin and utrophin on the lifetimes (τ) and amplitudes (***a***) of phosphorescence intensity decay of actin.

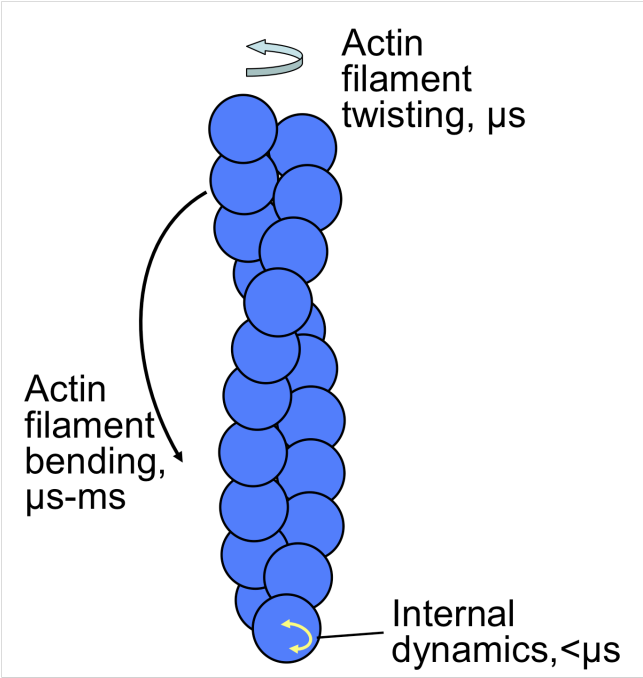

Figure A-6: Diagram of actin filament dynamics.